National University of Lesotho

Design and analysis for a feasibility study of a floating solar PV power system for Metolong Dam

Rorisang Christopher Moqulo

200900292

A dissertation submitted in partial fulfilment
Of the requirements for the degree of

Master of Science in Sustainable Energy

Offered by the

Energy Research Centre
Faculty of Science & Technology

June 2022

Abstract

Over the past years, an increasing capacity of floating solar photovoltaic (FSPV) technology utilizing water bodies to install solar power has been implemented, showing an alternative for countries where land use is constrained, land is not easily accessible, or land leasing is expensive. In addition to reducing land use competition, FSPV is promoted as a more efficient solar technology, bringing with it additional benefits such as reduced water evaporation and decreased algae growth. Based on previous field studies and industry insights, this study aims to analyse whether an FSPV project can be a feasible and cost-effective option for electricity generation and usage at Metolong Dam and water treatment works (WTW) located in Maseru district, Lesotho. Furthermore, PV module temperature analysis is another critical area, governing the efficiency performance of solar cells. In this study, the initial approach entailed the modelling of the Metolong reservoir water temperature (using Microsoft Excel) due to insufficient water temperature data at a selected location (since simulation software does not have features for FSPV). Then water temperature was used to investigate the photovoltaic (PV) module temperature on water bodies. The optimal sizing and performance prediction of a proposed power plant was modelled using a set of mathematical equations in a spreadsheet application (Microsoft Excel) and PVSyst software. Both models were compared to analyse the difference in annual electricity generation. Then, an economic analysis was performed to showcase the Levelized Cost of Electricity (LCOE) and Net Present Value (NPV). Finally, an evaporation model was proposed with the objective to quantify the potential savings an FSPV could provide using the calculations adapted from the Penman-Monteith model. The results indicated that this FSPV power plant would significantly contribute to the reduction of carbon dioxide (CO_2) emissions.

The recommended FSPV, with total installed capacity of 7.8 MWp, would consist of 3 platforms with an installed power of 2.6 MWp each. The study reveals that the proposed FSPV energy generation system is about 3.4% higher than ground-mounted PV (GMPV) generation system predicted by the PVSyst software due to the cooling effect provided by water just below the panels. From the simulation results, the value of performance ratio (PR) comes out as 90%, and the capacity utilization factor (CUF) value is 15.21% with a total effective energy generation at the output of the array of 17,345 MWh per year. The system could meet up to 70% of load demand during a typical day in winter months at the selected facilities. The FSPV system could cost US$ 10 Million with a payback period of 13 years, where the largest contributors to this cost are related to the floating structures and anchoring system of this plant. The proposed FSPV plant will substantially reduce the cost of energy as the plant cost is expected to be considerably reduced based on the low LCOE of 36.4 $/MWh. The economic feasibility of a FSPV system on a Metolong reservoir was thus established, and may be considered an efficient use option for electricity generation in Lesotho. Additionally, the shading provided by the FSPV system can save up to 84,136 m^3 of water annually. The annual reduction of greenhouse gas (GHG) emissions was analyzed and found to be 17,329 tCO_2 per year. Future studies should include more in-depth research into factors such as the impact of substation upgrade costs, variable interest rates, economies and environmental impacts.

i

Acknowledgments

I would like to express my sincere gratitude to my supervisors, Prof. Leboli Z. Thamae and Eng. Tawanda Hove, for all the patience they have taken with me during this difficult year. Secondly, I especially thank my family for their constant support and confidence during this intense but thoroughly enjoyable period.

I would like to thank Mr. Mokhothu Moerane from the Metolong Water Treatment Works for providing me with useful information on the operation of the Metolong Dam as well as data for some of my work.

I must express my gratitude to the people representing the Lesotho Electricity Company, Mr. Lebohang Mohasoa and Mr. Mareka Mosala who were open to share information with me.

Last but not least, I would like to acknowledge everyone who was instrumental in ensuring that this dissertation came to completion. Special thanks go to Ms Mathabo Moneri in that regard.

Table of Contents

List of Figures

Lists of Tables

Abbreviations

AC	Alternating Current
BOS	Balance of System
CAPEX	Capital Expenditure

CUF Capacity utilization factor (%) CdTe Cadmium Telluride

C-Si	Crystalline Silicon
DC	Direct Current
DHI	Direct Horizontal Irradiance
EPC	Engineering, Procurement, Construction
FIT	Feed-in-Tariff
FSPV	Floating Solar Photovoltaic
GHG	Green House Gas Emissions
GHI	Global Horizontal Irradiance
GMPV	Ground Mounted Photovoiltaic
GoL	Government of Lesotho
GWh	Gigawatt-hour
HDPE	High Density Polyethylene
IEA	International Energy Agency
IRENA	International Renewable Energy Agency
IRR	Internal Rate of Return kWh Kilowatt hour
LCOE	Levelised Cost of Electricity
MPP	Maximum Power Point
MPPT	Maximum Power Point Tracker
NOCT	Nominal Operating Cell Temperature
NPV	Net Present Value
NREL	National Renewable Energy Laboratory
O&M	Operation & Maintenance
OPEX	Operating Expenditure

PII	Permitting, Inspection, and Interconnection
PR	Performance Ratio
PV	Photovoltaic
SERIS	Solar Energy Research Institute of Singapore
STC	Standard Temperature Condition UN
	United Nation

Chapter 1 Introduction

1.1. Background

Energy is a comprehensive field that faces many challenges today, from developing access to electricity and grid connectivity, to climate change alleviation and moving to renewable energy solutions. Energy development is very often linked to education, social justice and economic growth and is therefore a key issue. As the United Nations set out in the "Sustainable Energy for All" (SEforALL) initiative, sustainable energy systems are the key to the development of sustainable societies [1].

However, the current energy systems around the world have been described as unsustainable and dangerous; leading to inequalities, human conflict and natural disasters. The current systems use conventional resources, mainly fossil fuels such as gas, oil or coal, to meet the world's energy and electricity needs. Though, traditional resources are becoming increasingly scarce and traditional energy use is one of the main reasons for the worsening of the climate and the increase in air pollution around the world [2]. The world has gradually realized the dangerous path of continuing the use of fossil fuels massively. As a result, a global interest has gathered in moving towards sustainable energy systems and solving these difficult challenges.

Additionally, many international and national conferences have been held around the world to find cleaner and more effective solutions under the guidance and influence of the United Nations and some major international agencies such as the International Renewable Energy Agency (IRENA) and the International Energy Agency (IEA). Countries have begun to come together and set ambitious goals for promoting clean energy systems [3]. At local level, NonGovernmental-Organisations (NGOs) and associations are also involved in the transition to a sustainable low carbon economy. The development of new alternative energy sources has always been considered as the key to sustainable development and the current challenges are actually driving technical development in the renewable energy sector. Overall, renewables generated an estimated 29.0% of global electricity in 2020, up from 27.3% in 2019 [4]. Thus, the share of renewable energy technologies in the global energy balance is systematically growing, especially in the electricity sector as shown in Figure 1.

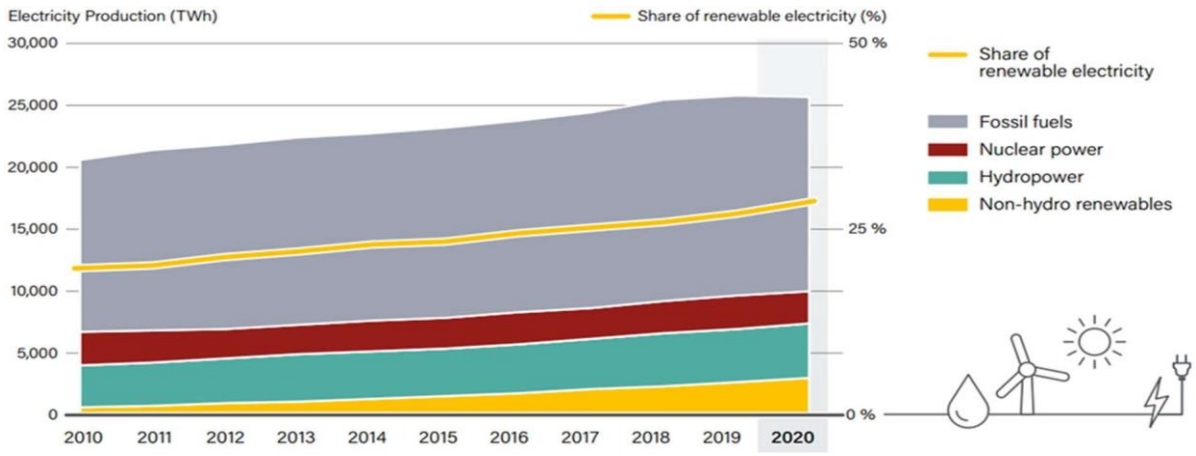

Figure 1- Global Electricity Production by Source, and Share of Renewables, 2010-2020 [4].

Solar energy is one of the most promising renewable technologies today. Solar energy is the richest resource in the world, which drives the development of technical solutions allowing for the efficient conversion of this energy. Indeed, the energy coming from the sun is by far greater than the annual energy consumption of humanity, as illustrated perfectly by Figure 2. Among the solar energy technologies, the fastest growing solution is the photovoltaic (PV) solar energy. In 2021, photovoltaic systems with a combined capacity of 171 GW were installed worldwide [5]. This increase, as shown in Figure 3, is mainly due to the lower prices of PV modules, which account for the majority of investments in PV systems [6]. Offering utility scale and cost-effective installations, large scale solar PV plants can nowadays be considered feasible solutions for investments in energy projects.

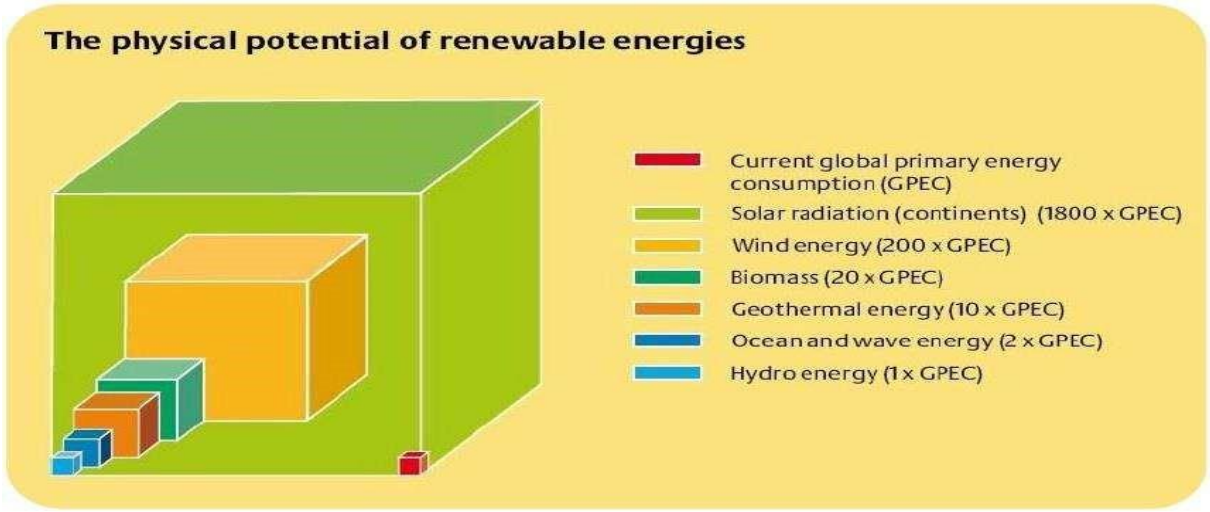

Figure 2- Global Energy Consumption and Energy Resources [7].

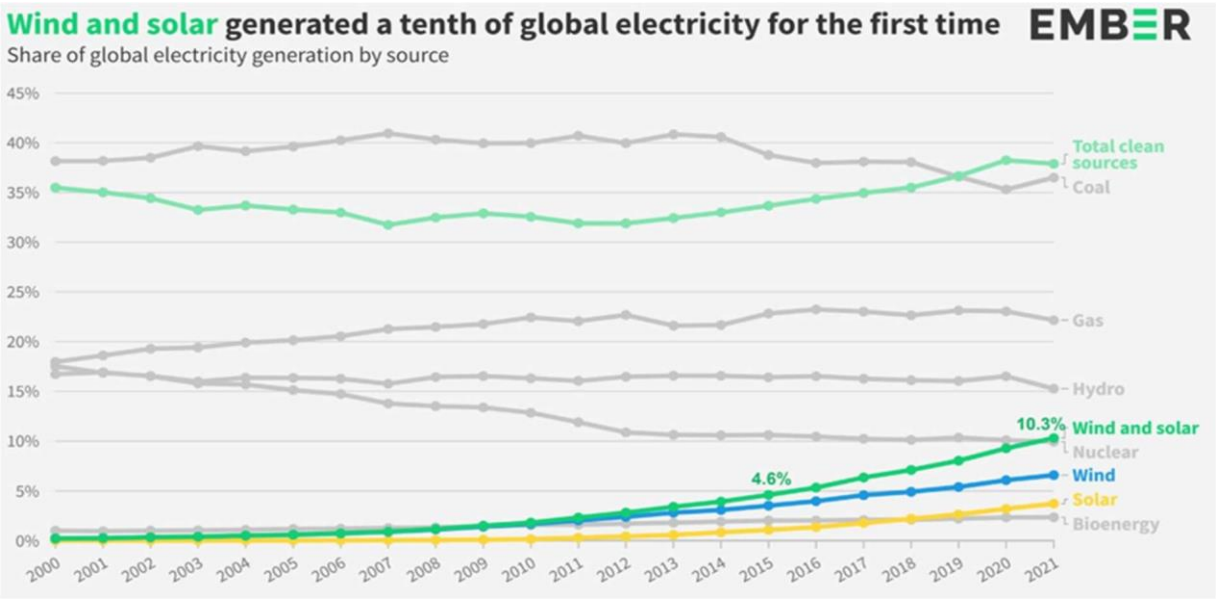

Figure 3- Annual additions of renewable power capacity, by technology and total [8].

In addition, solar energy has been considered one of the most exciting electrification solutions in Lesotho, where the sun shines for more than 300 days in a year [9]. The irradiation time ranges from 10.2 to 13.8 hours a day for both highlands and lowlands, with a high level of solar radiation on average 20-24 MJ/m^2/day on a horizontal surface [10]. As part of the national

sustainable development policy, one of the main objectives of the government in the energy sector is to promote the adoption of solar energy technologies. The draft renewable energy policy document includes the applications of solar PV (solar home systems (SHS), PV for clinics, PV for water pumping, PV mini-grids and PV for telecommunications) and solar thermal technologies (solar heaters, passive renewable solar energy technologies) in Lesotho [11]. Recently proposed electrification projects include the utility-scale PV solar park, small scale PV micro-grid and PV solar home systems, and other off-grid solutions [12], [13]. The use of solar PV will help achieve the country's renewable energy target.

1.2. Challenge

The construction of large PV systems requires a high availability of space, while many countries face a land scarcity [14]. Yet, in a sustainable economy, land plays a key role in agriculture or economic activities. Likewise, when implementing a solar PV system, landrelated problems such as land acquisition and availability often arise. The projects are then planned in large remote areas and this increases the cost of the investment in transporting electricity. Another challenge is the influence of ambient temperature on PV cell efficiency. Solar PV energy production is directly proportional to the amount of solar irradiance falling on the panel surface. Some portion of this irradiance is converted into electric energy and the rest of the solar energy heats up the solar panel. High solar irradiance causes overheating of the PV cells which in turn reduces the conversion efficiency and can lead to the thermal stress of solar panels [15]. Consequently, the physical drivers of reservoir evaporation might seems relatively straight forward given that the flux of water vapor from a reservoir is largely governed by the magnitude of the vapor pressure gradient between the water surface and the overlying air. Hence, reservoirs evaporate more water than the natural surface water flow before the dam was built because dams generally increase the surface area of the body of water. This means that more water is exposed to air and direct sunlight, thus increasing evaporation. This “lost” water is referred to as consumed because it is removed from the system. In some cases, this water consumption can be quite substantial [16].

To overcome these three main problems, a new concept which is installing solar PV systems on water bodies through floating structures has been proposed. Floating Solar Photovoltaics (FSPV) is a solar innovation with less than 14 years of technological development. A schematic diagram of a typical FSPV system is shown in Figure 4 [17]. The PV module is mounted on top of the floats/pontoons. There is a lightning protection system (connected to metal frames supporting modules and grounded). Floats are attached to the bottom of the reservoir with mooring lines and anchors. All electrical wires go to the combiner box which is then connected to the inverter. The inverter is then connected to a transformer ashore. The transmission line transfers electricity from the transformer to the grid. Further, the floating platform is composed of primary floats for supporting the PVs and secondary floats for maintenance, buoyancy and spacing the PVs appropriately. A hole in the middle, for passively cooling and ventilating the PV panel, is provided in the primary float, as shown in Figure 5.

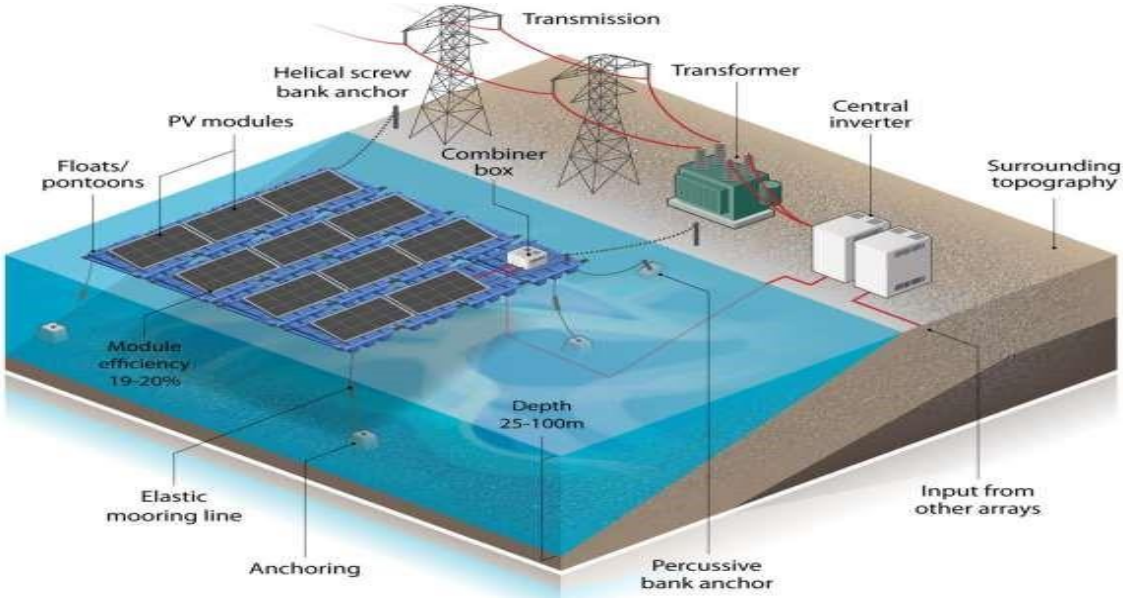

Figure 4- The layout of a typical floating PV system [17].

Figure 5- Floating structure [18].

A niche market a few years ago, the FSPV market accounted for 2.6 GW of the total global installed capacity at the end of 2020. China has emerged as the leader in this market with about 56% of the world's total output [19]. FSPV applications are particularly interesting for countries with irregular ground such as mountainous or coastal lands. These systems reduce the need of valuable land area, save drinking water that would otherwise be lost through evaporation, and show a higher efficiency of solar energy conversion as the panels are kept at a cooler temperature than they would be on land. This is crucial when people's livelihoods are dependent on land uses and water resources.

1.3. Objectives

Lesotho, a landlocked African state entirely surrounded by the Republic of South Africa [20], has excellent potential for FSPV on three reservoirs (Katse, Mohale, and Metolong) that are currently used for flood control, water storage, hydropower generation, or daily water usage. Hydropower in Lesotho is a significant component of the country's power resources. There are also plans to expand local generation particularly in large hydro up to 64% and PV up to 5% by 2030 to keep up with future demand and reduce the cost of imported electricity in the country [21]. Thus, the use of reservoirs for FSPV will help meet the renewable energy target of the country and take advantage of the already existing infrastructure of the dams.

To utilize water bodies in Lesotho and stay competitive within the floating solar market, this study explores the feasibility of installing an FSPV power system as a new cost-effective solution at the Metolong reservoir. The main goal of this thesis is to design and undertake analysis for feasibility investigation of an FSPV power system for the Metolong reservoir based on the analysis of the PV output potential, Levelized Cost of Energy (LCOE), GHG emissions reduction and water evaporation savings. To date, there is no scientific study focusing on the potential assessment of FSPV application in Lesotho. Thus, this study is the first and can pave the way for future studies.

This research work has its main focus on the techno-economic-environmental potential benefits of FSPV generation. Moreover, the study aims to model the proposed system in order to understand the impact on the electricity generation side. Further, this study aims to provide information on the use of solar PV on bodies of water in Lesotho as a convenient solution to improve access to electricity.

To accomplish the objectives of this study, the following three research questions will inform the analysis to be undertaken in this study:

- What is the potential for FSPV energy development at Metolong reservoir?
- Can the "FSPV" strategy help Water and Sewerage Company (WASCO) to meet its electricity demand using renewable energy source for water pumping from Metolong dam and electricity usage at Water Treatment Works?
- How much saving from water evaporation and emissions reduction can be achieved if FSPV system are being installed on the Metolong reservoir?

1.4. Justification of the study

Low access to electricity may be the main challenge facing Lesotho in the energy sector. Despite recent significant growth, the overall electricity availability in Lesotho covers less than 50% of the population, and energy shortages are projected to worsen in the coming years [20]. Moreover, households' electrification is unevenly distributed across the country; access is estimated at 71% in urban areas and 38% in rural areas [22]. Within the Lesotho Energy Policy [11], the Government of Lesotho (GoL) has put forward a framework to improve the energy security situation by reducing reliance on fossil fuels and imported electricity in the country by the year 2025. The policy further aims to reduce greenhouse gas (GHG) emissions from the

energy sector. One of the ways through which Lesotho can alleviate the challenges of the energy-water-nexus is to integrate renewable energy technologies to meet the peak power deficit. Furthermore, every year electricity tariffs increase on the energy and maximum demand charges for commercial and industrial customers in order to pay the heavy expenses from imported electricity. This is done in an effort to make profits and ensure smooth operations. However, it results in heavy tariffs which negatively affect consumers.

Loss of water resources due to evaporation is a well-known phenomenon stated to be as high as 40% worldwide [23] and its effect is particularly important in dry and arid regions. However, evaporation is a natural water cycle and some environmentalists may be concerned if it is disturbed. But in the case of a reservoir, the surface over which it occurs is artificially enlarged. Hence, it should be reduced as an environmental mitigation to save precious water. FSPV plants are deployed on the water surfaces; they provide shade to the water surfaces through the reduction of solar radiation reaching the water surface and by limiting the interaction of the wind on the water surfaces. The combined benefit of these may result in substantial reduction in the water evaporation losses though they cannot be stopped completely.

Available space has become a shrinking commodity due to the rising population. This has exponentially increased the cost of land thereby increasing the project cost. Since FSPV system can be installed over water surfaces, they have emerged as an effective solution to mitigate the issue of huge land requirement for PV systems.

As the Government of Lesotho (GoL) encourages the installation of solar stations in remote areas. It is therefore, imperative to conduct a thorough technical assessment of existing solar systems for system reliability, value of investments and current system performance in order to be able to determine their optimization through the use of renewable energy sources and ensure technical and financial sustainability. The outcome of this study will strengthen the policy formulation activities for the implementation of the FSPV program. This thesis is necessary to encourage the installation of power systems based on FSPV systems on existing water bodies in Lesotho. The study will also provide technical input on the methods and ways to optimize FSPV systems.

1.5. Thesis Outline

After this brief introduction, the research work will be structured as follows:

Chapter 2 outlined the literature review on FSPV performance, technology, energy-estimation methods, and environmental impacts. The review aimed to give a deeper knowledge and understanding of the energy potential development of FSPV systems. It will cover some background information pertaining to floating solar generation, and any recent developments in the industry. It also pointed out the important aspects that need to be considered for a good design of these systems. At the end of the same chapter, a brief review on identified gaps in literature for FSPV deployment was given.

Chapter 3 provided the details of the selected location; namely the resources availability and all the factors that led into choosing it. Furthermore, data collection and research methods was

discussed in this chapter. It will also include detailed justification of the importance of the chosen method as well as continuing to explain the methodology or explaining why that particular method was used to conduct this feasibility study. The technical modelling of the FSPV and economic analysis of the system alongside the quantification of the common suggested qualitative advantages of FSPV was discussed. At the end of this chapter, the environmental benefits modelling namely; reduction in evaporation and green-house-gas emissions was given.

Chapter 4 presented the results from the main simulation, the results from all sensitivity analysis, the results from the economical evaluation and the results from environmental benefits. Moreover, the initial capital cost and the levelized cost of electricity (LCOE) analysis methods have been used for the system, in order to estimate if the technical optimizations are profitable or not. The discussion regarding each presented result is also included in this chapter.

Chapter 5 is the conclusion chapter summarized the major results obtained throughout this entire work. It also presented further recommendations which can be carried out in future research on similar projects.

Chapter 2 Literature Review

Climate change related challenges, rapid population growth, the ever-increasing energy demand and the United Nations' call (through Sustainable Development Goal number seven SDG7) for an inclusive energy access strategy, have made access to alternative energy supplies imperative. This global energy trend also applies to Lesotho and according to the World Bank, the increase of electricity demand in Lesotho is associated with the growing rate of population with access to electricity and other developmental activities with increasing electricity usage [20]. This chapter aims to present a brief literature review of the parameters that control the FSPV technology during the design, implementation and maintenance stages of projects.

2.1. Performance of FSPV systems

The following section discuss a review of literature that documents existing installations and a list of some of the most recent, largest and unique installations. It also compares the behaviour of FSPV systems relative to land-based PV systems.

The solar energy market is working hard on increasing the efficiency of the PV module since solar energy is one of the sources available throughout the world. Study by [24], declared that a PV module technology is affected by several factors, which includes the distribution of solar intensity, ambient temperature, climate and the temperature coefficient of the module. It is proven that the electrical efficiency directly depends on the ambient temperature since increased temperature reduces the efficiency [24]. The voltage of a module is highly affected by the temperature thus the voltage maximum power point (Vmpp) increases at lower temperatures. For example, the maximum power output (Pmp) at 25˚C can reach 50.2 W meanwhile the same module at a temperature of 40˚C only reaches 46.5 W, at a constant radiation [25]. When the temperature increases, the band gap between the semiconductors in the PV module reduces, which means that the less energy can be absorbed by the panel [24]. Since most areas with the highest solar radiation are usually tropical regions, researchers have tried to integrate cooling systems in order to find the best solution of decreasing the module temperature [24]. The technique of air- and water-cooling systems has been studied and successfully proved to increase the efficiency of the module. The study conducted by [26], set up a hybrid PV water cooling system where a water flow system was placed at the back of a module. The result observed how the temperature of the module decreased by 20% and the power efficiency increased by 9%. In much the same way, the study by [27] found that a water cooling system provided higher efficiencies than using an air cooling system.

Comparing land-based PV with FSPV in the state of Hapcheon, China, the performance of 100 and 500 kW FSPV was compared with that of 1 MW PV plant 60 km south of Hapcheon, having similar global horizontal irradiance (GHI) and mean temperature. It was observed that 100 kW FSPV had an efficiency of 17.6% as compared to 13.5% of overland PV [28]. The efficiency of any solar panel depends on its module temperature. The water-cooling effect ensures ambient working temperature for the FSPV module. It was observed that there is a 3.5°C difference between land-based PVs and FSPVs [29]. It is also confirmed that FSPV systems produce at least 10% more energy than other land-based solar PV systems studied [30].

Similarly, another publication from the University of Malaysia simulated an 80W FSPV system using poly-crystalline cells. The experimental system shows 6% and 15% higher output power in short-term (2 hours at noon) and long-term simulations respectively, compared to the standard PV land modules [31].

A full-scale floating plant is located near Alicante, Spain, which was built in an agriculture reservoir to study the behaviour of the system. The top of the reservoir has a surface area of 4,700 m^2, but only 7% of such area has been covered with a fixed solar system. The cost of setting up FSPV systems was nearly 30% higher than a conventional grid [32]. Floating structure costs usually account for 25% to 34% of the total building cost for the plant, but these are still less than the cost of acquiring equivalent land area [33]. According to [34] and [35], operational and maintenance costs for FSPV systems are lower than for land-based systems, partially due to the readily available water needed for cleaning. Due to the lower ambient temperature on the reservoir, the system components are cooler, leading to lower maintenance costs. However, [33] found that soft costs, including labour, design & engineering, and supply chain logistics, contribute to the higher cost of FSPV and vary across projects. The uncertainty around these costs can deter developers and investors [33]. The study conducted by [36], had compared the LCOE of typical ground mounted solar PV grid connected system with the LCOE of FSPV Systems. The LCOE of grid connected system is lower than the FSPV system. However, other benefits such as water evaporation loss reduction and land use reduction compensate for the higher cost. This is due to the need for additional components such as mooring systems and supporting platforms. Added to this, is the material requirement of FSPV systems to resist harsher environments than land conditions. In a study conducted by [37], the authors estimated the cost of setting up 1 MW (1048 kW) fixed floating PV to be US$1 081 398. With the enhanced performance of FSPV relative to terrestrial PV, the focus moved towards optimising the systems supporting the PV modules in a water environment.

However, for the FSPV, the cost is still unclear as several technologies are still on the way to the market. Few FSPV projects exist compared to the ground mounted systems and they are limited to certain regions. This has to do with the fact that there are different types of fixings and anchoring which play a big part in the cost. Through extensive research from media releases and industry information, it was possible to summarize in Figure 6, the different FSPV project costs by the installed capacity [38]. The vertical axis represents the investment cost per installed Wp, the size of the bubble represents the size of the power plant (the legend of the size of each plot is in the upper right corner), and the colour of the bubble represents the region.

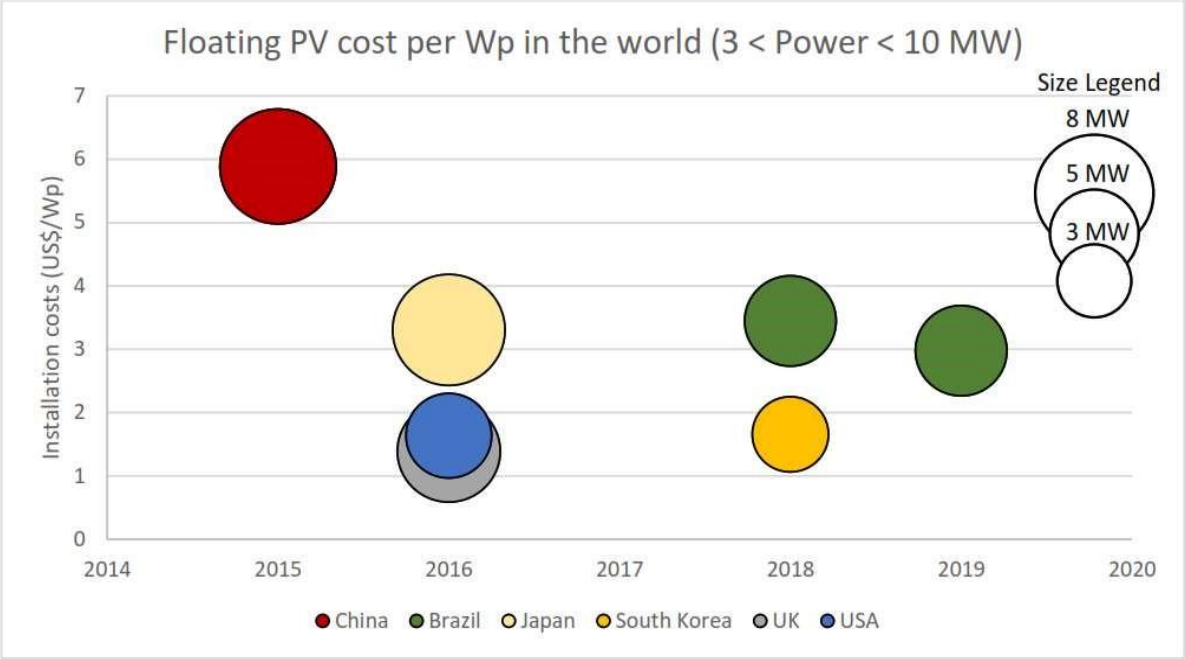

Figure 6- Specific cost of floating PV projects 3 MW and 8 MW [38].

When compared to the benchmark data, the commercial ground-mounted PV of 100 kW and 2 MW have been evaluated to range between 1.95 and 1.72 US$/Wp respectively, and for the fixed tilt utility, the scale ranges between 1.36 and 1.06 US$/Wp for 5 to 100 MW, respectively [39]. Thus, as expected with new technologies, implementation costs are relatively higher and become more competitive once large-scale projects are deployed. The a research on the several components included in the ground-mounted PV and FSPV systems were researched [57], [40], [41], [42] and summarized.

2.2. Review of FSPV technologies

The following section provides a list of some of the existing FSPV technologies, the authors disclaim that the list is comprehensive as some of the technologies studied in other papers have been omitted, including some found in the extensive works documented by [43] and [44].

The first floating solar PV structure dates back to 2007 [45]. In the initial days, pontoons were used to mount the FSPV system. Although robust in its structure, it was expensive and not specifically designed for the FSPV [44]. Only recently, an alternative approach to utilise highdensity polyethylene (HDPE) as a floating structure with galvanised steel supporting it became very popular due to its low manufacturing cost [35]. Few plants were set up with this technology, which proved to be successful [44]. Other companies followed suit and proposed an innovative solution to use plastic as the base material [45]. One such company, Ciel & Terre, utilised 100% HDPE and build a modular, robust floating structure [44]. This became widely popular and currently has the most installed capacity [46]. It meets the criteria of modularity, flexibility, robustness and safety, and thus, this floating structure has been adopted for the study. Both the enhanced performance of FSPV and the availability of scalable supporting structures meant that the focus moved towards accurately estimating the solar energy at a given

site. As FSPV becomes more popular, there are more than 100 projects around the world where FSPV has been installed in hydroelectric power plants and wastewater treatment facilities, mainly in Japan [33]. Figure 7 shows some of the major floating solar PV players compiled from 2019 [33]. It has been noted that some floating structure vendors produce their own mooring and anchoring solutions. However, the mooring and anchoring vendors as listed only produce these products.

Figure 7- Major FSPV players [33].

There are also many projects being studied and assessed for feasibility. A potential 1 MW FSPV system in Korea assessed using the System Advisor Model (SAM) software showed the production of 972 MWh/year, covering 87,650 m^2 of water surface [47]. A grid-tied 2 MW FSPV and electric transportation facility that covered 4,000 square meters (m^2) of a reservoir that would generate 2,685 MWh annually, cost around 1.6 million USD with a payback period of 6 years in Pondicherry, India [48]. Overall, feasibility studies for FSPV have been done in various continents, showing high potential in energy generation and competitive payback periods with other generation technologies.

Additionally, FSPV allows integration with other activities. Just as land-based PV systems can be used to provide shade for plants ("Agrivoltaic") that excel in low light, the FSPV can be integrated into aquaculture and fish farming. However, there is a lot of interest in integrating with hydroelectric dams which inundate large amounts of land that could otherwise be used for something else. The combination of the FSPV with hydroelectric power plants can lead to an increase in the total installed generation capacity of the plant [49]. According to the International Hydropower Association (IHA), this hybrid model was effective at the Longyangxia solar hydroelectric power plant in China [50]. With complementary control systems, differences in solar production can be reduced by hydroelectric power generation. Hydroelectric power plants can reduce their production when solar power is high and increase their production when solar power is low. Overall, there will be an increase in total energy generation and in turn, this will increase the reliability of power plants to reach the grid [51].

Another advantage of the hybrid model is the increased use of transmission lines. Turbines and power lines are often underutilized due to the low water volume during the dry season. Colocation will help resolve some of the problems by connecting the FSPV to the connection of the existing high-voltage grid of the hydroelectric power plant, saving on additional

transmission infrastructure costs typically faced by next-generation projects. To adapt to reservoir capacity, the FSPV does not need to cover a large reservoir area. Table 1 shows the number of area surfaces that must be covered with PV to match the same hydroelectric generating capacity.

Table 1- Percentage of reservoir area required for FSPV to match hydropower dam's capacity [49].

Dam/Reservoir	Country	Reservoir size (km^2)	Hydropower (GW)	Percentage of reservoir area required for FSPV to match dam's hydropower capacity (%)
Bakun Dam	Malaysia	690	2.4	3
Lake Volta	Ghana	8,500	1.0	<1
Guri Dam	Venezuela	4,250	10.2	2
Sobradinho Lake	Brazil	4,220	1.0	<1
Aswan Dam	Egypt	5,000	2.0	<1
Attaturk Lake and Dam	Turkey	820	2.4	3
Narmada Dam	India	375	1.5	4

As an additional benefit, water cooling of the FSPV array has been used as a method to increase PV module efficiency. In a no-shading-or-faults condition, a high operating temperature and reduced incoming irradiance due to soiling can affect the panels' efficiency. The body of water can be passively, or actively used to cool the panels. As water bodies provide an area free of trees, shading and contribute to a lower ambient temperature, PV deployment benefits [35]. The water taken from the water body supporting FSPV can be actively sprayed or used to create a water veil onto the module when the temperature is too high, or irradiance is too low due to soiling [44]. However, this method can reduce the water available for other benefits such as irrigation, drinking water, or hydropower.

FSPV, however, FSPV has some disadvantages. The system is prone to threats such as storms and corrosion of the metallic structure which can reduce the system's life. On September 9th, 2019, Japan's largest FSPV plan, a 13.7 MW project at Yamakura Dam, caught fire in the aftermath of Typhoon Faxai [52]. There are some environmental concerns such as the reduction of light penetration that can affect the growth of aquatic life [35].

2.3. FSPV Operating Cell Temperature

Hove and Mungofa [53] have carried out extensive studies on the efficiency, power and temperature of the module in the conventional photovoltaic system. Solar cells convert only a small part of the absorbed solar radiation into electrical energy and the remaining energy is dissipated as heat in the main area of the cell. Increasing the operating temperature of a solar cell and module reduces the band-gap which slightly increases a solar cell's short circuit current for a given irradiance but greatly decreases the open circuit voltage, resulting in a lower fillfactor and lower power output. The net effect gives a linear relationship for the electrical efficiency of a PV module as:

□ = □ 1 − □ (□ − □) ∗ □ [1]

where η_{ref} and β_{ref} are the electrical efficiency and temperature coefficient of the PV module, fm is the matching factor described as a ratio of power output of the PV array under varying operating conditions to its power output at maximum power point. T_m and T_{ref} are the PV module operational temperature and reference temperature, respectively.

The operating temperature of a solar cell depends on its exposure to radiation and heat exchange with its surroundings. Based on the long history of onshore photovoltaics, several models have been planned to approximate the operating temperature of cells and modules [44]. Two frequently used models are Sandia's cell temperature model and Faiman's cell temperature model [44]. The Sandia model is based solely on the experience found in various module designs and ground-based PV system installation conditions. As such, it may not always be applicable to FSPVs without experimental data for a particular FSPV technology. In the model proposed by Faiman, the cell temperature T_{cell}, is related to the ambient temperature T_{amb} and the wind speed v_{air} by:

□ = □ + _____ [2]

where U_0 is the constant heat transfer component, U_1 is the convective heat transfer component, and G_{POA} is the array irradiance plane. U_0 and U_1 measure how effectively the heat absorbed by the cell is released to the environment.

In practice, the U_1 use is often hindered by the lack of accurate wind speed measurements that represent the exact height and position of the module. It can be difficult to get these measurements. Therefore, a single U value is often derived without an explicit wind dependency. In equation (2), the reflection from the module is ignored. A more accurate specification of the module temperature considers the energy that is converted to current and reflected by the module.

(( )) (( )) □ = □ + _____ = □ + _____ [3]

τ is the transmittance of the glazing, α is the absorbed part of the irradiance and η(T) is the temperature-dependent efficiency of the solar cell.

This version is adopted in the widely used photovoltaic simulation tool PVSyst software. In the final expression (Equation 3), a single U-value is used without the explicit wind dependency. High U-values indicate a high heat exchange between the solar cell and the environment, resulting in lower module operating temperatures. For FSPV technologies that are in direct contact with water or very close to direct contact with water, the temperature of the water forms the environment on one side (or both sides for submerged structures). Since water has a significantly higher thermal conductivity than air (λwater = 0.6 W/mK, λair = 0.026 W/mK), water temperature and water flow dominate in such architectures. Therefore, the operating temperature of the module is likely to depend on the water temperature and water flow in addition to air temperature, wind and mounting structure [55].

Similarly, Kamuyu et al. [56] investigated a PV module temperature prediction model for the energy yield of floating PV. They used MATLAB to obtain equation coefficients of predictable environmental variables to derive FSPV models from the first module temperature operating models. Their proposed Model 1 and Model 2 coefficients for the FSPV model are expressed as follows:

□ = 2.0458 + 0.9458□ + 0.0215□ − 1.2376□ [4]

□ = 1.8081 + 0.92882□ + 0.021□ − 1.2210□ + 0.0246□ [5]

T_{m1} and T_{m2} explains the operation temperature behaviour of the FSPV module with seasonal variables, solar irradiance (G_T), ambient temperature (T_a), wind speed (V_w), and water temperature (T_w).

When comparing the theoretical prediction with the actual operating temperature of the PV field module, the corresponding model errors are between 2% and 4% depending on the number of embedded equation coefficients. Therefore, their study is useful to validate the results of other studies showing that FSPV systems produce 10% more energy than other terrestrial systems.

Another cell temperature prediction model called "MINITAB" is an advanced statistical program that has well-defined algorithms that describe the change of each dependent variable y with the interaction between the respective independent variables x [30]. MINITAB generates an equation showing the interaction between the dependent variable (module temperature) and the independent variables. Equation (6) derived from MINITAB is very accurate (0.1%) but carries the risk of equation complexity due to over fitting.

□ = −1.9034 + 1.12322 × □ + 0.028655 × □ − 0.6517 × □ − 0.0936 × □ − 0.001328 × □ − 0.000014 × □ + 0.08382 × □ − 0.00060 × □ × □ − 0.031334 × □ × □ + 0.001389 × □ × □ − 0.000981 × □ × □ + 0.000545 × □ × □ + 0.039145 × □ × □ [6]

However, one of the limitations is the absence of the water temperature data in some cases. Consequently, statistical models have been used extensively in water temperature forecasts because these models are relatively simple and require minimal data input. Linear regression models [57], [58], non-linear regression models [59], [60] and stochastic models [61] have been successfully developed in recent years for data related to different time scales. Although these statistical models relating water temperatures to air temperatures offer fairly simple approaches to water temperature prediction, other statistical models such as Box Jenkins and non-parametric models [50], and hybrid models based on statistical models such as air and water can do the modelling of the temperature of water [62]. Based on Mohseni et al. [59], the water temperature prediction was implemented and calibrated or validated using the R statistical software, with an optimization function to determine the best fit for the four parameters α, β, μ, and γ.

□ = □ + _____×
[7] where α is the estimated maximum temperature of the stream, μ is the estimated minimum

temperature of the stream, γ is the steepest slope of the function, and βair is the air temperature at the inflection point.

For the location data, a visual inspection of the function reveals the behaviour of the S-shaped curve used for the work by Mohseni et al. usually corresponds to a good fit with the NashSutcliffe coefficient close to unity, which represents the efficiency of the curve fitting and should be close to one [59].

With governments and institutions across the world incentivising the implementation of clean energy, these efforts have led to the availability of open-source energy estimation software. Widely used open-source software includes RETScreen (Natural Resources Canada), PVWatts (National Renewable Energy Laboratory, USA), PVSyst and PVGIS (European Commission). PVSyst version 7.2 was incorporated in the study to evaluate the proposed system.

PVSyst https://www.pvsyst.com is a widely used simulation tool for PV system designers and researchers. The software is capable of modelling both grid-connected and stand-alone PV systems. PVsyst is used for technical and economic evaluation of different PV system configurations in order to identify the most optimum design for energy generation. PVsyst together with 3D design capability is a useful tool for detailed designing and shading analyses. It is also possible to set local losses of the system, such as snow, shading and other system losses. This software is considered a standard for PV system design and simulation worldwide, the latest version is V7.2 and it has 30-days evaluation mode for DEMO, unlimited version is around USD 1,021. PVsyst V7.2 runs under any Windows operating system and Import irradiation data from PVGIS and NASA databases [63].

2.4. Impact of FSPV systems on evaporation

Surface water evaporation is a complex phenomenon and various factors affects the water evaporation from open water surface, some of these factors include water surface area, temperature, vapour pressure difference, wind effect, atmospheric pressure and quality of water. Due to increasing concern over climate change, the conservation of water becomes extremely important. An FSPV structure has its application in reducing water evaporation from water bodies. The rate of evaporation mainly depends on two factors: vapour pressure of air temperature and wind speed at a height of 10 m [37]. FSPV systems can help save up to 33% of the water from evaporating on a natural lake [35]. A feasibility study considering 1 MW FSPV was carried out over the Kishore Sagar dam in Kota, Rajasthan, India. The authors estimated the plant to generate 1,838,519 kWh of energy per year while saving 37 million litres of water from evaporation [64]. A similar study aimed at analysing large reservoir potential across the whole of India found that for each square kilometre of area, 1,250 million litres of water per year could be saved from evaporating [65]. Taboada et al., compared the evaporation potential of two identical preheated copper mine ponds with high-density polyethylene pontoons and PV covering 95% of the water area of one pond and the other pond left uncovered. Measurements during an 8-months' time span showed 90% water savings in the FSPV covered pond compared to the uncovered pond [66]. On analysing electrical generation and reduction in evaporation at a reservoir in Spain, it is seen that when the entire structure was covered with FSPV, it generated 425,000 kWh per year, saving 5,000 m^3 of water by covering a 4,490 m^2

surface reservoir with FSPVs, which is 25% of the total reservoir capacity [40]. The effect of solar panel on reducing water evaporation in Singapore reservoirs studied by [67] showed that floating solar panels above water bodies had a reduction effect of approximately 30% on evaporation rates. As per the experimental setup results, average daily evaporation rate was about 7 mm/day which was reduced to about 5 mm/day by covering water body surface using solar panels. Evaporation constitutes the physical process by which water in the liquid phase becomes atmospheric water vapour. In South Africa including Lesotho, the evaporation losses from our reservoirs are significant [68]. As shown in Figure 8, the evaporation rate is greater than 1 400 mm per year for most of the country. Evaporation has a significant influence on the yield of water supply reservoirs and on the economics of building reservoirs of various sizes.

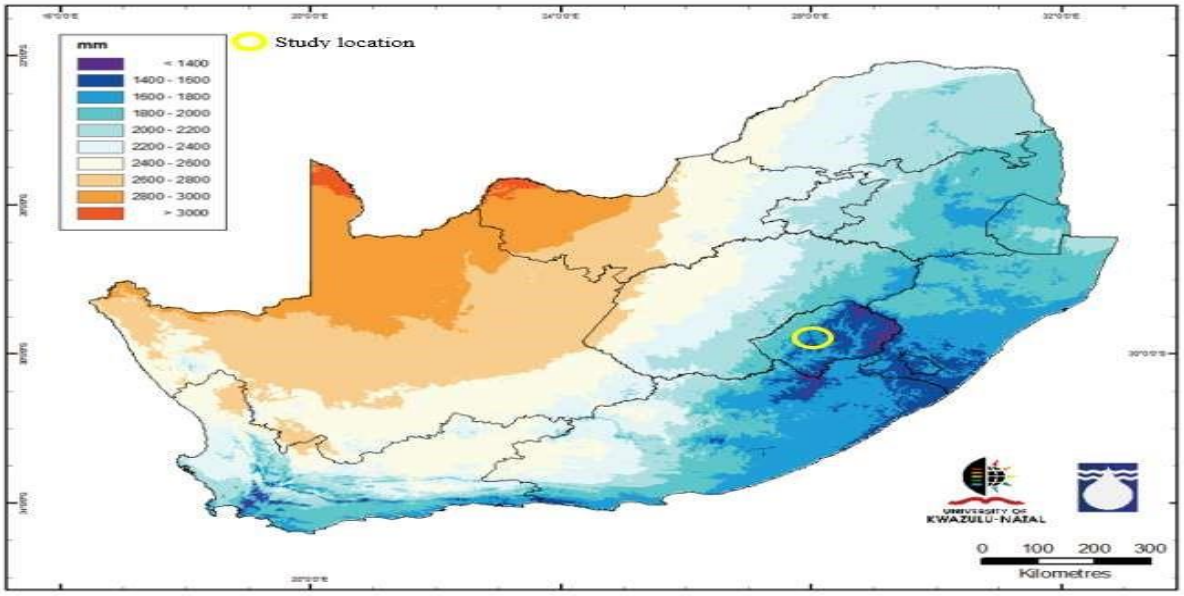

Figure 8- Map of evaporation from open-water surfaces across South Africa (mm/year) [68].

2.5. Environmental impacts of FSPV systems

Considering that water is one of the most important elements around the world, the installation of structures in direct contact with water raises concerns not only for safety, but also for the impact on the environment. If the selected reservoir is to be used for irrigation or for drinking water, special attention should be paid to the requirement to utilize this surface and if not available, be prepared when benchmarking other sites. Study by [69] assessed environmental impact of FSPV vs land-based PV system, in terms of water quality depletion, bird collision, water management and employment. As per the report, floating solar does not utilize chemicals and herbicide, hence less pollution. Floating solar also avoids use of precious agriculture land, hence causes less deforestation.

In a broader spectrum, the installation of FSPV in reservoirs can have several direct impacts in both the construction, management, and if necessary, decommissioning phases. During the construction stage, major impacts on the water basin may take place due to the need for keeping the system that can alter the geomorphology of the soil. However, in some initiatives such as Ciel et Terre [70], the complete structure can be commissioned outside a body of water and

only if a submerged mooring is required, an amendment to the basin bottom is required. Considering the operational phase, these structures, together with buoys or pontoons, will likely develop algae which can then appeal to other species in the case of lakes that will adapt under FSPV. Covering the surface of lakes with live fauna with PV panels can affect the natural brightness and cycle of micro-organisms which can have a negative impact on the environment [71]. As a result, the majority of commercially installed FSPVs are located above man-made reservoirs and sometimes abandoned mine pits, creating a hostile environment for the development of living species.

Furthermore, one of the biggest problems is getting to understand the compatibility of the material with water and how the constant contact between the metal structure and the HDPE float can affect the water quality. Companies are working on certifying their materials to be able to install structures above drinking water. For example, Ciel et Terre achieved drinking water compliance with BS 6920:2000 of the Water Regulation Advisory Scheme (WRAS), meaning that the material is compatible with the drinking water exposure in the UK [70].

The various aspects of FSPV integration covering performance, energy-estimation and environmental benefits have been extensively studied for large water bodies, like reservoirs and dams. In much the same way, this research work explores the suitability of using a large water bodies for solar energy generation in the Peri-urban set-up of Maseru district, Lesotho. The study solely covers energy estimation, quantifies the evaporation loses and provides a cost estimate. However, it does not include field studies and the environmental impact of solar panels on the reservoirs' ecosystem.

2.6. Identified Gaps in the Literature

Knowledge gaps remain regarding the costs of FSPV systems, potential negative impacts and validation of regular productivity. These gaps make it difficult for potential adopters to identify and quantify the actual benefits of FSPV systems, which may stifle investment in FSPV systems. The economies of scale of the FSPV system have not yet been clearly observed and investigated, but are envisioned in various studies [72], [33], [17], [42]. However, depending on the size of the sample studied, there was weak evidence of the economies of scale for FSPV. This statement was supported by the Institute for Local Self-Sufficiency (ILSR), which found that the costs of transmission and distribution of large-scale solar projects severely undermine the economies of scale [73]. The maintenance schedule and cost of FSPV are not readily available for research and comparison. In addition to standard PV site maintenance such as module cleaning, general site maintenance such as road management, safety equipment maintenance, fencing and equipment repairs, on-site metering including weekly or monthly meter readings, string measurements, FSPV may require more maintenance than a ground or roof mounted system [74].

The impact of FSPV on the ecosystem, that is, the impact of reservoir water retention on river hydrology and ecosystems due to the use of FSPV during the day instead of hydropower has not yet been addressed. Additionally, no empirical data is available from FSPV installations to support the claim that FSPV reduces algae growth or improves water quality. However, Far Niente Winery did not report any impacts on algal blooms, although the pond is used to unload wine purification equipment and this could affect algae growth [71]. A critical first step in

addressing this gap is to gather various water quality measurements (such as chloride, pH, and chlorophyll levels) and reveal the established system performance. In addition, from the literature reviewed, given that evaporation reduction is one of the stated primary co-benefits of FSPV structures and that it may want to extend water availability for other uses, this is a fundamental statistical gap that has to be addressed in addition research.

Floating solar PV does have the potential to reduce the availability of water bodies for recreational, ecosystem, and aesthetic purposes. None of the FSPV literature reviewed in this study addressed the need to consider environmental justice and quantify broader social and sustainability co-benefits and impacts of FSPV systems even though this is an area of increasing focus in the nexus literature. FSPV is an emerging market that is still in the early stages of adoption and needs further attention in the coming years. Despite some challenges and knowledge gaps, the rapid development of FSPV provides researchers with more data to study the strengths and weaknesses of the system and answer other questions.

The most widely documented and empirically supported benefit is increased panel efficiency leading to increased power production compared with a land-based PV system. For pontoon systems allowing air circulation behind the panel, an average 5–11% increase in power production has been reported in California (U.S.), Italy, Spain, and other locations [32], [71], [55]. However, the extent of panel efficiency improvements varies based on pontoon design and climactic zone; for example, a more humid environment has less evaporative cooling, which would result in fewer efficiency benefits [75]. Other studies use simulating software to obtain energy yield of FSPV systems, however the current version of softwares like, System Advisor Model (SAM), PVSyst, PV Watts, and others has no separate feature for FSPV systems. They depend on air temperature for simulations instead of using water temperature, because the operating temperature of the modules of FSPV are likely to depend on water temperature. Therefore relying on the results of other studies and adding 5-11% to the simulation software's energy output value. This thesis contributes by modelling correlation between air temperature and water temperature in the absence of water temperature at the site. Therefore, to investigate the PV module temperature on water for the energy yield of FSPV.

Chapter 3 Data and Research Methodology

The major objective in this thesis is to assess the prospective potential of floating solar PV installation on the Metolong dam/water body in Lesotho. Firstly, the chosen case study site for the implementation of a FSPV plant is described. The second part of the chapter provides a synopsis of data collection and analysis to summarize what the whole data entails. In the third part, Google Earth Pro was used to assess techno-geographical potential for FSPV on Metolong Dam. Then technical potential is evaluated in terms of installed capacity as MW and annual energy generation as MWh. System modelling, sizing and possible power production capacity of the FSPV system are discussed in the fourth part. Based on the estimated power production, the economic feasibility, evaporation reduction and reduction in greenhouse gas emissions are assessed in the fifth and sixth part, respectively. Figure 9 shows the 6-step study process used to assess the expected effects from the FSPV power system on the Metolong reservoir.

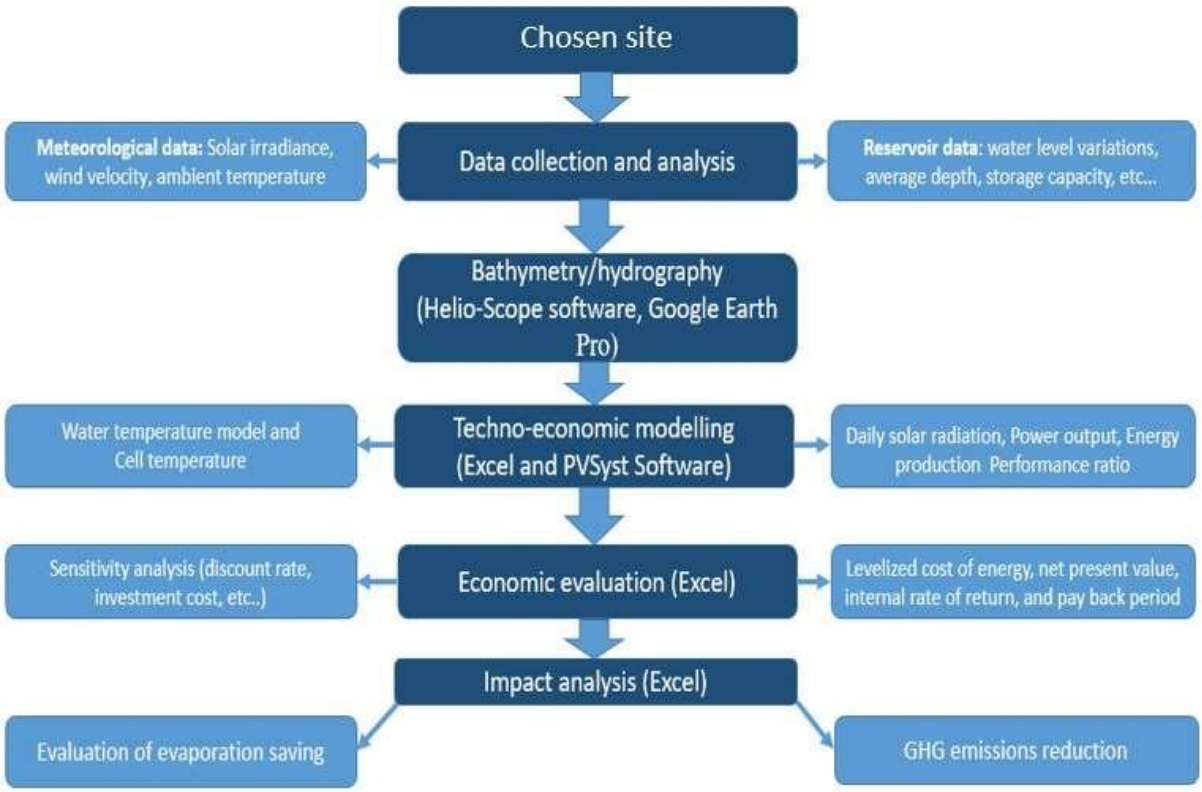

Figure 9-Overall procedure to assess the potential of a FSPV system in the study site.

3.1. Site location

The chosen site of Metolong dam in Maseru district, Lesotho, is located on the South of the Phuthiatsana River which flows through the Lowlands of central western Lesotho. The latitude and longitude of the location are: 29°20’4.33”S and 27°46’39.01”E. This location refers to the Metolong dam and water treatment works (WTW). The view and geographical location of the Metolong dam reservoir is shown in Figure 10.

Figure 10- Location of Metolong dam and Water Treatment Works (retrieved from Google Maps).

Metolong dam is a man-made effort with a 63 million cubic metres (Mm^3) capacity, 13.5 kilometers (km) reservoir length, 83 meter (m) height, 270 m crest width and a surface area of approximated to 2.8 square kilo-meter (km^2) [76]. This shows the scope to accommodate large number of solar PV panels. The purpose of this dam is to supply water to the capital city of Maseru and other towns such as Teyateyaneng, Roma and Morija. The production of pumping water and electricity usage at the WTW requires large quantities of electrical energy and the energy consumption bill is around 85,000 US$ per month. Furthermore, the dam is associated with a raw water pump station to supply untreated water to the Water Treatment Works (WTW). The WTW has an average capacity of 75 Mℓ/day and a peak capacity of 93.4 Mℓ/day. The infrastructure at the Metolong Dam site includes the two portable high-lift pumps each having a power output of 750 kW with a flow of 1297 ℓ/sec (using 20 hrs/day to give 93,4 Mℓ/day), roads, storm water drainage, water and waste water reticulation, power, and an electrical Sub-station. The power supply to the dam, the dam's pumping station and the sewage treatment plant are provided by the national grid. An 11 kV power supply with a total capacity of 10 MVA is provided by Lesotho Electricity Company (LEC) [77]. These are the additional facilities at the Metolong reservoir to support the FSPV power generation facility.

Additionally, the region has interesting resource availability for FSPV. Using PVSyst database [78] for the coordinates of the site, shows high beam insolation with average levels of 6.15 kWh/m^2/day, average temperature of 15.4 °C, average and wind speed at 10 meters height of 2.8 m/s which proves to be an interesting site to place FSPV. Therefore, the site shows extreme potential for the operation of FSPV by having large water body areas, high insolation, and low wind speed.

3.2. Metolong Dam and WTW energy demand

The plant is designed to supply only the daytime (sun-shine hours) load of the Metolong Dam plus WTW facilities, the size of the plant will be determined by the load demand of the Metolong Dam and WTW. Because the FSPV system is intended to supplement the existing power supply system (LEC) at the site, it is expected to operate in synchrony with the power supply, so net metering is highly recommended. When the power demanded is expected to be greater than what the FSPV system generates (at night or on cloudy days), the LEC's smallest unit kicks in and adds to the supply. If the capacity of the system is well designed, which means greater than the energy consumption of the facilities, the excess energy can be supplied to the national grid during the daytime and reused at night. The solar plant's ultimate goal is to supply the majority of the average daytime load while also leaving an enough reserve margin to accommodate potential growth in load demand and unforeseen load variation. The schematic picture of the FSPV system designed for the two facilities is given in Figure 11.

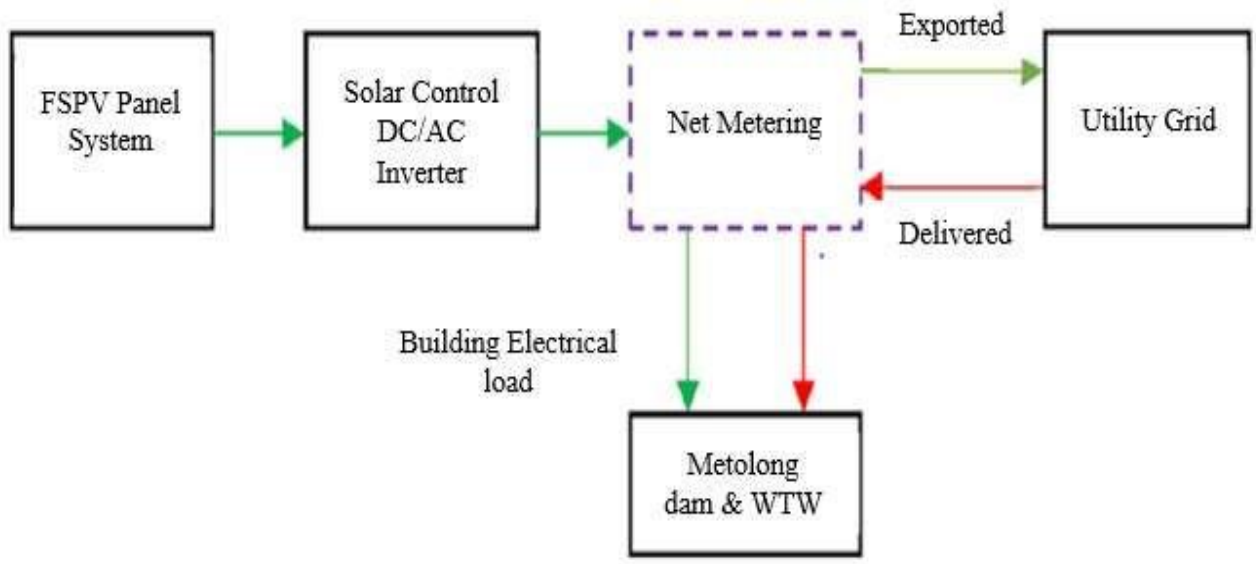

Figure 11- On grid FSPV power system for Metolong dam and Water Treatment Works.

Lesotho Electricity Company (LEC) is responsible for delivering power to the Metolong dam and WTW for water pumping and electricity consumption. The data from 2021 annual electricity consumption for water pumping and usage was obtained from LEC, shows that the annual electrical consumption in these facilities is about 15,391 MWh. The average power consumption during the day is around 1,219 kW. The diagram in Figure 12 shows the monthly profile of electricity consumption from the distribution power system measured in the most unfavourable case that took place in June 2021. The given diagram presents the results for measured apparent [kVA], and active [kW] power.

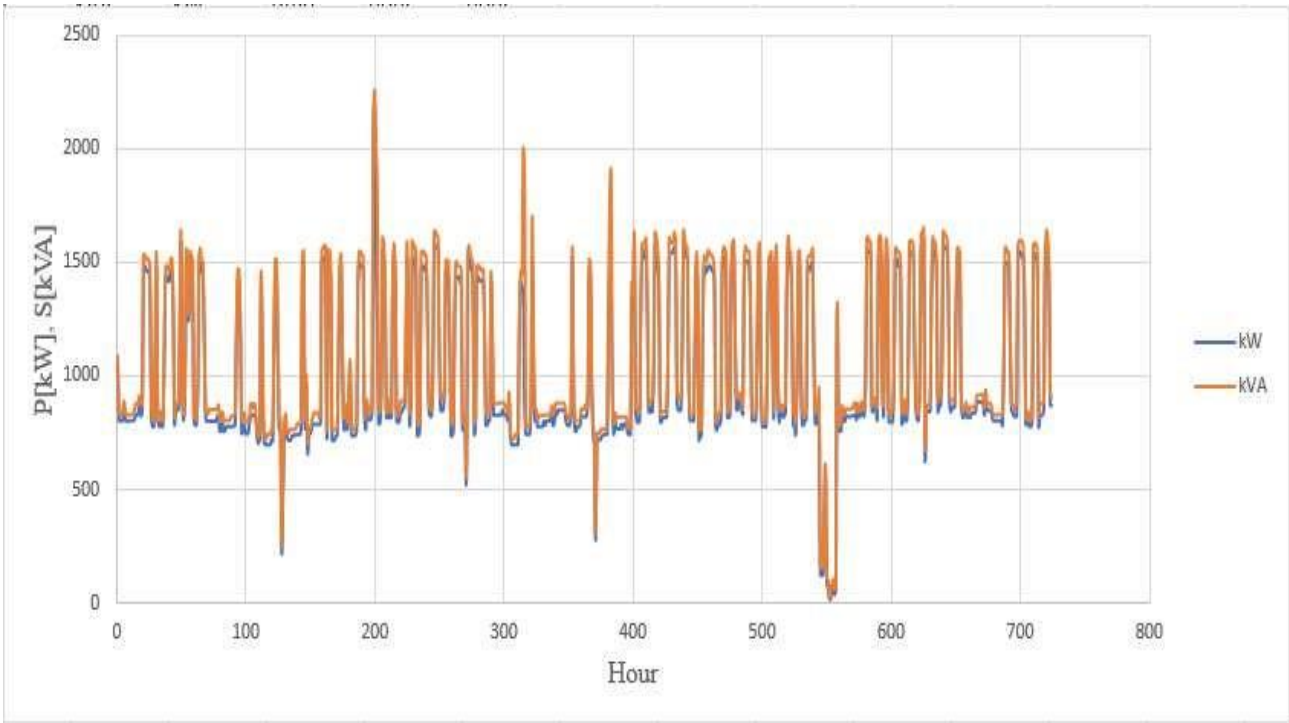

Figure 12- Electrical consumption of Metolong dam plus WTW - profile for June 2021.

3.3. Data Collection and Analysis

The available resource data employed in this thesis are for the time duration from 2012 to 2021 of hourly isolation (W/m^2), temperature profile (°C), and wind speed (m/s) which were retrieved from Photovoltaic Geographical Information System version 5 (PVGIS 5) databases in typical methodological year format (TMY) [79], by inserting the exact location of Metolong dam. TMY is a set of ground based meteorological data with values for every hour in a year of the given location. The reservoir data was collected from the Metolong Water treatment Works with information about the reservoir water level variations (see APPENDIX K) for the time duration from 2016 to 2021. Summary of values obtained for the reservoir parameters is shown in APPENDIX K. The access routes and electrical substation coordinates were extracted from Google Maps to show their locations. These data were then used to choose the possible geographical coordinates of the FSPV installation that are closest to the routes and substation infrastructure, which will further reduce cost for transmission lines and other necessary land acquisition.

The bathymetry map of Metolong dam was acquired through Lesotho Highlands Development Authority (LHDA) [53]. The bathymetry survey was done in July 2020. This information helps in determining several spots, which are at very low elevations, forming some small ponds. Then the data is used to determine the areas where stagnant water would remain during very low flows, and hence to find the best sitting for FSPV structures. Metolong bathymetry is shown in APPENDIX K. One of the mostly used applications of the FSPV on a reservoir surface is the relationship between the reservoir elevation and both its volume and surface area. These usually presented in a form of Storage-Area-Elevation (SAE) curves, table or both (see APPENDIX

K). Constructed only on the basis of the survey results. These data were used for computing storage parameters at different stage elevations of a detention facility or a naturally occurring reservoir, to mention but one use. Among the data required to conduct an evaporation calculation using the Penman–Monteith model, the wind speed (Ws), the atmospheric pressure (P), the maximum air temperature (Tw,max), minimum air temperature (Tw,min), sunshine hours and relative humidity were obtained from the Lesotho meteorology website at https://www.lesmet.org.ls.

3.4. Techno-geographical potential for FSPV on Metolong Dam

Technical potential for FSPV, as defined in this study represents the solar PV capacity installation in MW of a given PV technology. Apart from capacity, installations potential is also assessed in terms of energy generation in MWh. The assessment has been conducted for the feasibility case study as mentioned earlier, considering topographic limitations and environmental constraints. The primary benefit of assessing technical potential is in establishing benchmark estimate of solar PV capacity to be deployed. The key assumptions in estimating technical potential are physical constraints such as location, topographic constraints, and dead storage level in the driest month.

The area of the reservoir to be covered by the FSPV is the main variable in determining the overall scope of a project. In order to accurately assess the scale of the system, the reservoir area was first calculated by capturing the boundaries of the reservoirs. Metolong Reservoir boundaries was digitized from Google Earth Pro. As per the data obtained from Metolong Water Treatment Works, Metolong dam spans approximately 2,800,000 m^2 of water surface area at full storage level. However, this thesis proposes a portion of about 88,000 m^2 surface area close to the dam wall which would be utilized for FSPV which represents 3.1 % surface coverage. Hence, it was assumed that the proposed FSPV would not significantly change the ecosystem of the reservoir, especially with regard to any changes in the water temperature. Since FSPV will be a semi-permanent, moored installation, assessments are made using the lower range of surface area. Lowest surface area available for FSPV installation has been considered.

For estimating the geographical potential, the available surface area has been modelled in Helio-scope software using PV poly-crystalline technology 340 Wp modules with 17.8% efficiency. Each module represents about 2 m^2 surface area. In order to model the estimates, PV modules strings have been superimposed on Helio-scope as shown in

Figure 13. Considerations have also been made for other infrastructure development on water surface such as boat, docks and inter road distance for movement of cleaning equipment.

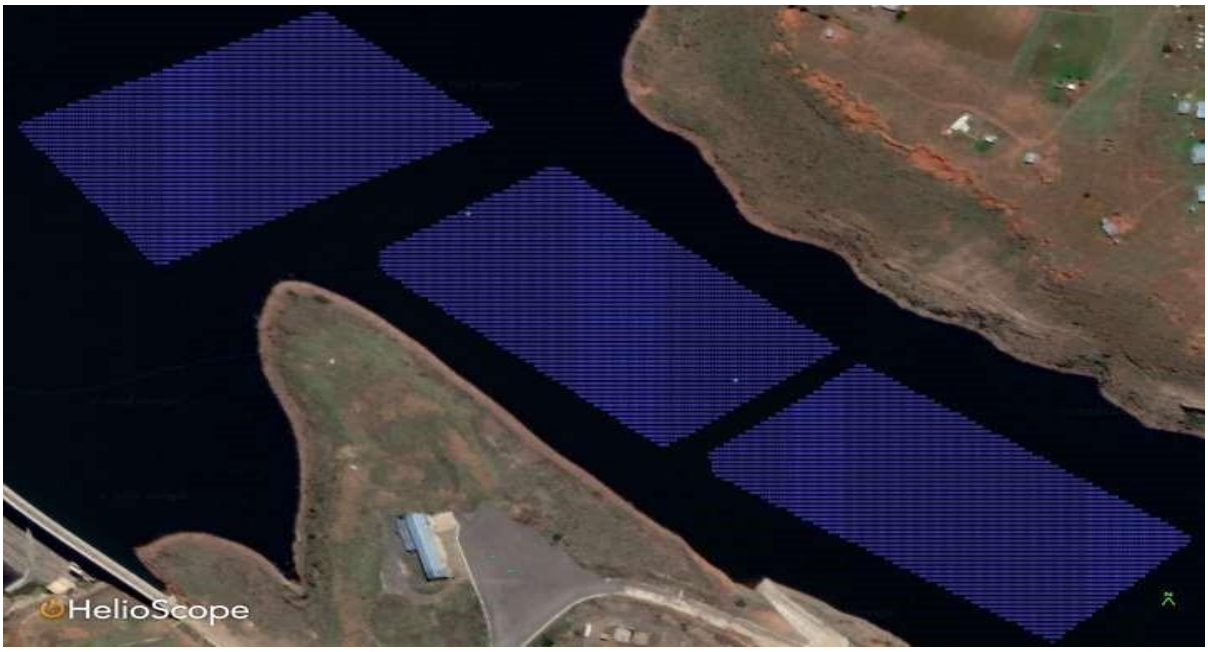

Figure 13- PV Modules superimposed on water surface (Source: Helio-scope).

Because moorings and anchoring are engineering challenges for size as well as cost impact depending on the level of complexity and requirements, this thesis proposed traditional bank installations use for mooring and anchoring. Such installations comprise a floating structure on which the PV modules are fixed, a buoy that resists the gravitational force of the structure, and a mooring system that fixes the horizontal load.

3.5. Modelling

For the FSPV design, the modelling to compute the energy yield will change slightly from the ground-mounted systems. The objective of this section is to show how it was performed through a set of linear and non-linear equations on a spreadsheet program that is, Microsoft Excel. Firstly, Metolong reservoir water temperature was modeled in a Microsoft Excel program using air temperature at the site. Then, water temperature was used to calculate the PV module temperature on water surface. Additionally, solar radiation on a tilted surface, cell temperature, the panels and inverters, DC to AC ratio and energy production were also calculated using Microsoft Excel program. Second layout was chosen to compare with the floating one. The layout to be compared was the ground-mounted PV (GMPV) system. PVSyst version 7.2 software [78] was used to simulate the GMPV system. Energy generation output was used to compare the two design under the same orientation. Table 2 summarizes the overall design parameters shared by both power plants. Other previous designs were also incorporated for the energy output comparison. The preliminary cost estimate is provided using the total coverage area. Lastly, greenhouse gas emissions was evaluated and evaporation losses are quantified using Penman-Monteith's model.

Table 2: common design parameters for FSPV and GMPV systems

Parameters	Value
Site location	29°20’4.33”S and 27°46’39.01”E
Power output	7.8 MWp
PV module	Jinko solar 340Wp
Tilt	Fixed 35°
Azimuth	North-facing (0°)
Module mismatch losses	2%
DC wiring losses	2%
Module efficiency losses	1.5%

3.5.1. Water temperature model

For the calculation of the annual water temperature at Metolong reservoir, as a function of air temperature, Equation 8 was formulated using trend-line options (polynomial order 5) on the curve, for which represents the efficiency of the curve fit and should approach unity.

□ = 0.000003283 ∗ □ + 0.000282436 ∗ □ − 0.00752866 ∗ □ + 0.066283159 ∗ □ + 1.022560256 ∗ □ − 1.037255244 [8]

where T_w and T_a are water temperature and air temperature respectively. The formulated Equation describes the relationship between the water temperature (Tw) and the air temperature (Ta) at the selected site.

The obtained average water temperature data was only for the duration time of six months JulyDecember 2020. Then the average air temperature data for the same months and year was retrieved from PVGIS Version 5. Using these data, non-linear curve was constructed using Microsoft excel program (Figure 14) showing relationship between air and water temperature at selected site. The water temperature results were then used to calculate the operating module temperature on water, then changes in the power generation efficiency. This study also comprehensively compared water temperature with modeled water temperatures with previous studies, namely, stochastic model [81], liner regression model [82] and non-linear regression model [59], based on geological survey gaging stations.

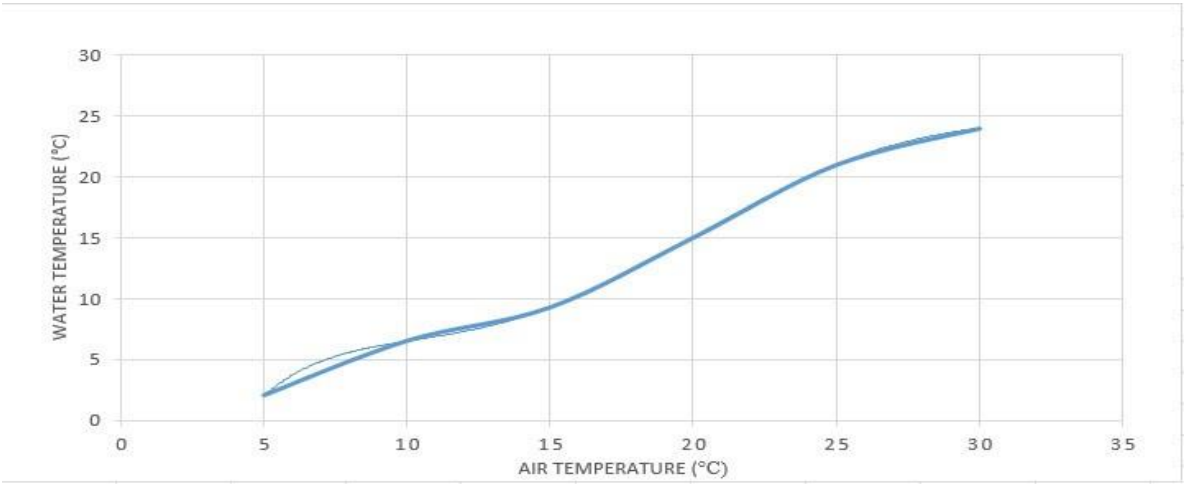

Figure 14- Relationship between air and water temperature at Metolong dam.

4.5.2. Performance analysis

For analysing the annual energy generated from the FSPV system, the estimation of irradiation levels at the location is the initial step. Irradiance can be Direct Normal Irradiance (DNI), Global Horizontal Irradiance (GHI) and Diffuse Horizontal irradiance (DHI). In order to measure the total irradiation incident on the horizontal surface, the GHI, DHI and DNI data for the Metolong reservoir location from 2012 to 2021, obtained from PVGIS 5 databases in TMY format, are used. The important parameters required in the calculation of irradiance are the solar angles and surface angles. Solar angles include the declination angle (δ), solar elevation angle (□), hour angle (ω), surface azimuth angle (□) and solar zenith angle (□), whereas surface angles include the angle of incidence(□) and tilt angle (β). The tilt angle (□) is obtained by taking the absolute value of latitude angle □, plus 5° [83]. Other geometrical inputs such as diffuse radiation on a tilted plane (□ ,), beam radiation on the tilted surface (□ ,) and reflected radiation (□ ,) were also calculated. Then solar radiation inputs are placed in equation (A.12) to determine the radiation on the tilted surface (□ ,). The equations of solar geometry calculations are explained in more details in

APPENDIX A. The variation in the solar elevation angle (□) to the azimuth angle (□) is useful to predict the length as well as the position of simple shadows like trees, hills, poles and buildings lying between the paths of the incident Sun rays and the panel in the location of the FSPV plant. The Sun-path diagram determined from these surface oriented solar angles helps in identifying the shadows in a particular location. The Sun-path chart for the Metolong reservoir in artesian coordinates with hours in Local Standard Time throughout the year is shown in APPENDIX F.

Shading loss due to trees is negligible in water-mounted PV systems. The row-to-row shading can be minimized by providing spacing between the individual PV panels and adjacent rows of panels, and by placing the panels with a minimum tilt angle. Even though the bottom edge of the second row of the PV array will be obstructed by the first row of the PV array, the reflected radiance on the shaded area will help in reducing the losses. The minimum spacing between the neighbouring arrays of PV panels was determined according to the day with the smallest

height of the Sun (see Error! Reference source not found.) and the location of the FSPV in the Metolong reservoir is selected accordingly to avoid the shadow cast by the nearby trees and mountains.

3.6. Module and Inverter selected for the proposed FSPV power plant

An adequate selection of the PV Plant components is very important in order to warranty the economic feasibility. As general items, performance, cost and warranty are the most important parameters to consider. The chosen PV module to be used in this study is made by Jinko Solar, one of the leaders in solar industry. The panel is built with 72 solar cells, has an efficiency of 17.52% and a rated power under STC of 340Wp. The power warranty is 25 years with a minimum power output of 80.7% for the selected module. The inverter selected to be used in this study is the EnSmart-L2500C-MV from the Turnkey solution. The inverter elected have a nominal AC output power of 2,750, with a high efficiency (99%), small total harmonic distortion (THD), less than 3% at nominal power and it is compatible with 5/60 Hz grid. APPENDIX B lists the product parameters of the PV module and the inverter employed for the FSPV system in this study.

3.7. FSPV power output and overall efficiency model

Power output P_{pv} is reliant on the radiation collected on the plane of the PV array, the PV module solar-electric conversion efficiency and its size and rated efficiency. The power output of the PV module or array of power rating P_{STC}, under random environmental circumstances was calculated using equation (9) [53]:

□ =___ ___* ' * □ [9]

where, P_{STC} (Watts) is the rated power of the PV Array at Standard Test Conditions (STC), η_{PV} is the operating efficiency, $G_{T,\beta}$ represents the irradiance measured on a tilted plane and G_{STC} is the reference irradiance.

Given that a typical value of the reduction of the power efficiency of the PV cells due to a temperature rise of a solar cell above a standard value (25 ºC) is 0.5%/ºC, the efficiency of a FSPV cell was calculated according to the Equation (10):

□ = □ * 1 − 0.005 * □ , − 25 * □ [10]

where: η_{stc} is an efficiency of a panel for a standard value of temperature of 25 C, F_m is the matching factor described as the ratio of the power output of the PV array under varying operating conditions to its power output at the maximum power point. A value of 0.9 is generally accepted in the PV system industry [84] and $T_{panel,FSPV}$ is the cell temperature on water bodies.

The NOCT method was used in this thesis. The manufacturer defines the temperature for the nominal exploitation conditions for each PV panel (NOCT-Operation Cell Temperature). By using this parameter, the temperature of a FSPV panel ($T_{panel, FSPV}$) was estimated on the basis of the water temperature T_{water} and solar irradiance $G_{T,\beta}$ falling onto a panel according to the following formula (11):

□ , = □ + _____ ∗ □ [11]

3.7.1. Performance ratio

When the entire simulation has been performed including the operation of the FSPV plant as well as all cost functions, techno-economic indicators can be calculated to examine the performance of the modeled system. In this subsection, the main indicators of the technoeconomic performance are presented and briefly explained.

The performance ratio (PR) is a very important factor to assess whether the FSPV system is well designed. It is defined as the ratio between the AC output power of the FSPV system and the theoretical energy that the system produces when all incident solar radiation is converted into energy, referred to the standard PV efficiency at STC. The PR includes both system losses (shading, incident angle modifier (IAM), etc.) and electrical losses (misalignment, wiring, etc.). The following equation was used to calculate such a power ratio.

□□ = _____, [12]
, η ,

3.7.2. Role of renewable energy plants

To better understand the role of renewable energy (RE) systems and their contribution to energy demand, it is necessary to understand a crucial aspect of their operation. In solar PV systems, as cell efficiency increases, the number of modules needed for a given capacity decreases. However, the capacity of the plant itself would remain the same. Of course, a system with more efficient modules would have a much smaller footprint compared to the one with less efficient. With this understanding, this thesis focuses on determining the adequate capacity of the FSPV system to meet the energy demand. The availability factor (AF) of a plant is the ratio of the number of hours for which the plant has active energy generation to the total number of hours in the time period of observation. For the present study, the availability factor was calculated using the following equations:

□□ = _____ [13]

Capacity Utilization factor (CUF) is the ratio of the total power generated by a PV system for 24 hours a day for a year, to the maximum yield that can occur simultaneously at nominal

power. Capacity factor depends on the amount of solar radiation and the number of days of sunlight available at the plant location. CUF was obtained by the following Equation:

□□□ = _____ * □□□□□□□□□□□□□ □□□□□□ [14]

3.7.3. Effects of Production of FSPV on Coverage of Consumption of Metolong dam and WTW.

The Demand Cover Factor (DCF) as a measure of efficiency of local production for coverage of consumption was used [85]. DCF is defined as the ratio to which the energy demanded by, in this case Metolong dam and WTW, is covered by the PV production, in this case the FSPV (Equation (15)):

$$\square\square\square = \frac{\int \{\ ,\ \}}{\int} \quad [15]$$

where P_S is the local power supply, in our case, this power is related on the power of the proposed FSPV and P_D is the local power demand, in our case, it is power consumption at Metolong dam and WTW. The term in $\{P_D, P_S\}$ represents the part of the power demand instantaneously covered by the local PV power supply or the part of the power supply covered by the power demand.

3.8. Sizing of FSPV array

Estimated daily power output of the FSPV plant was done for the typical day in winter month, i.e., day 168 recommended by [86], in which is the least productive in terms of average solar irradiance. Then long-term monthly power output was estimated. The sizing basically determines the necessary number of PV modules, how many of them are connected in series on each string and how many strings are connected in parallel as well as the number of arrays and inverters. Therefore, in this point the system was sized step by step following the procedure proposed by [87].

Calculate the power dimensions of the PV plant (see

APPENDIX C).

- Determine the inverter AC active power and DC input power

- Define the nominal power ratio (NPR)

Calculate the voltage dimensions (see APPENDIX D).

- Calculate voltage dimensions at module level Calculate voltage dimensions at string level.

Calculate the string dimensions and number of modules (see APPENDIX E)

- Minimum and maximum number of PV modules per string
- The number of strings per inverter
- Total numbers of PV modules

3.8.1. Simulation on PVSyst 7.2 Software

The PVSyst software is one of the most widely used software for designing and estimating the performance parameters of PV solar power plants. With the extensive options and built-in functions, this software gives almost accurate results compared to theoretical results. With this software, you can import the data of the various meteorological and personal data. Therefore for the estimation of power generation for the ground-mounted PV (GMPV) systems, the irradiation weather file data of the Metolong site was uploaded in the condition sets of the software PVSyst. Further, the software allows you to evaluate the main performance of the PV plant under the following circumstances: stand-alone, grid-tied and pumping system. In this thesis, the software (PVSyst 7.2) was used to calculate the annual energy yields of 7.8 MWp solar power system developed for the Metolong facilities. The PVSyst 7.2 dashboard is shown in Figure 15. Once the type of system has been selected the project design was done in different steps:

- Select the location of the system from the meteorological data base.
- Define the parameters of the project as the design conditions.
- In the orientation parameter, establish the type of PV field, if it is done by fixed panels, single axis solar tracking or double axis solar tracking. Then is necessary to specify the inclination of the panels and the azimuth.
- Select the system components, PV module and inverter model. In the same dashboard. It is also recommended to specify the desired power of the system and if it is going to be distributed in one or more subsets.
- It is necessary to consider losses of the different components of the system, modules, cable and transformer.
- Introduce economical parameters. Capital expenditures, operation and maintenance expenditures.

After introducing all the parameters for the system object of the study the simulation was done, obtaining the results of the simulations.

Figure 15- PVSyst 7.2 dashboard for system simulation.

3.9. Evaluation of Economic feasibility

In this section, the economic feasibility will be analysed through the scope of the Levelized Cost of Electricity (LCOE) and Net Present Value (NPV). At first, the LCOE was evaluated for the FSPV power plant. Several pieces of information will be needed to proceed with this evaluation, mainly the investment costs of the FSPV and maintenance costs that remain unclear due to the reduced number, maturity and track record of the projects. Moreover, the industry is highly concentrated on a few players, making it harder to obtain new and different standpoints. Next, the NPV of the proposed configuration will be analysed considering the different types of revenues that may exist and the variable costs. More details on LCOE and NPV analysis are shown in APPENDIX G and APPENDIX H respectively.

Table 3 shows the FSPV system design assumptions for the base case benchmark scenario. These assumptions are based on the median values provided by the FSPV developers and installers. The cost was assumed for a 7.8 MWp system. The cost includes 20% AC overloading, 25% module protection, and the test and survey cost are higher for floating solar systems due to bathymetric and hydrographic survey requirements [57].

The lifetime of the project was considered to be 25 years in which the performance degrades by 0.5% per year, starting to occur after year 2 [88]. The discount rate was considered to be 6.75%, taken from a recent survey performed by the professional services network Grant Thornton where hundreds of investors representing billions of pounds around the world answered what was the closest match for a discount rate for renewables projects such as solar, wind and hydro [89].

Table 3: Floating Solar PV cost, Simulation Inputs and Assumptions

Category	Modelled value	Description
System size	7.8 MW	Proposed average capacity of the system.
Module efficiency	17.52%	Average poly-crystalline module efficiency
Module price	$\$0.32/W_p$	Jinko-factory prices (polycrystalline module)
Inverter price	$\$0.18/W_{DC}$	Ensmart prices (inverters)
FSPV Structural components	$\$0.19/W_{DC}$	HDPE floating platform, (Recall fig. 14a) the structure most of the projects are based on, screws, rivets and elastic joints to keep the structures cohesive as well as the foundation and anchoring.
BOS	$\$0.054/W_{DC}$	Conductors, conduit and fittings, transition boxes, switchgear, panel boards, and other parts
Installation, commissioning	\$0.067/W	Modeled labor rate assumes national average non-unionized labor rates.
EPC overhead (percentage of equipment cost)	9% (over equipment)	Costs and fees associated with EPC overhead, inventory, shipping, and handling.
Sales tax	15%: National average	Sales tax on equipment
Burden rates (percentage of direct labor)	18%:national-wide average	Workers compensation, federal and state unemployment insurance, FICA, builders' risk, public liability
PII	$\$0.04/W_{DC}$	For construction permits fee, interconnection study fees for existing substation, testing, and Commissioning.
Developer overhead (DO)	$\$0.0067/W_{DC.}$ Varies by system size. (30% DO)	Includes overhead expenses such as payroll, facilities, travel, legal fees, administrative, business development, finance, and other corporate functions.
Contingency	4%	Estimated as mark-up on EPC cost; value represents actual cost overruns above estimated cost

Profits	7%	Applies a fixed percentage margin to all costs, including hardware, installation labor, EPC overhead, and developer overhead.

3.9.1. Sensitivity analysis

Sensitivity analysis by changing discount rate between 0% and 10% that results in changes in the NPV was performed to investigate the range of variability in this thesis. The prices of mooring and anchoring systems are significantly high and expected to decrease due to the increasing the use of FSPV power systems. Moreover, the solar PV modules and inverter prices have fallen since 2010 [13]. This thesis considers the investment cost decrease of 5%, 20%, 30%, 40% and 50% to investigate the changes in LCOE.

3.10. Evaluation of environmental feasibility

The environmental impact of the FSPV power plants play an important role in determining the feasibility of the projects. The environmental factors that this thesis focuses on are the greenhouse-gas emissions and the conservation of water resources. An assessment of potential greenhouse gas (GHG) emission reductions compared to the current grid mix was conducted based on the potential PV generation over the FSPV projected lifetime and the emissions that would have occurred from producing an equivalent amount of electricity from the current grid mix. The Carbon dioxide (CO_2) emissions for one year and during the service life of a PV, life cycle CO_2 emission from the PV, annual CO_2 mitigation, net CO_2 reduction for a PV system and earned carbon credits are calculated in more details using equations shown in APPENDIX I.

Another possible environmental benefit of the FSPV for the reservoir is the reduction of the evaporation of water from the reservoir. Water conservation is critical to meeting irrigation needs and daily domestic water use, and can sometimes be overlooked in environmental impact assessments. The evapotranspiration rate (ET_0) in millimetres per day (mm/day) was calculated using the variation of the Penman formula developed by [90], that requires relative humidity, mean air temperature, wind speed, and solar radiation data (see equations detailed in APPENDIX J). The total volume of water that evaporates from free surfaces and the reduction in reservoir water evaporation after the construction of the FSPV are also calculated using equations (J.7) and (J.8) respectively.

Chapter 4 Results and Discussions

This chapter presents the results for the technical, economic, and environmental feasibility of FSPV power generation at the Metolong dam in Lesotho. These are discussed in terms of the FSPV operating temperature model, the potential energy production. The energy generation section will be analyzed with the input of the design results to compare if the FSPV is more

efficiency than the GMPV power system. Latter, the economic, potential GHG emissions, and evaporation reduction results are discussed.

4.1. FSPV Operating Temperature Model

The annual temperature profile at the selected reservoir has been simulated using the proposed water temperature model compared to the ambient temperature at the chosen site as shown in Figure 16. From the figure, it can be observed that the air temperature fluctuated between -5 °C and 32 °C while water temperature fluctuated between -7 °C and 24 °C annually. Water temperatures at selected site are lower at same air temperature during the warming seasons (April to September) than they are during the cooling seasons (October to March). During cooling seasons, air temperatures are higher than the water temperatures by 3 °C to 4.5 °C. Thus, the cooling time predict a lower temperature when the panels will be in direct contact with the water surface. Equation (8) was used to correlate the water temperature and the dependent variable (air temperature) at the Metolong reservoir.

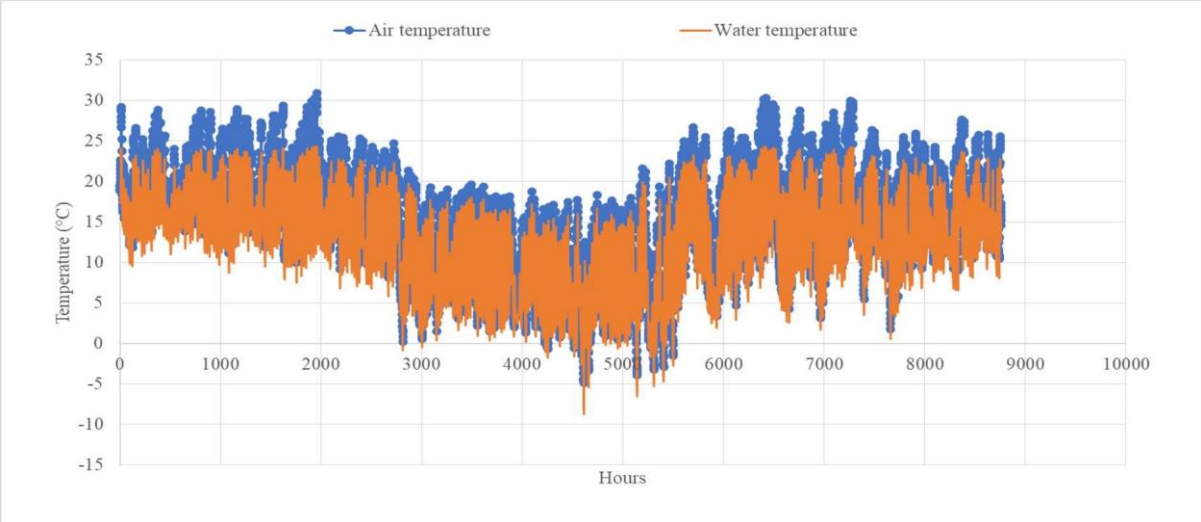

Figure 16- Annual performance of the air and water temperature

4.1.1. Comparative models for water temperature and air temperature

The performance of the proposed water temperature model is compared to other popular models that are used to predict water temperature, namely, linear regression, non-linear regression, and stochastic models. A selected group of water temperature models are presented in Table 4 for comparison. The models incorporate a reference, stating for example air temperature (Ta) as a dependent variable. Owing to the complexities involved, some authors presented explicit correlation in addition to implicit relations requiring iterations.

Table 4: Regression expressions of standard models.

Standard models	Expression	R_2	Reference

Proposed model	□ = 0.000003283 ∗ □ + 0.000282436 ∗ □ − 0.00752866 ∗ □ + 0.066283159 ∗ □ + 1.022560256 ∗ □ − 1.037255244	0.99	Present study
Linear model	□ (□) = 4.971 + 0.66 ∗ □ (□)	0.91	Senlin Zhu et al.(2018) [91]
Stochastic model	□ (□) = 7.149 + 6.661 ∗ □□□ 2□/365 (□ + 578.734) + 0.006 ∗ □ (□) + 0.011 ∗ □ (□ − 1) + 0.014 ∗ □ (□ − 2)	0.95	Senlin Zhu et al.(2018) [91]
Linear model	□ (□) = 0.204 ∗ □ (□)	0.84	Lori.A.Krider et al. (2013) [58]
Non-linear model	$□(t) = \frac{28.64}{1 + e^{0.15*(13.56-T_a\ t}}$ ())	0.94	F. Laanaya et al.(2017) [92]

From Table 4, the R-squared value obtained in this study is in agreement with previous measurements made by Zhu et al [91] which estimate the daily water temperature of the Missouri River with the aid of only the mean air temperature. They found that the stochastic model clearly outperforms the standard linear model based on the logical S-shaped function [59], and the models show high correlation coefficient values with the least value being R= 0.9508. In much the same way, Krider et al [58] use simple linear regressions to examine the weekly air-water temperature relationships for 40 groundwater-fed streams in south-eastern Minnesota [46]. Laanaya et al evaluated a statistical scheme to model average water temperature based on daily average air temperature and average discharge at the SainteMarguerite River, Northern Canada [92]. Overall, regression models for streams/lakes with high R^2 values offer promise for use as predictive tools for future climate conditions.

To support the decision making for all models, this thesis connects the dependent variable, hourly average of water temperature (Tw), to the explanatory variable, hourly average of air temperature (Ta) at the selected site (Metolong reservoir) to obtain seasonal forecasts of the Metolong reservoir temperatures profile as shown in Figure 17. It can be observed that the total annual degree hours in the three models have a similar pattern. The winter months exhibited the lowest monthly degree day accumulations of -6 °C, 2 °C and 5 °C for the proposed model, linear model and stochastic model respectively. In general, monthly degree day accumulations also increased in summer months. Thus, the summer months would predict lower temperatures when the panels are in direct contact with the water surface. In addition, monthly degree days for all models' accumulations also increased with the air temperature.

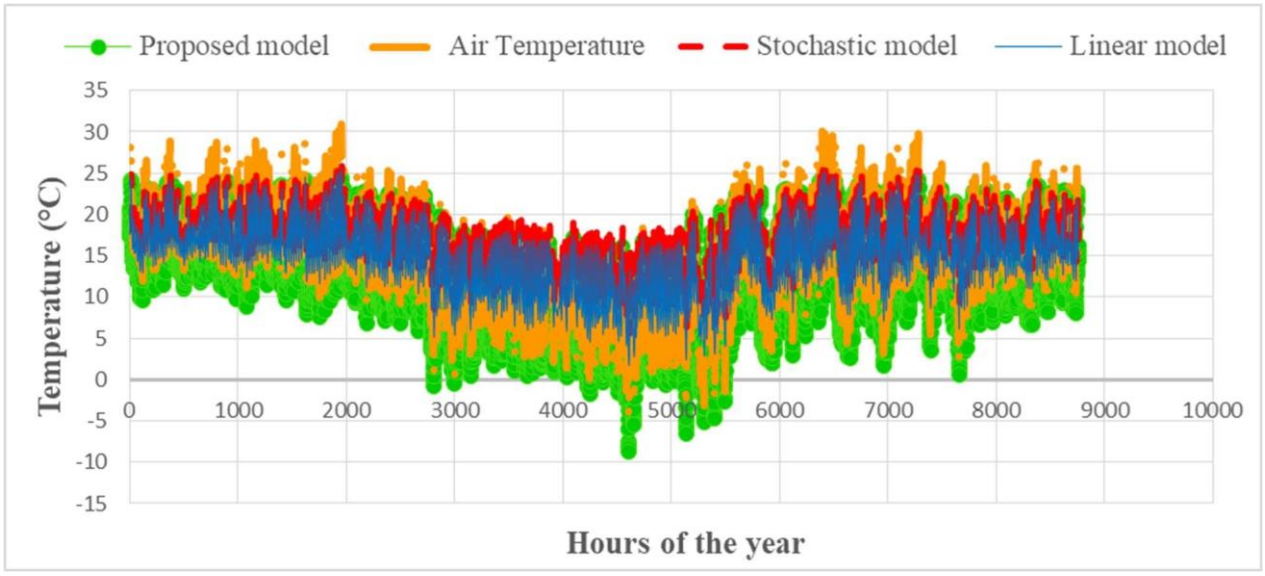

Figure 17- Water temperature comparison.

4.2. Cell temperature distribution of floating PV systems

The second interesting parameter to be assessed is the cell temperature on both the ambient temperature and modelled water temperature. Due to the presence of water below the panels, the FSPV is expected to operate under lower temperatures, which is beneficial for the energy output. Figure 18 compares the monthly average cell temperature during operational hours between the module on land and water designs in each of the months. Equation 11 was used to obtain both module temperatures. Under the solar irradiance of 800 W/m^2 and wind speed of 1 m/s, the PV module reaches the highest average temperature, i.e. 34.15 °C on the terrestrial PV system and 30.81 °C on the FSPV system for the month of January. The lowest average temperature is 16.02 °C on the terrestrial PV system and 13.6 °C on the FSPV system for the month of July. On a yearly average, the cell temperature on the water surface at a selected site is about 2.73 °C lower than the cell temperature that would be on land-based counterpart.

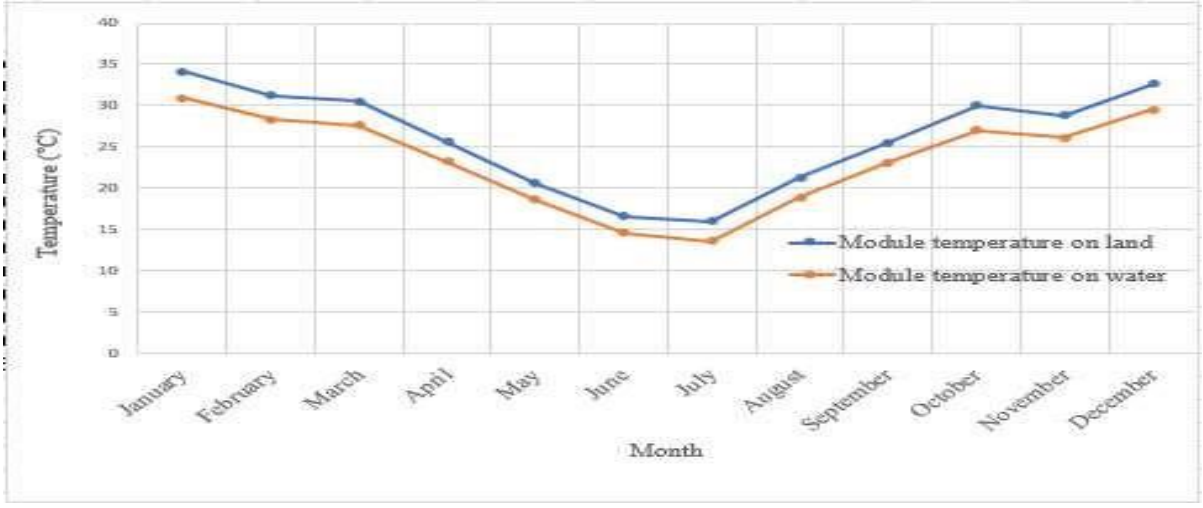

Figure 18- Hourly average cell temperature per month.

For the proposed FSPV technology that is in direct contact with water or very close to direct contact with water, the temperature of the water forms the environment on one side or both. Since water has a significantly higher thermal conductivity than air, the water temperature and water flow dominate in such architectures. Therefore, the operating temperature of the modules is likely to depend on the water temperature and water flow in addition to air temperature, wind and mounting structure.

The results on temperature distribution are in a similar pattern as the results of [29]. In his study, it was found that, the temperature of the floating panels is approximated to be 3.5 °C lower than the ground-mounted systems, which is close to the result obtained in this thesis. In addition, higher intensity of solar radiation can help to increase the generation efficiency of PV cells, and so can higher wind speeds. Although solar radiation and wind speed remained stable in the simulation, the changes in practical solar and wind conditions should be considered in practical design of floating solar PV systems in order to reach a higher generation efficiency.

4.3. Average hourly radiation available to the PV array

For each month, the average day, N, (day 168) recommended by Hove [86] is used for the simulation on Equation (A.1) using Microsoft Excel spreadsheet. Daytime hourly values of the radiation available per unit array area, G_{array}, are calculated using the location, collector orientation and radiation data as illustrated in Table 5 for the month of June at Metolong, Lesotho. In Table 5, N is the day number of the average day for the month, δ is the sun's declination on the average day of the month calculated by equation (A.1), φ is the latitude of the location (-29.34) and ω is the hour angle calculated by equation (A.2) from a knowledge of φ and δ. G (h) and G (d) are the average hourly global irradiance on the horizontal plane and diffuse irradiance on the horizontal plane respectively, obtained from PVGIS software. G (t,β) and R (b,β) are the total solar radiation over the tilted surface and beam radiation on the tilted surface calculated by equation (A.12) and (A.10) respectively. θz is the solar zenith calculated by equation (A.3) and θ(array) is the solar incidence angle calculated by using equation (A.6). β is the tilt angle which is 35° in this study.

Table 5: Determination of average hourly radiation available to the array (location: Metolong, Lesotho, latitude: -29.336, month: June.

Hours	G(h) (W/m^2)	G(d) (W/m^2)	N	φ[rad]	δ[rad] Eqn. (A.1)	ω[rad] Eqn. (A.2)	θz Eqn. (A.3)	θ (array) Eqn. (A.6)	R(b,β) Eqn. (A.10)	G(t,β) (W/m^2) Eqn. (A.12)
5-6	0.00	0.0	168	-0.512	0.408	-1.833	-0.402	-0.197	0.491	0.000
6-7	0.00	0.0	168	-0.512	0.408	-1.571	-0.194	0.039	-0.201	0.000
7-8	191	51	168	-0.512	0.408	-1.309	0.013	0.276	21.84	8.993
8-9	378	75	168	-0.512	0.408	-1.047	0.205	0.496	2.411	134.1
9-10	531	85	168	-0.512	0.408	-0.785	0.371	0.685	1.844	283.2
10-11	635	83	168	-0.512	0.408	-0.524	0.498	0.830	1.665	422.9
11-12	666	99	168	-0.512	0.408	-0.262	0.578	0.921	1.593	535.4
12-13	640	90	168	-0.512	0.408	0.000	0.606	0.952	1.572	556.1
13-14	544	91	168	-0.512	0.408	0.262	0.578	0.921	1.593	427.1
14-15	395	84	168	-0.512	0.408	0.524	0.498	0.830	1.665	250.4
15-16	214	56	168	-0.512	0.408	0.785	0.371	0.685	1.844	84.00
16-17	13.0	13	168	-0.512	0.408	1.047	0.206	0.496	2.411	56.00
17-18	0.00	0.0	168	-0.512	0.408	1.309	0.013	0.276	21.84	0.000
18-17	0.00	0.0	168	-0.512	0.408	1.571	-0.194	0.04	-0.201	0.000

4.4. System daily power output and sizing results.

An assessment of technical potential of floating PV on Metolong dam for 3.1% of the total submerged area has been conducted. Considering of infrastructure development on water surface such as boat, docks and inter road distance for movement of cleaning equipment, the total PV installed capacity on the available surface area of 88,000 m^2 is estimated as 7.8 MWp.

By using equation 9 daily power and long-term monthly power output of 7.8-MW floating solar power plant was estimated using the Microsoft Excel applications after inputting all necessary data derived from PVGIS 5 software at the chosen site. Table 6 demonstrates how the FSPV array size is determined when the solar radiation is low at Metolong dam. The simulation was done for the month of June which is the least productive in terms of average solar radiation and higher consumption over the year at Metolong facilities. The last row from Table shows the daily average sums or averages of the FSPV system performance parameters.

Table 6: Computation of FSPV power output performance.

Solar Time (hour)	Gt (Wh/m²) Eqn. (A-12)	Tw (°C) Eqn. (8)	η(pv) Eqn. (10)	Tcell (°C) Eqn. (11)	P_{PV} (MW) Eqn. (9)	Energy (MWh)
7	6.7	5.4	0.192	5.6	0.08	0.08
8	129.9	7.4	0.190	11.4	1.45	1.45
9	275.7	9.6	0.188	18.2	4.05	4.05
10	411.3	12.0	0.186	24.8	4.80	4.80
11	518.3	12.5	0.186	28.7	5.66	5.66
12	536.6	13.1	0.185	29.9	5.84	5.84
13	412.0	13.7	0.185	26.6	4.89	4.89
14	243.6	11.7	0.187	19.4	3.67	3.67
15	84.0	9.9	0.188	12.5	0.93	0.93
16	56.0	8.1	0.190	9.8	0.62	0.62
17	13.0	6.5	0.191	6.9	0.15	0.15
Sum or (averages)	244.3	10.0	0.188	17.6	2.922	29.43

Note: Gtilt (Wh/m^2) - Global incident on a collector Plane. T(water) - Water temperature. η(pv) - PV efficiency. T_{cell}- operating cell temperature. P_{PV} – PV power output.

Additionally, this thesis presents a comparison made between the production of the FSPV and consumption of the Metolong Dam plus WTW for a typical day during a year. Daily power production is illustrated in Figure 19, highlighting power generation on a typical winter day. The daily consumption of the Metolong Dam-WTW is also shown to understand the difference in performance strategies during day time. It can be observed that the simulated solar power plant averagely begins to generate power at about 6:30am with an average power generation of 0.08 MW. This increases with the intensity of the solar irradiance to a peak of 5.84 MW at 12:00 noon when it then begins to drop as the sun sets back to as low as 0.2 MW at 4pm. The proposed floating solar power plant will averagely cater for most of the average load demand at Metolong between 7am and 2:50 pm. This means that during this period, the electricity from LEC either does not need to come on or does not need to run at maximum. In total, the 7.8 MWp FSPV system produces 29,431 kWh of energy, compared to the total consumption of 42,000 kWh of the Metolong facilities.

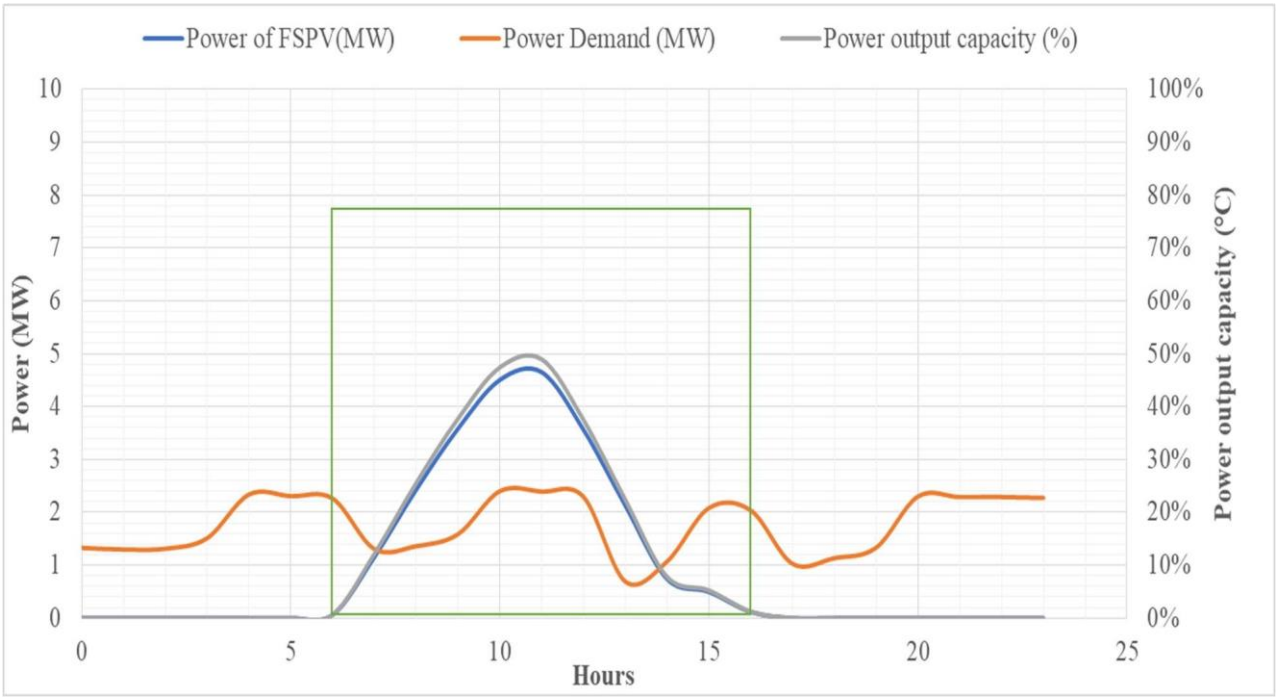

Figure 19- Average daily production of FSPV and daily consumption of Metolong dam plus WTW on a winter day.

The availability factor (AF) of a plant is the ratio of the number of hours for which the plant has active energy generation to the total number of hours in the time period of observation. Usable solar energy is typically available for 9-11 hours a day. This corresponds to an availability factor of 39.5 % (Equation 13) for typical winter months. Ideally, as shown in figure 19, the ratio of average power generated per hour per day to the plant rated capacity, would, approximately, be the ratio of the area under the generation curve to the area corresponding to the rectangular window (power ratio). The pattern of the generation curve is primarily dependent on the quantum of incident solar radiation at different time intervals. The nature and distribution of this radiation may not always be as smooth as indicated in the power output capacity curve. However, we consider a smooth profile for initial assessments. Also, the availability of energy may not always correspond to around 9-11 hours a day; it could be less than that depending on the season. Nonetheless, we consider a conservative power ratio of 0.37. Multiplying this power ratio with the availability factor would give the capacity utilization factor (CUF) (Equation 14) estimated to 14.6% (0.37*0.3958) for winter for the entire location.

Furthermore, in this thesis, the calculation of Demand Cover Factor (DCF) is obtained based on both the average daily diagram of energy consumption of Metolong facilities and average daily production of FSPV on an annual level (Figure 19). The use of Equation (15), DCF = 0.70 for the analyzed case, means that it can be expected that the proposed FSPV would covers almost 70% of daily consumption of Metolong facilities on average during a year. But because it produces more at some given time during the day than the Metolong Dam-WTW can consume, the FSPV system can export about 7,600 kWh to the grid in typical winter months; therefore, the net-metering is recommended in the absence of storage.

However, the Floating Solar power plant in this study is intended to supply power to meet the daytime load demand at the Metolong Dam and WTW. During the day, preference is given to

the generation from the solar power plant, except for times when the power generated by the solar power plant will not be enough to meet the demand at Metolong; at these times, the power from the Lesotho Electricity Company (LEC) will supply energy in synchronization with the solar power at the Metolong Dam and WTW. Based on the considered results, the daily level, it can be concluded that the production of the FSPV power plant would cover a part of consumption of Metolong facilities but without significant reversible flows of energy. An increase in the value of the DCF could be achieved by implementing battery storage which could be used to cover the night-time electricity consumption of Metolong dam and WTW.

Table 7 and Table 8 show the results obtained after simulating the polycrystalline grid connected FSPV system respectively. It is shown that by applying the PV modules and inverters proposed to be used in this thesis, for each field, it is necessary to install 415 strings by equation (E.1) with 19 modules in series (equation (E.6)). By using equation (E.9) the total number of PV modules obtained is 23,655 each with a rated power of 340 Watts and installed in at least a total area of 46,639.095 m^2 equation (E.5). The losses considered are related to the component selection as well as the auxiliary losses or consumption of the inverter. Also following the calculations provided in this study and the data from the Sun path chart, the module row spacing is 2.777 m according to equation (F.2). This space allows us to confirm that there are no losses due to a joint shadowing of PV modules in the power plant, while the total installed nominal power output is 8200 kW or 8.2 MW.

Table 7: FSPV plant power and voltage dimensions.

AC Active Power (Eq. C.1)	2,475 kW
DC Input Power of the inverter (Eq. C.2)	2,507.6 kW
Nominal Power Ratio (NPR) (Eq. C.3)	0.92
FSPV plant voltage dimensions	
Maximum Open circuit voltage (Eq. D.1)	51.623 V
Minimum MPP Voltage (Eq. D.2)	35.832 V
Maximum FSPV Module Current (Eq. D.3)	9.331 A

Table 8: Technical specification of the designed FSPV system

Module power output	340 Wp
Pnom Array	8,200 Kw
Maximum number of PV modules per String. (Eq. E.6)	19
Minimum number of PV modules per String. (Eq. E.7)	18
Maximum string voltage (Eq. E.4)	980.8 V
Minimum string Voltage (Eq. E.5)	613.8 V
Maximum number of strings per inverter (Eq. E.1)	415
Minimum number of strings per inverter (Eq. E.2)	402
Number of modules (Eq. E.9)	23,655
Number of inverters (2750 kWac)	3 units, total 8250 kWac
Module spacing	
Module height difference (Eq. F.1)	1.122 m
Module row spacing (Eq. F.2)	2.777 m
Minimum module row spacing (Eq. F.3)	1.964 m
Modules row width (Eq. F.4)	3.566 m
Area of FSPV (Eq. F.5)	46,639.095 m^2

4.5. Layout of proposed FSPV

The proposed site for the three rectangular structures of the FSPV power plant is the northernmost water body in the Metolong reservoir map. This study recommends a solution where the platform with PV panels supports a yawing system, planned to increase the insolation falling onto the FSPV power plant according to the azimuth angle of the Sun. Figure 20 presents bathymetry results, the layout configuration of the proposed FSPV on the reservoir consisting of three platforms which were constructed using the Helio-Scope software. This study used Eagle 72P 340W poly-crystalline model panels to construct the proposed FSPV power plant. In the case of the inverter proposed for the FSPV power system, it is necessary to consider the grid requirements; considering that parameter, the inverter proposed to be installed is the EnSmart-L2500C-MV from the Turnkey solution. The selected inverter has a nominal AC output power of 2,750 kW with a high efficiency (99%) and a small total harmonic distortion (THD) of less than 3% at nominal power. The proposed installed power of the PV panels on each platform is 2.6 MWp along with one string inverter which makes a total of three solar inverters, and the total installed DC power of the power plant is 7.8 MWp. The modules are tilted at an angle of 35° from the base obtained by taking the absolute value of latitude angle □, plus 5°. Furthermore, the active area, that is, the total area estimated in electricity generation by the incident solar irradiation is 46,639.095 m², and balance of unbuildable area, represents

about 41,000 m^2 which makes 88,000 m^2 including the space between the modules in the same row and the spacing between adjacent rows. The spacing also includes the gap for maintenance, cleaning purposes and combiner boxes. So, practically 1.67% (approximately) of the total submergence area has been utilized for FSPV installations. The remaining 1.46% area accounts for maintenance, row shedding considerations. An extra area was provided on the right end of the floating structure to accommodate the junction boxes and other electrical devices.

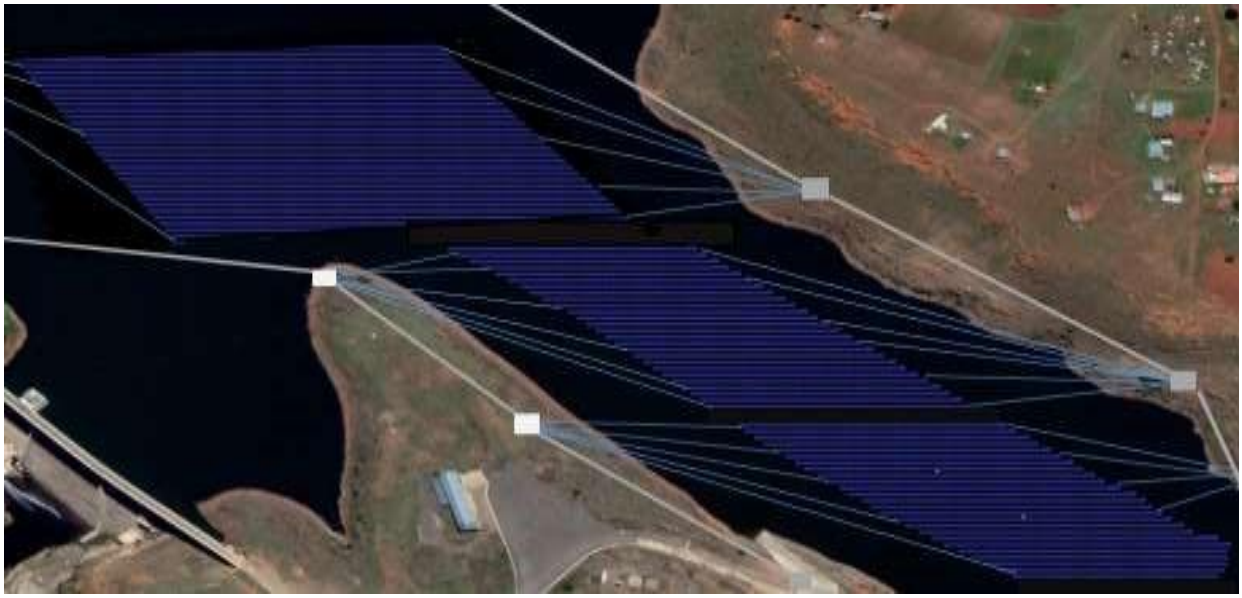

Figure 20- Layout of the proposed floating SPV power plant.

Because moorings and anchoring are engineering challenges for size as well as cost impact depending on the level of complexity and requirements, this study proposed traditional bank installations use for mooring and anchoring. Such installations comprise a floating structure on which the PV modules are fixed, a buoy that resists the gravitational force of the structure, and a mooring system that fixes the horizontal load.

Figure 21 below was modelled using the Metolong bathymetry survey, Storage-Area-Elevation (SAE) curve as mentioned in chapter 3.

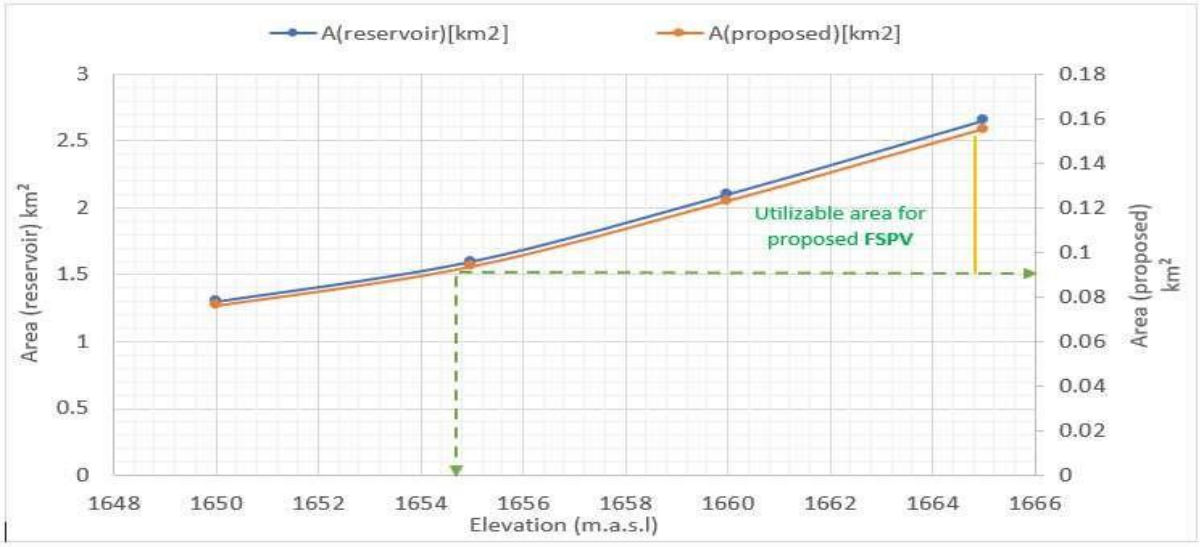

Figure 21- Relationship between the proposed area and reservoir area at Metolong.

It shows the relationship between the actual reservoir area, actual elevation and proposed reservoir area for FSPV system. Also, it can be observed that the utilizable area for the proposed power plant can be reached when the actual area ranges between 1.5 and 2.7 km^2, while the corresponding proposed area ranges between 0.085 and 0.15 km^2. If the water level reaches below 1653 m.a.s.l, it means that the calculated area of the floating structures will be greater than the proposed area of the reservoir, causing the floating structures to hit the reservoir banks, thereby damaging the structure. Hence, the maximum and minimum water levels on the reservoir have to be considered for the entire lifetime of the FSPV plant, including exceptional weather events such as floods or storms. However, it is noted that since 2017, the minimum average level of water is 1665 m.a.s.l. at the Metolong Dam as mentioned from the reservoir vs rainfall curve (see APPENDIX K).

4.6. Energy generation

4.6.1. Energy generation and solar irradiance simulation

The simulation was done using a spreadsheet application (Microsoft Excel) for equations (9), (10), (11) and (A.12). Typical monthly results are shown in

Figure 22 to understand the effect of irradiance on the energy output of the system. It can be observed that, the total energy production of the system depends upon the solar radiation intensity and its availability. As the solar radiation increases, the energy output also increases. Also, with decrease in solar radiation, the energy generation decreases. The maximum availability of the radiation on the tilted surface is recorded for October due to maximum sunshine hours, which results in the maximum monthly average daily energy of 1,652 MWh. The minimum monthly average electricity generation is recorded in June at 1,269 MWh due to the decrease of the solar radiation.

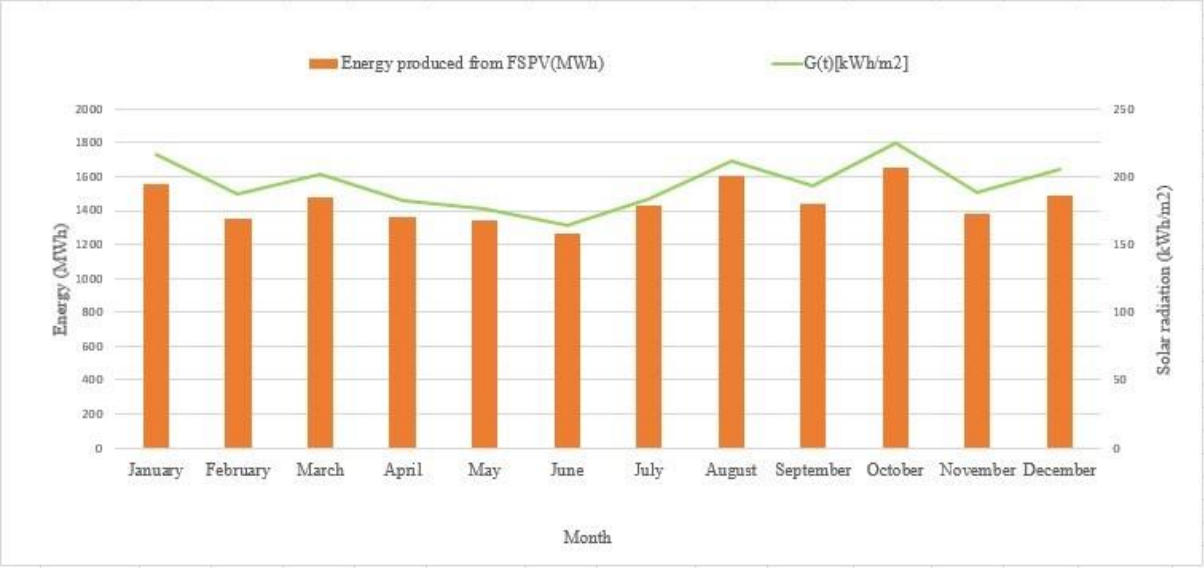

Figure 22- Average monthly energy production, Energy consumption and solar radiation.

Table 9 shows the calculated values of monthly production, monthly consumption and mean daily insolation for each month. The calculated array nominal energy at standard testing conditions (STC) is 18,212.3 MWh. The average efficiency of the PV array at STC is 20.0%. The effective energy at the output of the array (E_Array) at the maximum power point is 17,345 MWh per year. The various losses which occur in this stage are losses due to temperature, loss due light induced degradation, loss due to module array mismatch and the Ohmic writing losses. The available energy on an annual basis at the inverter output facility is 17,067 MWh, which is the energy to be used at the Metolong Dam-WTW facilities, and the surplus is injected into the grid. Here, two losses were possible; one is the inverter loss during inverter operation and the inverter loss over nominal inverter power. The energy consumption at Metolong facilities is recorded as 15,391 MWh per year which is 12.7% lower than the energy generated by FSPV power plant annually. This means that, by covering 3.1% of the 2.8 km² water storage reservoir, the floating solar would be able to provide clean energy for Metolong facilities for a whole year. Further, the study by [93], indicates that by 2025, the energy consumption under the forecast for the most likely scenario in Lesotho is approximated to be 990,352 MWh. Hence, the proposed FSPV system will covers approximately 1.75% of Lesotho's predicted 2025 energy demand under most likely scenario.

Table 9: Balance and main results of the proposed system

Month	G(h) kWh/m^2	G(tilt) kWh/m^2 (Eq. A.12)	T(water) °C (Eq.8)	$E_{DC,Array}$ MWh	E_{User} (MWh)	$E_{AC, Inverter}$ MWh	Eff. PV (Eq.10)	PR (Eq.12)
January	238.89	215.98	20.76	1552	1283	1527	19.3	0.88
February	191.66	186.73	19.52	1356	1283	1334	19.5	0.89
March	182.37	202.19	18.15	1475	1283	1451	19.6	0.88
April	142.35	182.48	14.67	1358	1283	1336	20.0	0.90
May	120.35	176.31	10.32	1341	1283	1319	20.5	0.93
June	104.71	163.85	6.871	1269	1283	1248	20.8	0.94
July	118.39	183.39	5.006	1429	1283	1406	21.0	0.95
August	154.43	211.15	9.000	1608	1283	1583	20.5	0.93
September	165.64	193.17	14.04	1440	1283	1417	20.1	0.91
October	220.17	225.3	16.46	1652	1283	1625	19.7	0.90
November	205.43	188.45	17.25	1383	1283	1361	19.8	0.90
December	235.61	205.25	19.90	1484	1283	1460	19.5	0.88
Year	2080	2334.3	14.33	17345	15391	17067	20.0	0.90

Note: G (H)-Global horizontal irradiation; G (tilt) - Global incident in a collector Plane. T (water) - Water temperature. $E_{DC, Array}$ - Effective energy at the output of the array. E_{User} - Energy supplied to the user. $E_{AC, Inverter}$ - Available Energy at Inverter Output. Eff. PV-Photovoltaic efficiency. PRPerformance Ratio.

4.6.2. PVSyst simulation results

The results obtained after simulating the 7.8-MWp connected PV system show that for each field, it is necessary to install 740 strings with 31 modules in series. For this system, 22,940 modules will be needed and are going to be installed in at least a total area of 42,860 m^2. The losses considered are related to the component selection as well as the auxiliary losses or consumption of the inverter.

Table 10 shows the parameters of the simulation and the characteristics of the fields. The total amount of energy generated from the solar PV array for the entire year is 16,757 MWh and the annual average performance ratio is 83.2 %.

Table 10: 7.8 MWp PVSyst results of the system

Month	G(h) kWh/m^2	G(tilt) kWh/m^2	T(amb)	$E_{DC,Array}$ MWh	E_{User} (MWh)	$E_{AC,\ Inverter}$ MWh	Eff. PV	PR
January	246.1	220.5	21.29	1421	1307	1395	16.97	0.81
February	204.0	200.9	20.57	1295	1181	1270	16.97	0.81
March	195.5	218.0	18.85	1411	1307	1384	17.04	0.81
April	157.6	201.8	14.91	1341	1265	1317	17.49	0.84
May	135.8	202.6	11.26	1379	1307	1355	17.92	0.86
June	117.1	185.5	7.67	1284	1265	1261	18.21	0.87
July	128.0	196.0	7.42	1355	1307	1331	18.20	0.87
August	155.2	213.9	10.87	1449	1307	1424	17.84	0.85
September	182.7	216.2	14.71	1429	1265	1403	17.40	0.83
October	227.4	234.8	18.00	1521	1307	1493	17.05	0.82
November	241.6	223.4	18.97	1441	1265	1414	16.98	0.81
December	252.8	222.2	20.76	1432	1307	1405	16.96	0.81
Year	2243.8	2537.7	15.41	16757	15391	16450	17.40	0.83

4.6.3. Performance comparison

The energy generated annually by the FSPV power system is compared with that of the GMPV generation systems. Following the comparison,

Figure 23 shows the compared production capacity in FSPV and GMPV systems. The results of FSPV were calculated using Equation (9). It was found that the annual energy generation by the FSPV power system is about 3.4% higher than that of the GMPV power system with the same power. This is thanks to the water-cooling effect on the PV module performance and reduction in the temperature of the PV module. In addition, the temperature impact can be observed through the distribution of the insolation of the GMPV plant and the FSPV plant. Indeed, it was found that the insolation on the tilted surface for the GMPV plant in comparison

with the FSPV is 7.9% higher. This can be explained by the fact that the air temperature above the reservoir surface is visibly lower than the land surface temperature; therefore, there is a drop in the PV panel efficiency due to the higher temperatures for the PV power plant installed on land than in case of the FSPV.

Meanwhile, FSPV yield higher energy compared to ground-mounted solar plants as mentioned in chapter 2 by [28], [31] and [30] showing 4.1%, 6% and 10% better efficiency on average respectively. The energy generation increased by 3.4% for the FSPV system in this study, which is far from the results obtained by other previous studies. However, most of the energy measurements presented in the literature are performed under the microscale and experimental conditions, ranging from cells to modules and at different geographies. However, the result of this study confirms that water has a cooling effect on the panels and one could expect an increase in efficiency when installing floating PV in similar regions in Lesotho.

Based on the cooling effects obtained in the simulation, the study further calculated the efficiency under the cooling effects. Figure 24 shows a monthly comparison of the panel's efficiency in two modes. These results of FSPV efficiency were calculated using Equation (4). It is found that the cell efficiency is 17.4% for GMPV cells and 20.0% for FSPV cells, respectively. With the electricity temperature coefficient of 0.45 %/°C and the operating temperature difference of 2.73 °C, the annual average increment in panel efficiency for the FSPV system was found to be 2.6% compared with the GMPV system. In addition to ambient temperature, radiation intensity and wind speed will also influence on the efficiency of PV systems. Taking all of the factors into account, the electricity generation efficiency of FSPV systems would be 2.6 -3% higher than GMPV systems under similar ambient conditions.

The outcomes of the present assessment are also compared with other solar PV systems across the globe based on the available literature and summarised in

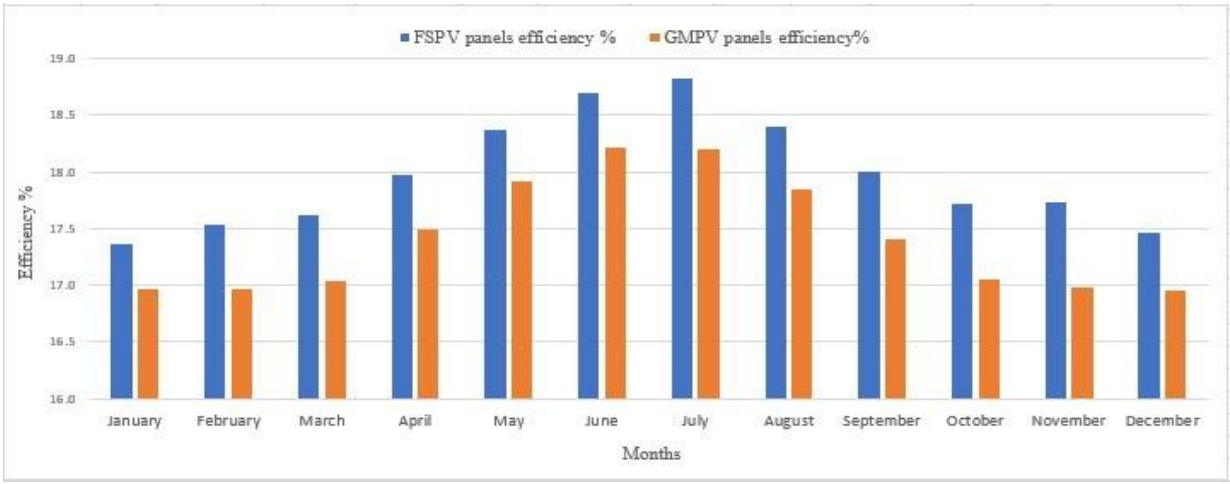

Figure 24- Monthly comparison of panel's efficiency.

Table 11 . It can be observed that, the energy production of the FSPV generation system is significantly higher than that of the PV energy production evaluated by other studies over the

entire year. Despite the increased energy yield due to the cooling effect of the FSPV systems and the lower operating and maintenance assumptions, their cost are still higher compared with the cost of ground-mounted systems as mentioned in chapter 2.

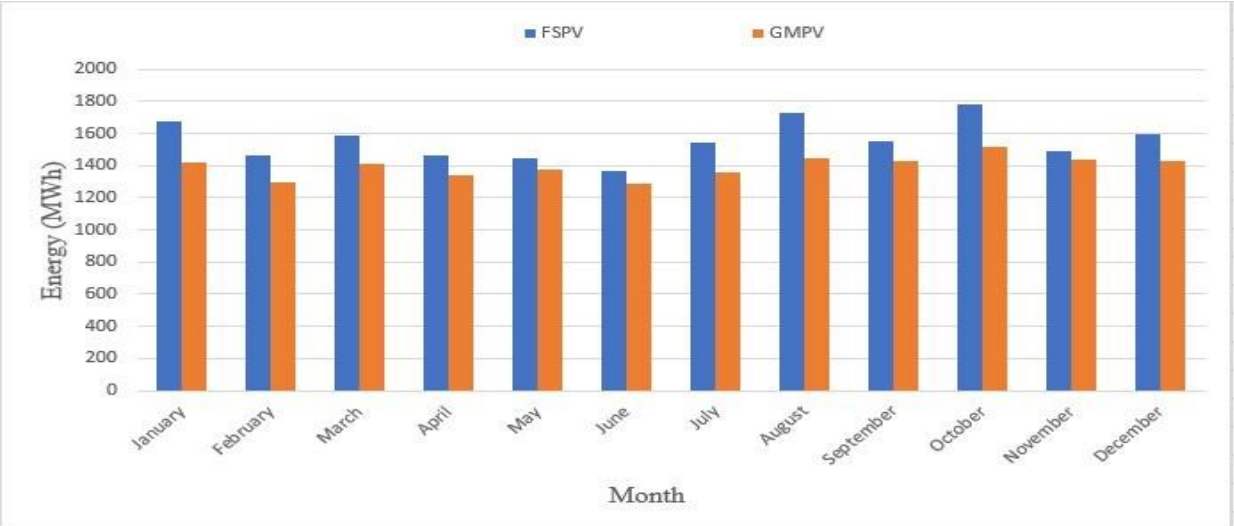

Figure 23- Monthly comparison of array energy for 7.8-MWp solar plants.

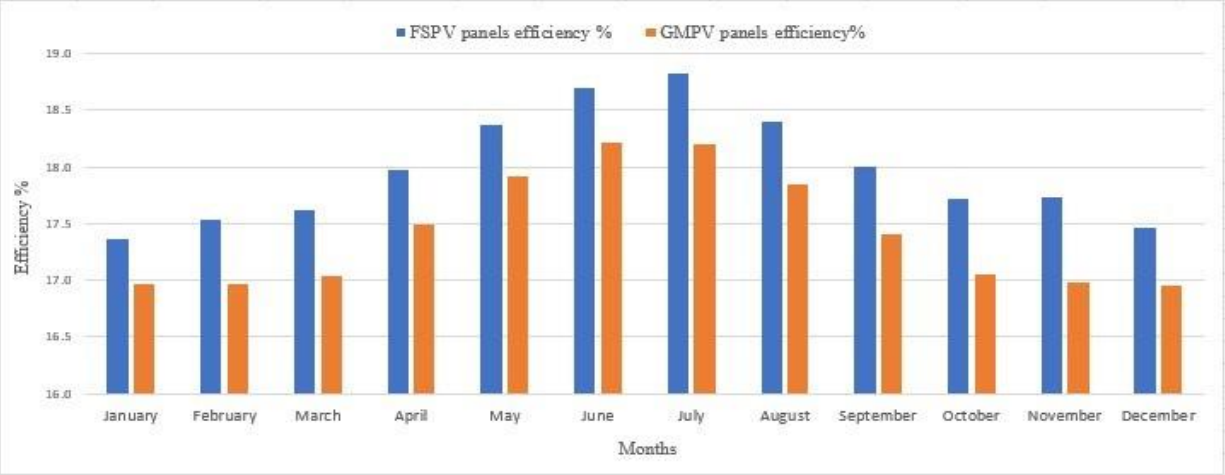

Figure 24- Monthly comparison of panel's efficiency.

Table 11 Performance comparison of the FSPV system with other systems

Site	Year	System size	$E_{DC,Array}$ (MWh)	Mod. Eff. (%)	CUF (%)	PR (%)	LCOE (US$/MWh)	Reference

Metolong (proposed FSPV)	2022	7.8-MW	17,345	17.5	15.21	0.9	34.2	Present study
Metolong (proposed GMPV)	2022	7.8-MW	16,757	16.0	-	0.83	-	Present study
Peddapalli	2015	10-MW	15,798	13.3	17.68	0.9	-	Kumar and Sudhakar, 2015 [94]
Kolar	2013	3-MW	4,204	13.25	15.69	0.7	-	Padmavathi & Daniel, 2013 [74]

Note: $E_{DC,\ Array}$ - Effective energy at the array output in MWh; Mod. Eff. - module efficiency in %; LCOE - Levelised Cost of Energy (US$/MWh).

4.7. Economic calculations

Economics are a major factor in the realisation of a commercial project and unless a positive return on investment is guaranteed, the project stands little chance of being undertaken. As per the literature review, the cost of the floating systems is greater than the conventional ground mounted systems as mentioned in chapter 2. However, the cost of buying and levelling large hectares of land is avoided in this water infrastructure system when compared to conventional PV systems. The FSPV system cost model assumes a contingency rate of 4% due to its relative newness and an extra shipping and handling cost of 9% for the floats and anchoring system. 7% of the profits were added, which applies a fixed percentage margin to all costs including hardware, installation labor, engineering, procurement and construction (EPC) overhead, and developer overhead. The cost breakdown of the FSPV system components is shown in

Figure 25. From the figure, it is clearly that the high cost associated with the construction and installation of the floating structures, followed by the PV modules which are approximated to 30% and 26% of the total cost of the proposed FSPV system respectively.

Table 12 summarizes the calculated input parameters based on Table 3 in the previous chapter to carry out the estimation of the production costs of the FSPV. The total cost of the floating platform was found out to be 3,034,000 USD, including mooring and anchoring mechanism, which shares the largest portion of the FSPV system cost. The cost of PV panels and other electrical components to be used in the installation of the FSPV system is 5,092,200 USD. By adding other cost (i.e. EPC overhead, Sales tax and others) which is about 1,911,376 USD, the total cost of the FSPV system without tracking system in the Metolong reservoir of 7.8-MW

capacity is around 10.0 Million USD. No bank loan has been considered for constructing the proposed FSPV power system.

Further, during the initial stages of this thesis, techno-economic models were carried out to determine whether the floating PV arrays would be economically feasible alternative renewable solutions when augmenting the electricity supply at the Metolong Dam and WTW site and with grid integration. The LCOE is one of the parameters that is widely used to compare different energy sources costs and it is normally a measure that tells if a renewable technology has become cost-competitive against the traditional energy generation. Meanwhile, the NPV can show which project should be chosen given different investment alternatives. A known trend is that renewables have drawn nearer to fossil fuel technologies in terms of economic feasibility. Several factors may explain this: reduction in costs coming from technological improvements and competitive procurement, meaning that new types of market strategies and financing have enabled the deployment of more projects.

Table 13 summarizes the economic results obtained after simulating the FSPV systems. The Levelized Cost of Energy (LCOE) represents the average revenue per unit of electricity produced that would be required to recover the costs associated to the construction and operation of a generation plant. A high LCOE is associated with a high cost production and consequently, less returns. Using equation (G.1), the LCOE was found to be 36.4 US$/MWh. The LCOE result obtained is in accordance with the 10 MWp FSPV system benchmark performed in United States (U.S) which represents the expected typical size of FSPV systems to be installed over the next couple of years. The project LCOE was 37.8 US$/MWh, while the total estimated initial investment cost of the project was $12.9 Million [42]. Since the proposed project is 7.8 MWp with the LCOE of US$36.4/MWh and initial investment cost of $10.0 Million, the value sits closely to this benchmark which reinforces the realistic results of the model.

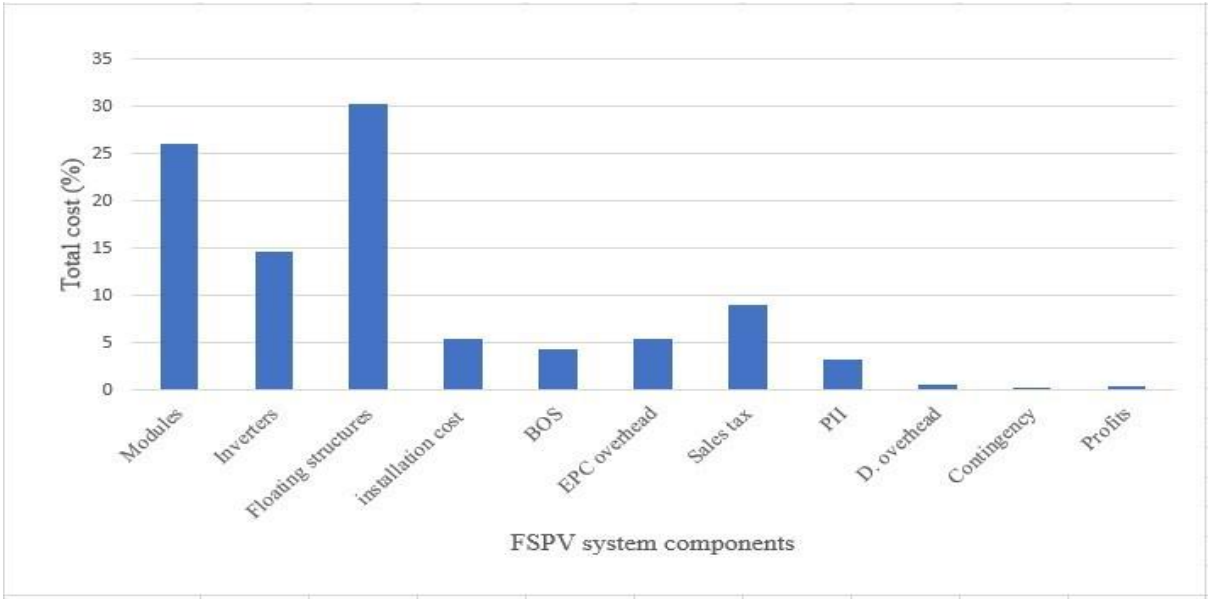

Figure 25- Cost breakdown of FSPV-system components in Metolong reservoir

Table 12 Estimated input parameters.

	Value	Unit
Modules	2,624,000	USD
Inverters	1,476,000	USD
Floating structures	3,034,000	USD
installation cost	549,400	USD
BOS	442,800	USD
EPC overhead	549,072	USD
Sales tax	915,120	USD
PII	328,000	USD
D. overhead	54,940	USD
Contingency	21,963	USD
Profits	42,281	USD
Total cost (CAPEX)	10,037,576	USD
O&M	237,800	USD/year
Operating cost (OPEX)	237,800	USD/year

From an economic point of view, the total investment of the plant (CAPEX) is 10,037,576 US$, with the chosen panels, inverters, floating structures and anchoring design. The total operating cost per year (OPEX) is 237,800 US$, considering the maintenance and equipment replacement over the years.

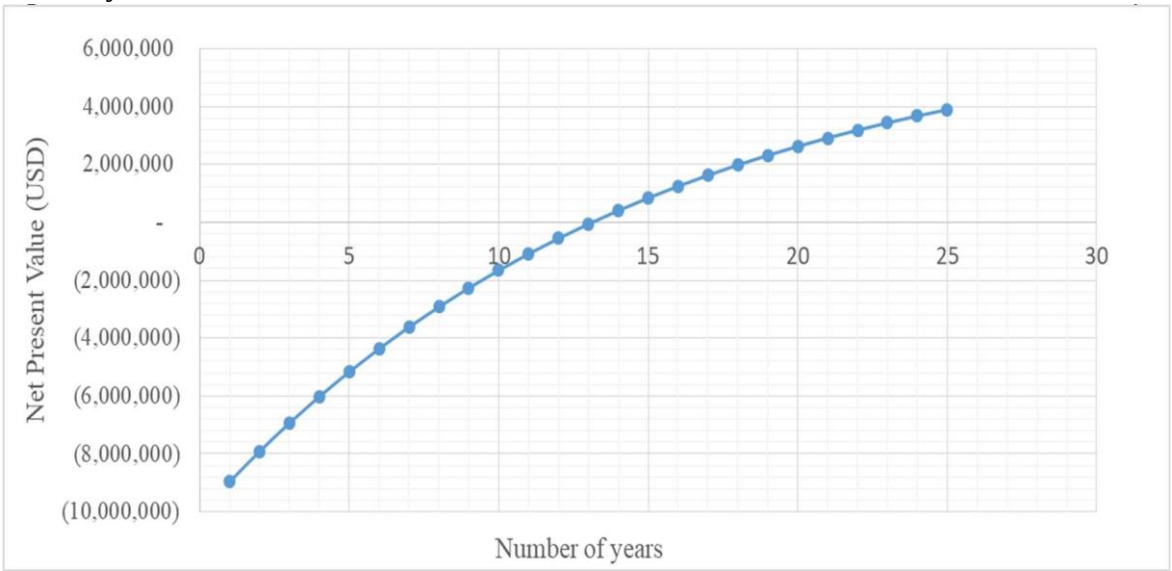

Figure 26 shows the simulated NPV for each year over the 25 years lifespan. Considering the cash flows generated during the operating lifespan, the payback period was calculated to be about 13 years. The NPV calculated over 25 years stood at 3,946,724 USD, which suggests that the combined present value of all cash inflows exceeds the present value of cash outflows by 3,946,724 USD. Hence, the project is an acceptable one since it adds 3,946,724 USD to the value of the project.

Table 13: Economic results.

	Value	Unit
Net Present Cost (NPC)	3,496,724	USD
LCOE	0.0364	US$/kWh
FSPV Pay Back	13	Years
Internal Rate of Return IRR	10.5	%

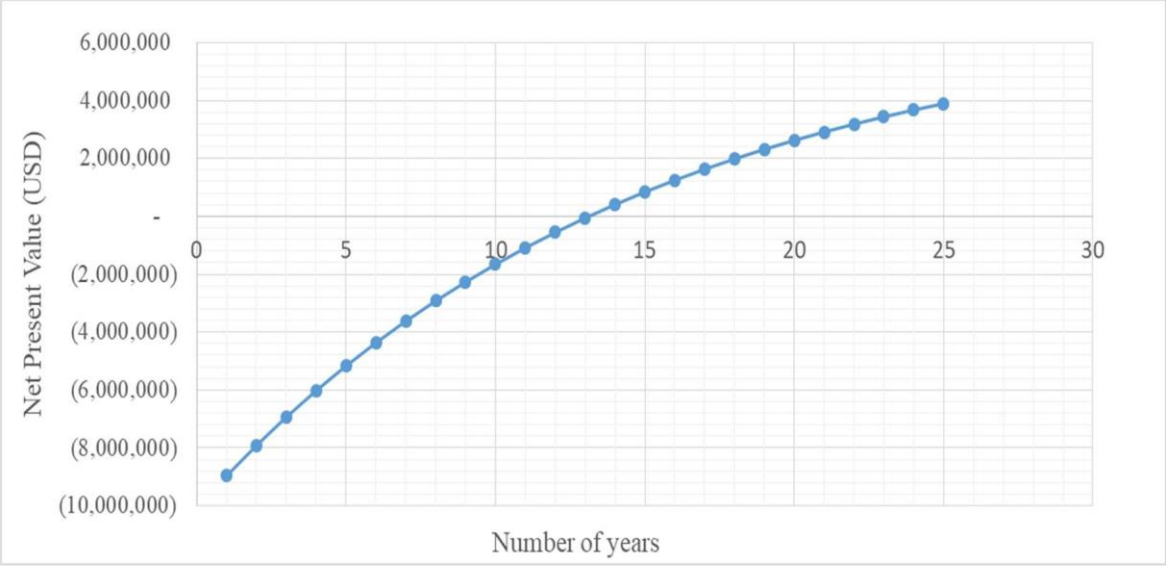

Figure 26- Net present values of the floating photovoltaic system.

Contribution to the Metolong Dam-WTW facilities and Lesotho's energy supply. Metolong dam and WTW typically face demand charges (M/kVA) based on their peak demand during each billing period [96]. Because peak demand is based on how and when a customer uses electricity, even customers that consume similar amounts of electricity and are billed under the same utility rate may incur vastly different demand charge expenses, depending on their peak demand. Hence, the demand charges assumed to be 2,671.7 kVA occurring each month throughout the year. The basic energy charge plus demand charge is estimated to be 850,405.74 US$ per year at Metolong Dam plus WTW. Based on the total energy consumption at these facilities, the cost of energy from current conventional energy charge is estimated to be 0.0553 US$/kWh (55.3 $/MWh). The estimated FSPV LCOE of 36.4 $/MWh is less than the current

energy cost at these facilities. Based on that, the FSPV system will save about 289,776.46 US$ (5.2 Million Maloti) in the first commencement year in a comparison to using conventional gird electricity which confirms that the FSPV system is beneficial and suitable for the electrification of Metolong Dam for water pumping and WTW electricity usage. Hence, to reduce the cost of energy, it is important to introduce and operate energy systems that can offer supply electricity during all periods and especially during peak periods where LEC which charge a premium price for electricity.

Furthermore, the study assume that the construction of the proposed FSPV would be of a great importance on the state level in view of the fact that the Metolong facilities are one of the biggest consumer of electricity in Lesotho and are located on a terrain that has very good technical preconditions for the construction of the proposed power plant. Its construction would to a large extent resolve the electricity deficit problem, reduce losses in the transmission grid, while reducing importation of energy from primarily fossil-based generation systems by Eskom [97]. The study deem that these are sufficient motives for the government to analyze the extension of subsidies for such a plant. Also, one of the basic objectives of subsidies based on the feed in tariff principle is to provide a contribution to the development of new technologies, which would be achieved with the construction of the proposed power plant. This is a significant addition to the overall energy sector and it will substantially reduce the cost of energy as the FSPV plant cost is expected to be considerably reduced based on the low LCOE of 36.4 $/MWh.

4.8. Sensitivity analysis

4.8.1. Change in discount rate

In this section, various sensitivity analyses have been performed on the FSPV system. The variated parameters of this study are: LCOE, NPC, discount rate and change in investment cost.

The NPC is very sensitive to the discount rate. Different discount rates may apply to different technologies as they may be subject to different risk profiles. Some argue that a risk-free discount rate is the best way to compare technologies. Therefore, a developer must make realistic assumptions, sometimes limited by the cost of financing. In this sensitivity analysis, discount rates were introduced between 0% and 10% to analyse how the NPV of the FSPV changes as shown in Figure 27. It was found that, NPC decreases with the increasing interest rate.

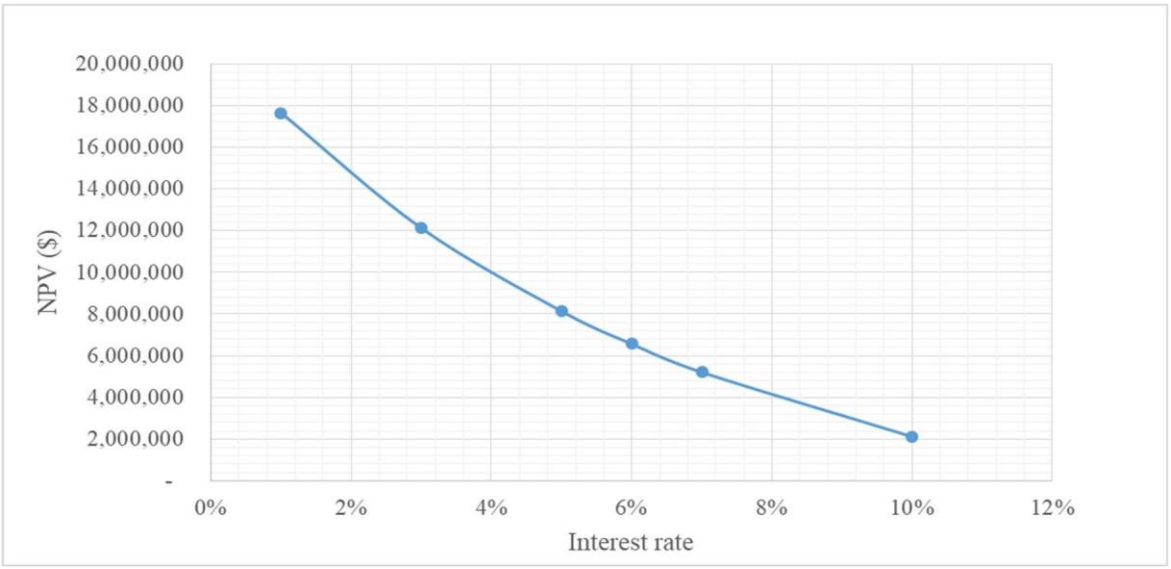

Figure 27- Change in discount rate.

4.8.2. Change in Investment cost

The costs of components such as modules, inverters, anchoring and mooring structures take up a large part of the investment costs. As reported by IRENA (2018), the solar PV module and inverter prices have fallen dramatically since 2010 [13]. On the other hand, the prices of mooring and anchoring systems are significantly high and expected to decrease, when increasing the use of FSPV. This study considers a price decrease of 5 %, 20 %, 30%, 40% and 50%. The LCOE decrease with the decreasing cost and varies between 36.4 and 25.3 $/MWh at 5% to 50% of the cost reduction respectively as shown in Figure 28.

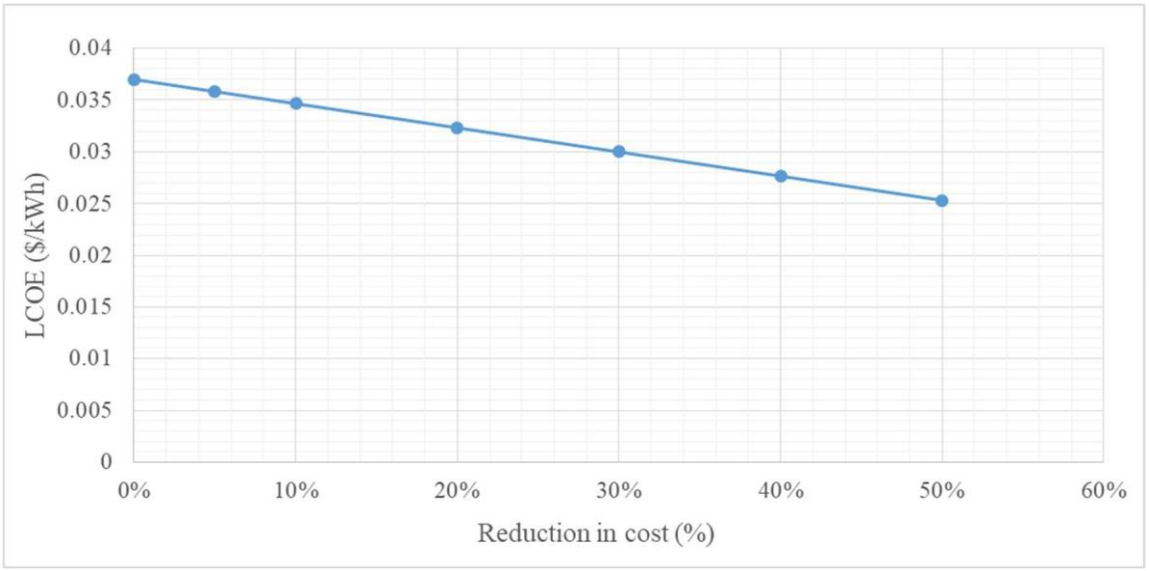

Figure 28- Change in Investment cost.

4.9. Environmental benefits

4.9.1. Avoided emissions

For the environmental assessment, several assumptions are made to calculate GHG emissions. First, the avoided GHG emission was based on the mixed emission of the national grid. No data is currently available at the regional emission level to compare with the national emission. The environmental impacts of renewable energy infrastructure are being studied more intensively in order to quantify the holistic benefits of such systems. One of the clearest advantages of the solar PV system is the avoided emission compared to the emission of fossil fuel power plants.

In addition, a solar PV system emits greenhouse gases due to its embodied energy. Since the life cycle of CO_2 emissions for the polycrystalline silicon module is assumed to be 0.053 kgCO2-eq. /kWh, the net CO_2 emission of the PV system over its lifetime of 25 years is found to be 24,621 tCO_2eq using Equation (I.2). The annual CO_2 reduction by the system is 17,329 tCO_2eq using Equation (I.3) and the net CO_2 mitigation for the entire lifespan is 406,013 tCO_2eq by Equation (I.4). The annual saving that can be earned from carbon credit is 311,062 US$ as per the actual annual electricity generation data using Equation (I.5). To put this numbers into perspective, according to the African Development Bank (AFDB) [98], the share of emission from the energy sector in Lesotho has grown steadily, reaching about 30% of national emissions, and producing an annual total of 1,079 Gg CO_2eq (1,079,000 tCO_2eq). One of the dominant source is the importation of energy from predominantly fossil-based generation systems by Eskom. The implementation of the proposed FSPV system will reduce coaldominated electricity imports from South Africa and reduce emissions by over 1.6% annually Therefore, FSPV can add low-emissions and renewable generation system to domestic electricity sources.

4.9.2. Calculation of the reduction of water evaporation from Metolong reservoir after the building of the FSPV.

The co-benefit scenario will attempt to combine the proven benefits of using solar energy with the benefits that covering a water reservoir with PV modules could have. In this case, it will account for the gains in evaporation. The 2020 data from the Lesotho meteorological services website were used for the calculation of the water evaporation from the Metolong reservoir. Table 14 presents the input data in the first five rows. The water evaporation from the Metolong reservoir is calculated for an average day in each month, namely, the average daily decrease of the altitude level of water due to water evaporation. Figure 29 presents the calculated water evaporation values from the Metolong reservoir.

Table 14: Input meteorological parameters and calculated water evaporation from Metolong reservoir for an average day in each month.

Month	Jan	Feb	Mar	Apr	May	Jun	Jul	Aug	Sep	Oct	Nov	Dec
Tmax (°C)	27.1	26.2	25.2	21.1	16.1	9.6	10.4	12.1	18.7	21.9	21.0	22.6

Tmin (ºC)	19.1	17.1	15.1	12.1	3.0	2.0	2.0	4.0	12.1	14.1	14.1	18.1
RH (%)	52	59	58	58	56	55	51	41	35	40	45	51
Sun-hours	11.6	11.5	9.5	7.5	7.6	7.5	7.6	7.4	9.3	11.8	11.7	11.5
v (m/s)	4.50	4.20	4.22	4.24	4.50	4.9	5.00	5.30	5.50	5.10	4.80	4.50
E(mm/day)	7.27	6.40	5.44	4.09	3.30	2.3	2.63	3.55	5.51	6.59	6.51	6.62

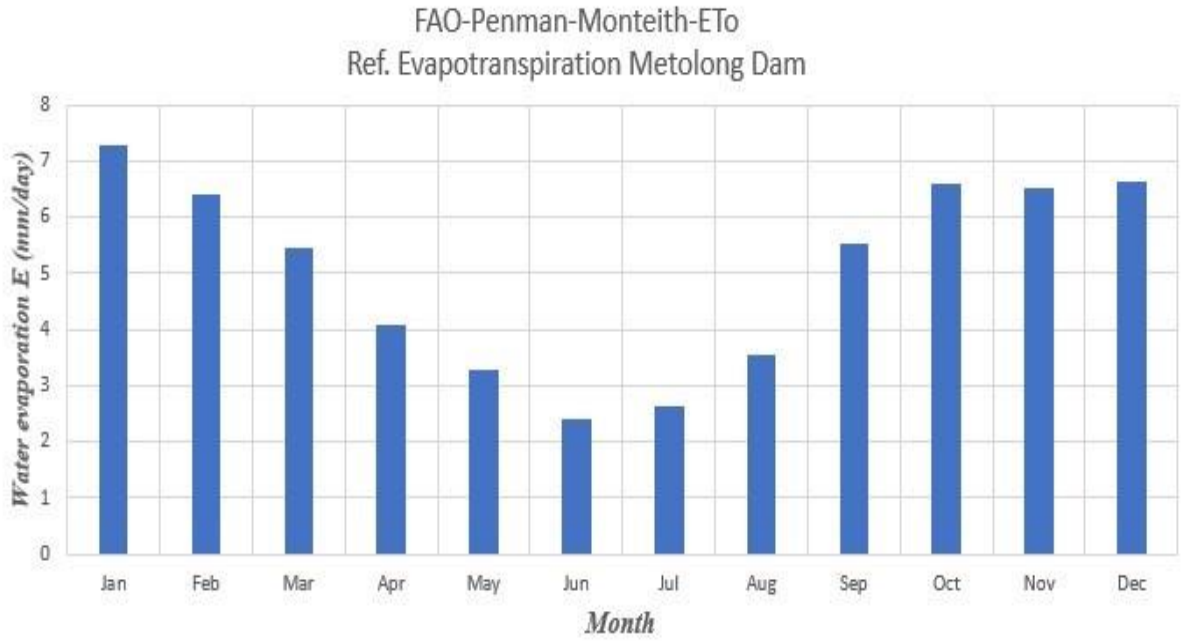

Figure 29- Reduction of the depth of Metolong reservoir due to water evaporation for an average day in each month.

The proposed floating power plant will only cover 3.1% of the reservoir's surface area. The modelling results show that for the region chosen, the most intensive evaporation occurs in January. The estimated value of the decrease of water level in this month is about 7.27 mm daily. The smallest intensity of water evaporation is in June and it is about 2.39 mm daily. The total water evaporation from the Metolong reservoir in an average year is about 5.2 Million m^3 (Equation J.7) at the rate of 184 cm. These results agree with previous studies showing an estimated rate of 180 to 200 cm/year of evapotranspiration for Lesotho, as it was observed in figure 8 in chapter 2 [68].

With regard to the calculated water evaporation values from the free surface of the Metolong reservoir and the area employed by the FSPV, according to Equation (J.8), the drops of water

evaporation for each month were obtained. The data are graphically presented in Figure 30. The total annual reduction of water evaporation after the construction the FSPV on the Metolong reservoir was found to be 84,136.12 m^3 obtained by the summation of monthly water evaporations. This outcome within range with results obtained by [37] showing that, covering roughly 69,000 m^2 or 0.069 km^2 could save up to 124,000 m^3/year.

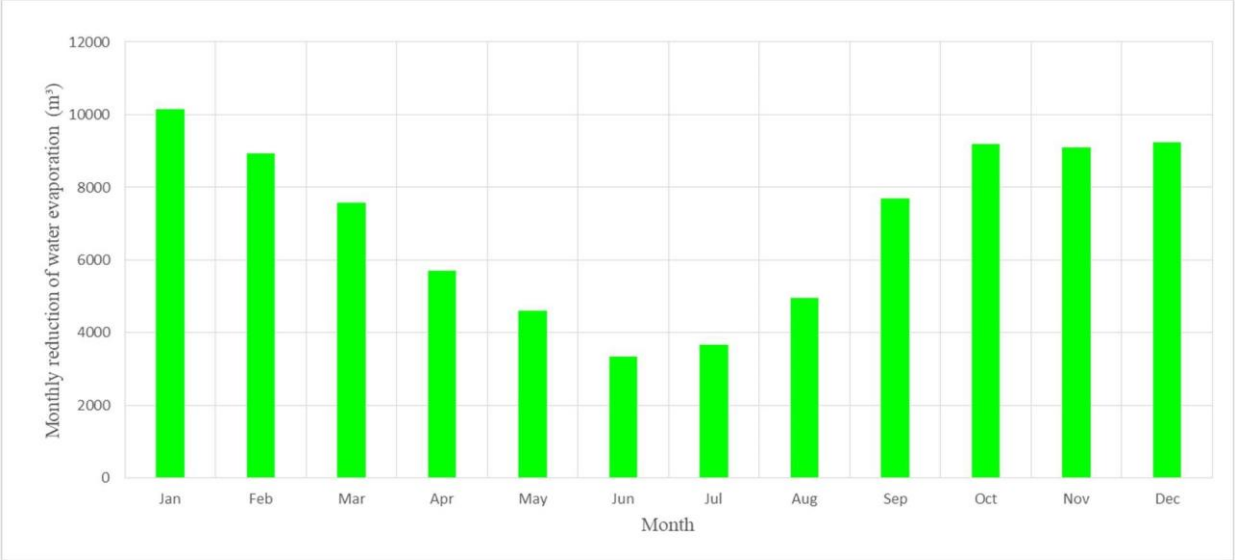

Figure 30- Monthly reduction of water evaporation at Metolong reservoir after building the FSPV.

Chapter 5 Conclusion and Recommendations

Solar power came after years of development and cost reduction that made it competitive in today's market. In addition, being a free resource, the production of electricity with solar does not pollute and is part of the sustainable development proposed by various summits and international agreements. In this thesis, the technical-economic-environmental analysis of FSPV was carried out for the Metolong dam and WTW field in Lesotho.

In chapter one, it provided an overview of the components and benefits of FSPV technology. The nascent of FSPV industry is one which is growing rapidly, and the technology is becoming a promising source of renewable energy. It is also established that the FSPV system will be used to cover the surface of water bodies in the near future. The cooling effect of water will improve the energy efficiency of the technology. The added advantage apart from higher energy generation, includes improved water quality and decreased evaporation. Therefore, this technology will be a good source of income for reservoir hosts. It has also been stated that the installation of FSPV technology will solve the problems of land acquisition.

In chapter two of this thesis, the state-of-the-art was conducted on FSPV systems design and operation from multiple regions of the world. The papers written, and studies conducted on these technologies features a small, but developing, community of academic researchers, independent researchers and companies. Much of the work has been conducted with regards the design, implementation and technical performance of individual technologies and augmenting features that provide additional performance benefits. Several of the technoeconomic studies lack the consideration of cooling benefits of placing FSPV devices on water and should be implemented in future studies. There is a lack of studies in the areas of environmental impacts, dynamic modelling, hydrodynamics, aerodynamics, mooring configuration and coupled aero-hydro-elastic modelling. Furthermore, a lot needs to be understood in terms of how to model these complex multi-body systems in response to wind, waves and currents, how to design these structures to withstand the harsher marine environments, and whether particular design concepts, such as rigid, semi-rigid or flexible systems are more suitable solutions for marine environments. However, in this thesis, through a deep literature review, we identified and combined the empirically supported and unsupported benefits of FSPV systems as well as gaps in the knowledge base. These identified research gaps, when addressed, could help justify the adoption of FSPV systems, reduce the risk associated with developing FSPV projects, and attract lower-cost capital and more investment in this new application of PV.

In chapter three, the methodology of study reveals that the project is feasible to be implemented due to the reachable topography, availability of resources and nearby infrastructure at the site. The technical potential assessed for FSPV installation on Metolong dam in this thesis, provides a guiding information towards planning and modelling floating solar installation on water bodies. These guidelines can be used as a basis to estimate the overall FSPV potential on the water bodies at a regional scale. In this work, several layouts have been presented and a technical analysis of floating and ground-mounted PV was performed. A technical model was developed to estimate the energy yield of a FSPV power system and, with these results, two different scenarios were proposed and analyzed to understand the technical feasibility of this technology compared to the ground-mounted PV.

In chapter four, the main results and findings were provided. Since one of the limitations is the insufficient water temperature data at the chosen location and the simulation software does not have features for the floating solar PV, a correlation between the air and water temperatures model was developed, and the water temperature was used to estimate the energy yield of a FSPV power plant. For the specific reservoir studied, the results indicate that changes in the air temperature directly influence the water temperature. The changes are functions of the change in air temperature and are modulated by other factors such as the relative input of the surface water and season time of the year. Although perhaps the model is not appropriate for all reservoirs around the world, in this study, changes in the air temperature impact the water temperature most significantly during summer months. It was found that air temperatures usually exceed the corresponding water surface temperatures with temperature differences greater than 2.7 °C.

Regarding the technical aspects, this study presented a technical feasibility assessment for covering the Metolong Dam and WTW's energy demand using the FSPV system. The analysis was carried out by using the load of the Metolong Dam and WTW. The FSPV system size, design and energy output were estimated using a set of equations applied in the Excel

application. The second layout (ground-mounted system) was carried out using PVSyst software. Energy generation output was used to compare the two design. The simulation output results shows that the FSPV system could generate around 17,345 MWh per year. The required area to install the FSPV system was found to be 88,000 m^2, accommodating 23,655 solar modules including the space between the modules in the same row, spacing between adjacent rows, the gap for maintenance, cleaning purposes and combiner boxes, which could be facilitated on a portion of the Metolong reservoir occupying about 3.1% to the total surface area. The optimal use of this area was presented visually and factually by using the Helio-scope software. The performance ratio analysis shows that the average PR for a year was 90%. Generally, it was found that the proposed FSPV is in fact more efficient than the groundmounted system of the same size, which in this case was 7.8 MWp. This could be observed due to the overall increase of 3.4% more energy produced per year by the FSPV, which in turn would provide an accumulated surplus of 588 MWh in the first commencement year. This performance was the result of the yearly average decrease in the cell temperature of the floating panels. Thus, a negative impact of a higher temperature on the production of the FSPV is reduced in water surface temperature than in air temperature.

In terms of economic feasibility, the FSPV system's payback period was 13 years, and the net present value was USD 3,946,724 over the 25 years estimated lifetime of the project. The levelized cost of energy was found to be 36.4 US$/MWh. Based on that, the FSPV system will save about 289,776.46 US$ (5.2 Million Maloti) per year in a comparison to using conventional gird electricity which confirms that the FSPV system is beneficial and suitable for the electrification at Metolong Dam for water pumping and WTW applications. In addition, a sensitivity analysis was also carried out for the system; four sensitivity cases were used for four different parameters (change in discount rate, change in investment cost, NPV and LCOE). Hence, this study concluded that the NPV and LCOE are most sensitive to the initial investment cost, and then to the discount change.

In addition, a solar PV system emits GHG due to its embodied energy. Since the life cycle of CO_2 emissions for the polycrystalline silicon module is assumed to be 0.053 kgCO2-eq/kWh, the net CO_2 emission of the PV system over its lifetime (25 years) has been calculated and was found to be 24,621 tCO_2-eq. The annual CO_2 mitigation by the system was 17,329 tCO_2eq, and the net CO_2 mitigation for the entire lifespan is calculated as 406,013 tCO_2eq. The annual saving from the earned carbon credit was 311,062 USD as per the actual annual electricity generation data. It was concluded that the implementation of the proposed FSPV system will reduce coal-dominated electricity imports from South Africa and reduce emissions by over 1.6% annually. Therefore, will add low-emissions and renewable generation system to domestic electricity sources.

The water evaporation calculation performed in this study predicts a significant water saving potential at the Metolong reservoir. The evaporation calculation using the Penman equation data has shown an annual evaporation estimate of 5.7 million m^3 for the reservoir, whose water level in the summer months decreases to a critical height that isolates it from the rest of the reservoir. It was also found that the proposed FSPV can save 84,136.1 m^3 of water annually. It was concluded that the effect of evaporation reduction has a very positive effect on agriculture and water supply as well as the survival of living organisms in this part of the reservoir.

Finally, since the marginal price of the system and the prices for renewable energy certificates are constantly changing, it is necessary to check the economics on a regular basis. The results of this study have important implications for future large-scale floating PV systems in Lesotho. For the successful deployment of FSPV power, the key is a rigorous feasibility assessment and planning for the redistribution of benefits in order to minimize environmental damage and community rejection.

5.1. Limitations and suggestions for future work

Based on the work presented, several limitations were identified throughout the analysis and could be further improved in future work. Given the limited literature availability and track record of floating PV projects, future work is needed to explore policies that sustain the development of this technology while also minimizing negative externalities. To accomplish this, a full life cycle analysis study is needed on this technology. Improvements in future analysis should account for:

- Collecting more data to further refine the correlation between air-water temperature model that could be extended to perform optimization studies on water temperature strategy as well as improving the energy production accuracy of the results shown here.
- Modelling of a cell temperature equation accounting for real data, mainly measuring the water temperature and energy yield of a floating installation.
- To actually install floating solar PV in individual reservoirs, more work is needed for the accurate analysis of accessibility, detailed topography, and other conditions need to be implemented.
- The lifetime analysis of costs and revenues surrounding the effects of the PV system design and the energy-water nexus is needed to understand the whole economic feasibility of FSPV applications.
- There is a need to scientifically relate the biotics of an ecosystem with the coverage ratio of solar panels to ensure a balanced trade-off between energy production and environmental protection.
- Since most of the floating solar plants are in their nascent stages of operation, a simulation of their biological activities and studying their behaviour would ensure the holistic suitability of FSPV systems

References

[1] S. Karlsson-Vinkhuyzen, ‘The UN, Energy and the Sustainable Development Goals’, 2016, pp. 115–138. doi: 10.1057/978-1-137-55631-8_5.

[2] B. Johansson, D. K. Jonsson, A. Månsson, L. J. Nilsson, and M. Nilsson, ‘Transition to a Low Carbon Energy System and Energy Security- Synergies and Conflicts’, p. 14.

[3] B. Saerbeck, M. Well, H. Jörgens, A. Goritz, and N. Kolleck, ‘Brokering Climate Action: The UNFCCC Secretariat Between Parties and Nonparty Stakeholders’, Glob. Environ. Polit., vol. May, May 2020, doi: 10.1162/glep_a_00556.

[4] L. Ranalder et al., ‘Renewables in Cities - 2021 Global Status Report - REN21’, 2021, doi: 10.13140/RG.2.2.28518.14403.

[5] D. Henner, REN21. 2017. Renewables 2017 Global Status Report. 2017.

[6] X. Ju, C. Xu, X. Han, H. Zhang, G. Wei, and L. Chen, ‘Recent advances in the PV-CSP hybrid solar power technology’, Abu Dhabi, United Arab Emirates, 2017, p. 110006. doi: 10.1063/1.4984480.

[7] K. Larchet, ‘Solar PV-CSP Hybridisation for Baseload Generation’, p. 92.

[8] Maciej Zielinski; Jeremy Fletcher; Matt Ewem; Nicolas Fulghum; Pete Tunbridge, ‘Global Electricity Review 2022.’, EMBER.

[9] B. M. Taele, K. K. Gopinathan, and L. Mokhuts’oane, ‘The potential of renewable energy technologies for rural development in Lesotho’, Renew. Energy, vol. 32, no. 4, pp. 609–622, Apr. 2007, doi: 10.1016/j.renene.2006.02.014.

[10] B M Taele, L Mokhutšoane, and Himanshu Narayan, ‘Solar energy resources potential and sustainable production of biomass energy in Lesotho’, 2010, doi: 10.13140/RG.2.1.2962.0882.

[11] Government of Lesotho, ‘Lesotho Energy Policy 2015–2025’, Maseru, Lesotho, 2015.

[12] ‘Lesotho Renewable Energy-Based Rural Electrification Project (LREBRE).’, United Nations Development Programme, 2013.

[13] IRENA, ‘Global Atlas for Renewable Energy’. Accessed: Jul. 01, 2021. [Online]. Available: https://www.irena.org/ globalatlas

[14] R. Y. Shum, ‘A comparison of land-use requirements in solar-based decarbonization scenarios’, Energy Policy, vol. 109, pp. 460–462, Oct. 2017, doi: 10.1016/j.enpol.2017.07.014.

[15] H. Ibrahim and N. Anani, ‘Variations of PV module parameters with irradiance and temperature’, Energy Procedia, vol. 134, pp. 276–285, Oct. 2017, doi: 10.1016/j.egypro.2017.09.617.

[16] P. K. Kenabatho and B. P. Parida, ‘Evaporation losses as a major factor in determining allowable yield from water supply reservoirs: the case of Botswana’s major reservoirs’, WIT Trans. Ecol. Environ., vol. 83, p. 8, 2005.

[17] ‘World Bank Group, ESMAP and SERIS. 2019. Where Sun Meets Water: Floating Solar Handbook for Practitioners. Washington, DC: World Bank.’

[18] ‘SERIS Annual Report 2020.’, Solar Energy Research Institute of Singapore (SERIS), National University of Singapore (NUS), 2020.

[19] Cox, Molly., ‘Floating Solar Landscape 2021.’, Wood Mackenzie., United States, Wood Mackenzie., 2021. [Online]. Available: https://www.woodmac.com/reports/power-markets-floating-solar-landscape-2021476537.

[20] F. Pasanisi et al., ‘A Cooperation Project in Lesotho: Renewable Energy Potential Maps Embedded in a WebGIS Tool’, Sustainability, vol. 13, no. 18, p. 10132, Sep. 2021, doi: 10.3390/su131810132.

[21] M. Senatla, M. Nchake, B. M. Taele, and I. Hapazari, ‘Electricity capacity expansion plan for Lesotho – implications on energy policy’, Energy Policy, vol. 120, pp. 622–634, Sep. 2018, doi: 10.1016/j.enpol.2018.06.003.

[22] International Energy Agency (IEA), International Renewable Energy Agency (IRENA), United Nations Statistics Division (UNSD), World Bank (WB), and World Health Organization (WHO), ‘Tracking SDG7: The Energy Progress Report.’, 2020. Accessed: Jul. 01, 2021. [Online]. Available: https://trackingsdg7.esmap.org/

[23] Mohit Acharya and Sarvesh Devraj, ‘Floating Solar Photovoltaic (FSPV): A Third Pillar to Solar PV Sector ?’, Energy Resour. Inst. TERI, 2019.

[24] P. K. Dash and N. C. Gupta, ‘Effect of Temperature on Power Output from Different Commercially available Photovoltaic Modules’, vol. 5, no. 1, p. 5, 2015.

[25] V. J. Fesharaki, M. Dehghani, J. J. Fesharaki, and H. Tavasoli, ‘The Effect of Temperature on Photovoltaic Cell Efficiency’, p. 6.

[26] H. Bahaidarah, A. Subhan, and P. Gandhidasan, ‘Author’s personal copy Performance evaluation of a PV (photovoltaic) module by back surface water cooling for hot climatic conditions’, Energy, vol. 59, pp. 445–453, Sep. 2013, doi: 10.1016/j.energy.2013.07.050.

[27] Y. Tripanagnostopoulos, T. Nousia, M. Souliotis, and P. Yianoulis, ‘Hybrid photovoltaic/thermal solar system’, Sol. Energy, vol. 72, pp. 217–234, Mar. 2002, doi: 10.1016/S0038-092X(01)00096-2.

[28] Y.-K. Choi, ‘A Study on Power Generation Analysis of Floating PV System Considering Environmental Impact’, Int. J. Softw. Eng. Its Appl., vol. 8, pp. 75–84, Jan. 2014, doi: 10.14257/ijseia.2014.8.1.07.

[29] L. Liu, Q. Wang, H. Lin, H. Li, Q. Sun, and R. wennersten, ‘Power Generation Efficiency and Prospects of Floating Photovoltaic Systems’, Energy Procedia, vol. 105, pp. 1136–1142, May 2017, doi: 10.1016/j.egypro.2017.03.483.

[30] W. Charles Lawrence Kamuyu, J. Lim, C. Won, and H. Ahn, ‘Prediction Model of Photovoltaic Module Temperature for Power Performance of Floating PVs’, Energies, vol. 11, no. 2, p. 447, Feb. 2018, doi: 10.3390/en11020447.

[31] Z. A. A. Majid, M. H. Ruslan, K. Sopian, M. Y. Othman, and M. S. M. Azmi, ‘Study on Performance of 80 Watt Floating Photovoltaic Panel’, J. Mech. Eng. Sci., vol. 7, pp. 1150–1156, Dec. 2014, doi: 10.15282/jmes.7.2014.14.0112.

[32] C. Ferrer-Gisbert, J. Ferrán-Gozálvez, M. Santafé, P. Ferrer-Gisbert, F.-J. Sanchez-Romero, and J. B. Soler, ‘A new photovoltaic floating cover system for water reservoirs’, Renew. Energy, vol. 60, pp. 63–70, Dec. 2013, doi: 10.1016/j.renene.2013.04.007.

[33] Cox, M., ‘Floating solar update: Bigger projects and climbing capacity. Wood Mackenzie Power & Renewables.’ [Online]. Available: https://www.woodmac.com/news/editorial/floating-solar-update-2019/

[34] P. Ranjbaran, H. Yousefi, G. B. Gharehpetian, and R. Astaraei, ‘A review on floating photovoltaic (FPV) power generation units’, Renew. Sustain. Energy Rev., vol. 110, pp. 332–347, May 2019, doi: 10.1016/j.rser.2019.05.015.

[35] ‘Sahu, A., Yadav, N., Sudhakar, K. (2016). Floating photovoltaic powerplant: A review. Renewable and Sustainable Energy Reviews, 66, 815-824.’.

[36] L. Wästhage, ‘OPTIMIZATION OF FLOATING PV SYSTEMS’, p. 52.

[37] M. Rosa-Clot, G. M. Tina, and S. Nizetic, ‘Floating photovoltaic plants and wastewater basins: an Australian project’, Energy Procedia, vol. 134, pp. 664–674, Oct. 2017, doi: 10.1016/j.egypro.2017.09.585.

[38] B. P. Martins, ‘Techno-economic evaluation of a floating PV system for a wastewater treatment facility’, p. 90.

[39] D. Feldman, K. Wu, and R. Margolis, ‘H1 2021 Solar Industry Update’, NREL/PR-7A40-80427, 1808491, MainId:42630, Jul. 2021. doi: 10.2172/1808491.

[40] M. Santafé, J. B. Soler, F.-J. Sanchez-Romero, P. Ferrer-Gisbert, J. Gozálvez, and F. Gisbert, ‘Theoretical and experimental analysis of a floating photovoltaic cover for water irrigation reservoirs’, Energy, vol. 67, Apr. 2014, doi: 10.1016/j.energy.2014.01.083.

[41] M. Davis et al., ‘Wood Mackenzie | U.S. Research Team’, p. 17.

[42] Ramasamy, Vignesh, and Robert Margolis, ‘Floating Photovoltaic System Cost Benchmark.’, National Renewable Energy Laboratory, NREL/TP-7A40-80695. [Online]. Available: https://www.nrel.gov/docs/fy22osti/80695.pdf.

[43] S.-H. Kim, S.-C. Baek, K.-B. Choi, and S.-J. Park, ‘Design and Installation of 500-kW Floating Photovoltaic Structures Using High-Durability Steel’, Energies, vol. 13, no. 19, p. 4996, Sep. 2020, doi: 10.3390/en13194996.

[44] R. Cazzaniga, M. Cicu, M. Rosa-Clot, P. Rosa-Clot, G.M. Tina, C. Ventura, ‘Floating photovoltaic plants: Performance analysis and design solutions’, Renew. Sustain. Energy Rev., vol. 81, Part 2, pp. 1730–1741, 2018, [Online]. Available: https://www.sciencedirect.com/science/article/pii/S1364032117309103

[45] K. Trapani and M. Redón Santafé, ‘A review of floating photovoltaic installations: 2007-2013: A review of floating photovoltaic installations’, Prog. Photovolt. Res. Appl., vol. 23, no. 4, pp. 524–532, Apr. 2015, doi: 10.1002/pip.2466.

[46] S. Oliveira-Pinto and J. Stokkermans, ‘Assessment of the potential of different floating solar technologies – Overview and analysis of different case studies’, Energy Convers. Manag., vol. 211, p. 112747, May 2020, doi: 10.1016/j.enconman.2020.112747.

[47] J. Song and Y. Choi, ‘Analysis of the Potential for Use of Floating Photovoltaic Systems on Mine Pit Lakes: Case Study at the Ssangyong Open-Pit Limestone Mine in Korea’, Energies, vol. 9, no. 2, p. 102, Feb. 2016, doi: 10.3390/en9020102.

[48] A. K. Singh, D. Boruah, L. Sehgal, and A. P. Ramaswamy, ‘Feasibility study of a grid-tied 2MW floating solar PV power station and e-transportation facility using “SketchUp Pro” for the proposed smart city of Pondicherry in India’, J. Smart Cities, vol. 2, no. 2, Mar. 2017, doi: 10.18063/JSC.2016.02.004.

[49] ESMAP & SERIS, ‘Where Sun Meets Water: Floating Solar Market Report.’ [Online]. Available: http://documents.worldbank.org/curated/en/579941540407455831/pdf/131291- WP-REVISED-P161277PUBLIC.pdf

[50] International Hydropower Association (IHA)., 'Case study: A hybrid hydropower and floating PV system in
Portugal.' [Online]. Available:
https://www.hydropower.org/sites/default/files/publicationsdocs/case_study_-_a_hybrid_hydropower_and_floating_pv_system_in_portugal.pdf

[51] J. Farfan and C. Breyer, 'Combining Floating Solar Photovoltaic Power Plants and Hydropower Reservoirs:
A Virtual Battery of Great Global Potential', Energy Procedia, vol. 155, pp. 403–411, Nov. 2018, doi: 10.1016/j.egypro.2018.11.038.

[52] 'Bellini, E. (2019). Japan's largest floating PV plant catches fire after Typhoon Faxai impact. PV Magazine.'

[53] T. Hove and E. Mungofa, 'Towards the Optimal Sizing of Solar-Powered Pump-Pipe-Storage Systems', in Proceedings of the ISES Solar World Congress 2019, Santiago, Chile, 2019, pp. 1–12. doi: 10.18086/swc.2019.34.02.

[54] D. Faiman, 'Assessing the Outdoor Operating Temperature of Photovoltaic Modules', Prog. Photovolt. Res. Appl., vol. 16, pp. 307–315, Jun. 2008, doi: 10.1002/pip.813.

[55] H. Liu, V. Krishna, J. Lun Leung, T. Reindl, and L. Zhao, 'Field experience and performance analysis of floating PV technologies in the tropics', Prog. Photovolt. Res. Appl., vol. 26, no. 12, pp. 957–967, Dec. 2018, doi: 10.1002/pip.3039.

[56] W. Charles Lawrence, J. Lim, C. Won, and H. Ahn, 'Prediction Model of Photovoltaic Module Temperature for Power Performance of Floating PVs', Energies, vol. 11, p. 447, Feb. 2018, doi: 10.3390/en11020447.

[57] J. Morrill, R. Bales, and M. Conklin, 'Estimating Stream Temperature from Air Temperature: Implications for Future Water Quality', J. Environ. Eng.-Asce - J Env. ENG-ASCE, vol. 131, Jan. 2005, doi: 10.1061/(ASCE)0733-9372(2005)131:1(139).

[58] L. A. Krider, J. A. Magner, J. Perry, B. Vondracek, and L. C. Ferrington, 'Air-Water Temperature Relationships in the Trout Streams of Southeastern Minnesota's Carbonate-Sandstone Landscape', JAWRA J. Am. Water Resour. Assoc., vol. 49, no. 4, pp. 896–907, Aug. 2013, doi: 10.1111/jawr.12046.

[59] O. Mohseni, H. G. Stefan, and T. R. Erickson, 'A nonlinear regression model for weekly stream temperatures', Water Resour. Res., vol. 34, no. 10, pp. 2685–2692, Oct. 1998, doi: 10.1029/98WR01877.

[60] M. T. H. van Vliet et al., 'Coupled daily streamflow and water temperature modelling in large river basins', Hydrol. Earth Syst. Sci., vol. 16, no. 11, pp. 4303–4321, Nov. 2012, doi: 10.5194/hess-16-4303-2012.

[61] A. Rabi, M. Hadzima-Nyarko, and M. Šperac, 'Modelling river temperature from air temperature: case of the River Drava (Croatia)', Hydrol. Sci. JournalJournal Sci. Hydrol., vol. 60, Sep. 2015, doi: 10.1080/02626667.2014.914215.

[62] S. Piccolroaz, E. Calamita, B. Majone, A. Gallice, A. Siviglia, and M. Toffolon, 'Prediction of river water temperature: a comparison between a new family of hybrid models and statistical approaches: Prediction of River Water Temperature', Hydrol. Process., vol. 30, no. 21, pp. 3901–3917, Oct. 2016, doi: 10.1002/hyp.10913.

[63] N. Umar, B. Bora, C. Banerjee, and B. S. Panwar, ‘Comparison of different PV power simulation softwares:
case study on performance analysis of 1 MW grid-connected PV solar power plant’, p. 15.

[64] ‘Mittal, D., Saxena, B. K., & Rao, K. V. (2017). Potential of floating photovoltaic system for energy generation and reduction of water evaporation at four different reservoirs in Rajasthan. 2017 International Conference On Smart Technologies For Smart Nation (SmartTechCon). doi:10.1109/smarttechcon.2017.8358376’.

[65] P. Sharma, B. Muni, and D. Sen, ‘DESIGN PARAMETERS OF 10KW FLOATING SOLAR POWER PLANT’, vol. 2, no. 1, p. 6, 2015.

[66] M. Taboada, L. Cáceres, T. A. Graber, H. Galleguillos, L. F. Cabeza, and R. Rojas, ‘Solar water heating system and photovoltaic floating cover to reduce evaporation: Experimental results and modeling’, Renew. Energy, vol. 105, pp. 601–615, May 2017, doi: 10.1016/j.renene.2016.12.094.

[67] G. K. X. Melvin, ‘EXPERIMENTAL STUDY OF THE EFFECT OF FLOATING SOLAR PANELS ON REDUCING EVAPORATION IN SINGAPORE RESERVOIRS’, p. 50.

[68] M. Van Dijk and S. Van Vuuren, ‘Destratification induced by bubble plumes as a means to reduce evaporation from open impoundments’, Water SA, vol. 35, no. 2, May 2012, doi: 10.4314/wsa.v35i2.76731.

[69] G. D. Pimentel Da Silva and D. A. C. Branco, ‘Is floating photovoltaic better than conventional photovoltaic? Assessing environmental impacts’, Impact Assess. Proj. Apprais., vol. 36, no. 5, pp. 390–400, Sep. 2018, doi: 10.1080/14615517.2018.1477498.

[70] Ciel et Terre, ‘Ciel et Terre’, 2018. Accessed: Dec. 29, 2018. [Online]. Available: https://www.ciel-etterre.net.

[71] S. Gadzanku, H. Mirletz, N. Lee, J. Daw, and A. Warren, ‘Benefits and Critical Knowledge Gaps in Determining the Role of Floating Photovoltaics in the Energy-Water-Food Nexus’, Sustainability, vol. 13, no. 8, p. 4317, Apr. 2021, doi: 10.3390/su13084317.

[72] IHA, ‘Case study: A hybrid hydropower and floating PV system in Portugal.’, London, 2018.

[73] J. Farrell, ‘RELATED ILSR PUBLICATIONS’, p. 35.

[74] Bengt Jaeckel, ‘SolarPower Europe: O&M Best Practices Guidlines’, Jun. 2016.

[75] Marco Antonio Esteves Galdino and Marta Maria de Almeida Olivieri, ‘Some Remarks about the Deployment of Floating PV Systems in Brazil’, J Electr. Eng., vol. 5, no. 1, Jan. 2017, doi: 10.17265/23282223/2017.01.002.

[76] ‘Metolong Dam Environmental and Social Impact Assessment volume 1 – Main Report Final Report 2008.’

[77] ‘Metolong Water Treatment Works (WTW): Environmental Management Plan. Report Number: 122809299-2, January 2010.’

[78] L. A. Kumar, V. Indragandhi, and U. Y., ‘PVSYST’, 2020, pp. 349–392. doi: 10.1016/B978-0-12-8194164.00009-0.

[79] C. Haydaroğlu and B. GÜMÜġ, ‘EXAMINATION OF PVGIS AND SUNNY DESIGNWEB PHOTOVOLTAIC SYSTEM WEB-BASED SIMULATION PROGRAMS AND EVALUATION OF THE RELIABILITY OF RESULTS’, p. 9, 2016.

[80] ‘LHDA. Bathymetric survey at the Metolong Dam.’, Jul. 2020.

[81] M. Hadzima-Nyarko, A. Rabi, and M. Šperac, ‘Implementation of Artificial Neural Networks in Modeling the Water-Air Temperature Relationship of the River Drava’, Water Resour. Manag., vol. 28, pp. 1379–1394, Mar. 2014, doi: 10.1007/s11269-014-0557-7.

[82] B. Webb, P. Clack, and D. Walling, ‘Water-Air Temperature Relationships in A Devon River System and the Role of Flow’, Hydrol. Process., vol. 17, pp. 3069–3084, Oct. 2003, doi: 10.1002/hyp.1280.

[83] M. Mpholo, D. Steuerwald, and T. Kukeera, Eds., Africa-EU Renewable Energy Research and Innovation Symposium 2018 (RERIS 2018): 23–26 January 2018, National University of Lesotho On occasion of NULISTICE 2018. Cham: Springer International Publishing, 2018. doi: 10.1007/978-3-319-93438-9.

[84] M. Benghanem, ‘Estimation of daily flow rate of photovoltaic water pumping systems using solar radiation data’, Results Phys., p. 6, 2018.

[85] R. Baetens et al., ‘Assessing electrical bottlenecks at feeder level for residential net zero-energy buildings by integrated system simulation’, Appl. Energy, vol. 96, pp. 74–83, Aug. 2012, doi: 10.1016/j.apenergy.2011.12.098.

[86] T. Hove, ‘A method for predicting long-term average performance of photovoltaic systems’, Renew. Energy, vol. 21, no. 2, pp. 207–229, Oct. 2000, doi: 10.1016/S0960-1481(99)00131-7.

[87] ‘Planning of a PV Generator - Planning Guidelines’, p. 37.

[88] P. Gilman, N. A. DiOrio, J. M. Freeman, S. Janzou, A. Dobos, and D. Ryberg, ‘SAM Photovoltaic Model Technical Reference 2016 Update’, NREL/TP--6A20-67399, 1429291, Mar. 2018. doi: 10.2172/1429291.

[89] G. Thornton, ‘Renewable energy discount rate survey results - 2018’, p. 36.

[90] John D. Valiantzas, ‘Simplified versions for the Penman evaporation equation using routine weather data, Journal of Hydrology.’, vol. 331, no. 3–4, pp. 690–702, 2006, [Online]. Available: https://doi.org/10.1016/j.jhydrol.2006.06.012.

[91] S. Zhu, E. K. Nyarko, and M. Hadzima-Nyarko, ‘Modelling daily water temperature from air temperature for the Missouri River’, PeerJ, vol. 6, p. e4894, Jun. 2018, doi: 10.7717/peerj.4894.

[92] F. Laanaya, A. St-Hilaire, and E. Gloaguen, ‘Water temperature modelling: comparison between the generalized additive model, logistic, residuals regression and linear regression models’, Hydrol. Sci. J., vol. 62, no. 7, pp. 1078–1093, May 2017, doi: 10.1080/02626667.2016.1246799.

[93] M. Mpholo et al., ‘Lesotho electricity demand profile from 2010 to 2030’, J. Energy South. Afr., vol. 32, no. 1, pp. 41–57, Feb. 2021, doi: 10.17159/2413-3051/2021/v32i1a7792.

[94] B. Shiva Kumar and K. Sudhakar, ‘Performance evaluation of 10 MW grid connected solar photovoltaic power plant in India’, Energy Rep., vol. 1, pp. 184–192, Nov. 2015, doi: 10.1016/j.egyr.2015.10.001.

[95] K. Padmavathi and S. A. Daniel, ‘Performance analysis of a 3 MWp grid connected solar photovoltaic power plant in India’, Energy Sustain. Dev., vol. 17, pp. 615–625, Dec. 2013, doi: 10.1016/j.esd.2013.09.002.

[96] LEWA, ‘LEWA’S Determination of Lesotho Electricity Company (LEC) Tariff Application for 2020/2021’, 2021.

[97] ‘Green Climate Fund. “Readiness Proposal with DBSA for the Kingdom of Lesotho.” 2018.’ [98] Lesotho,

African Development Bank (AFDB), ‘Lesotho Energy Programme’.

[99] T. M. Klucher, ‘Evaluation of models to predict insolation on tilted surfaces’, Sol. Energy, vol. 23, no. 2, pp. 111–114, 1979, doi: 10.1016/0038-092X(79)90110-5.

[100] ‘Jinko Solar.’ [Online]. Available: www.jinkosolar.com

[101] ‘EnSmart power conversion and energy storage.’ [Online]. Available: www.ensmartpower.com

[102] ‘Sun path chart program.’ [Online]. Available: httpo://solardat.uoregon.edu/SunChartprogram.php

[103] K. Huyen Nguyen, N. Huong Giang Vu, and X. Truong Nguyen, ‘The Status and Potential Assessment of Solar Power Energy Development in Vietnam’, Int. J. Energy Power Eng., vol. 9, no. 5, p. 69, 2020, doi: 10.11648/j.ijepe.20200905.11.

[104] H. Hondo, ‘Life cycle GHG emission analysis of power generation systems: Japanese case’, Energy, vol. 30, pp. 2042–2056, Aug. 2005, doi: 10.1016/j.energy.2004.07.020.

[105] A. Biswas, D. Husain, and R. Prakash, ‘Life-cycle ecological footprint assessment of grid-connected rooftop solar PV system’, Int. J. Sustain. Eng., vol. 14, no. 3, pp. 529–538, May 2021, doi: 10.1080/19397038.2020.1783719.

[106] D. Jordan and S. Kurtz, ‘Photovoltaic Degradation Rates—an Analytical Review’, Prog. Photovolt. Res. Appl., vol. 21, Jan. 2013, doi: 10.1002/pip.1182.

[107] S. K. Yadav and U. Bajpai, ‘Energy, economic and environmental performance of a solar rooftop photovoltaic system in India’, Int. J. Sustain. Energy, vol. 39, no. 1, pp. 51–66, Jan. 2020, doi: 10.1080/14786451.2019.1641499.

[108] NASDAQ, 2018. [Online]. Available: https://dqydj.com/2018-nasdaq-return/

[109] Edward T Linacre, ‘Data-sparse estimation of lake evaporation, using a simplified Penman equation, Agricultural and Forest Meteorology.’, vol. 64, no. 3–5, pp. 237–256, 1993, [Online]. Available: https://doi.org/10.1016/0168-1923(93)90031-C.

[110] H. L. Penman, ‘Natural Evaporation from Open Water, Bare Soil and Grass.’, R. Soc. Lond. Ser. Math. Phys. Sci., vol. 193, pp. 120–145, 2011, [Online]. Available: http://www.jstor.org/stable/98151 .

APPENDICES

APPENDIX A: Solar Position and Solar Radiation for Fixed-Tilt Surfaces.

One of the most important aspects of working with solar technologies is to know the available solar resources at the point of interest. To know this, it was necessary to estimate the position of the sun according to the movements of the earth. As it is well known, the earth revolves around the sun, also rotating around its own vertical axis and tilting around one of its vertical planes. These movements cause the Sun's "position" relative to a point on Earth to change every instant. An accurate calculation of the sun's position is necessary to obtain the accurate irradiance estimates.

The solar geometry modelled using a set of meteorological data with values for every hour in a year for a given geographical location. The first step in this process is to calculate the declination angle (δ) which measures the tilt that the Earth has with its vertical axis along a year. The declination was calculated as follows using Equation (A.1):

□ = □□□□ 0.39795 ∗ □□□2□ ——)] [A.1]

Using N as the days of a year, January 1st is 1 according to the Gregorian calendar. In parallel, the hour angle (ω) defines the angular displacement of the sun east or west of the local meridian due to the rotation of the earth on its axis at 15^0 per hour. The hour angle is zero at solar noon when the sun is above the local meridian, morning negative and afternoon positive. It was calculated using Equation (A.2):

□ = 15(□ − 12) [A.2]

Once this information is known, the calculation of the sun's angles could begin. The first was the solar zenith. It is the angle between the normal vector of a point on the earth's surface and the center of the sun. It was determined with Equation (A.3):

□ = acos (cos(□) cos(□) cos(□) + sin (□)sin (□) [A.3]

where φ_{ltd} is the local latitude in degrees and referenced to the North. The elevation angle is the angle between the horizon and the center of the Sun. It was easily calculated with Equation (A.4):

□ = 90 − □ [A.4]

After this, it was necessary to calculate the solar azimuth. This angle represents the direction of the Sun and it is referenced clockwise due south. It was determined with Equation (A.5). However in this study, a collector is located in the Southern hemisphere facing north (equatorfacing), then surface azimuth, □ = 0^o (by the sign convention adopted here).

□ = sin(□) □□□□ ( ) ( ) ( ) / ( ) ( ) = 0 [A.5]

Finally, the solar incidence angle was calculated with Equation (A.6). It measures the angle between a particular surface normal and the center of the Sun. It is important to have the surface normal aligned as much as possible to the solar beams if the higher irradiance flux is desired.

$$\square = \sin(\square)\sin(\square + \square) + \cos(\square)\cos(\square + \square)\cos(\square) \quad [A.6]$$

The variable β is the tilt angle of the surface.

After defining the sun's position, the sun's flux over a given area could be calculated. In this point, the focus is on fixed-tilt surfaces. This is the case with the FSPV solar systems without a tracking system. Solar radiation consists of three main components: beam, diffuse and ground reflected. The sum of these three components forms the global total solar radiation on a tilted surface. This behaviour calculated using the hourly data from the PVGIS 5 in TMY format which returns the components and total global solar radiation given the solar geometry. After the local meteorological data with the beam (G_b) and the horizontal radiation (G_h) have been obtained, the first thing to determine is the diffuse radiation. It was calculated using the following equation:

$$\square = \square - \square\cos(\square) \quad [A.7]$$

where $\square$ is the solar zenith angle, diffusivity is the percentage of radiation that reaches the Earth after being scattered by other particles (such as water or air in a cloud) along the way. Diffuse radiation on a tilted plane was calculated using the model developed by Klucher [99] illustrated on Equations (A.8) and (A.9)

$$\square_{,} = \square \quad 0.5\ 1 + \cos^{-}) \quad 1 + \square\square\square^{-})] [1 + \square\square\square(\square)\square\square\square] \quad [A.8]$$

$$\square = 1 - \quad —) \quad [A.9]$$

Usually, the meteorological data that can be found shows the beam and global total radiation over horizontal surfaces. It is necessary to correct this in order to obtain the radiation on the tilted surface. This was done using Equation (A. 10):

$$\square_{,} = \square\cos(\square) \quad [A.10]$$

Last component is the ground reflected radiation. It represents the share of solar radiation that reaches the surfaces after being reflected by the ground surface (Equation (A.11).

$$\square_{,} = \_\square\square(1 - \cos(\square)) \quad [A.11]$$

Where ρ is the ground albedo and it is equal to 0.2 but for the water surface, the albedo value range recorded by [55], ranges between 5% and 7% at Singapore's FSPV test bed can be used. Once the three components are known then it is possible to obtain the global total solar radiation over the tilted surface by Equation (A.12)

□ , = □ , + □ , + □ , [A.12]

As it was mentioned before, this procedure was used only in the cases where the PV modules are fixed-tilt. In the case where they have a single or double axis tracking angle, some modifications in the angles must be done.

APPENDIX B: Components specifications (PV module and Inverter)

The datasheet for the modules and inverter used in the simulation are listed in this appendix. All data sheets are from the manufactures website.

Engineering Drawings

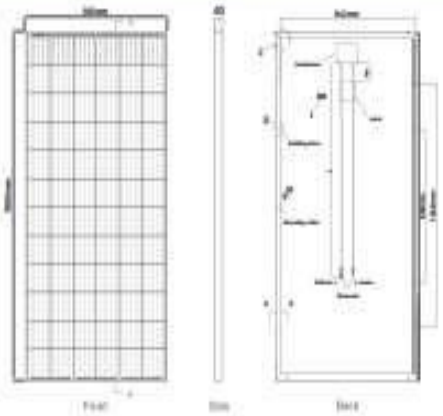

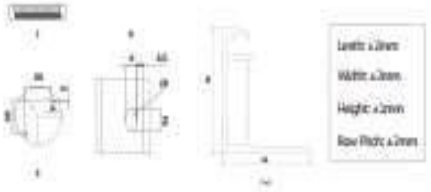

Electrical Performance & Temperature Dependence

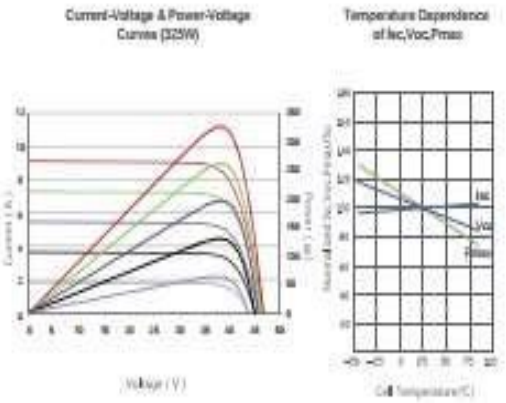

Mechanical Characteristics

Cell Type	Poly-crystalline 157×157mm (6 inch)
No.of cells	72 (6×12)
Dimensions	1956×992×40mm (77.01×39.05×1.57 inch)
Weight	22.5 kg (49.6 lbs)
Front Glass	3.2mm, Anti-Reflection Coating, High Transmission, Low Iron, Tempered Glass
Frame	Anodized Aluminium Alloy
Junction Box	IP67 Rated
Output Cables	TÜV 1×4.0mm², Length: 1200mm or Customized Length

Packaging Configuration

(Two pallets=One stack)

27pcs/pallet, 54pcs/stack, 648 pcs/40'HQ Container

SPECIFICATIONS

Module Type	JKM320PP-72 JKM320PP-72-V		JKM325PP-72 JKM325PP-72-V		JKM330PP-72 JKM330PP-72-V		JKM335PP-72 JKM335PP-72-V		JKM340PP-72 JKM340PP-72-V	
	STC	NOCT	STC	NOCT	STC	NOCT	STC	NOCT	STC	NOCT
Maximum Power (Pmax)	320Wp	237Wp	325Wp	241Wp	330Wp	245Wp	335Wp	249Wp	340Wp	253Wp
Maximum Power Voltage (Vmp)	37.4V	34.7V	37.6V	35.0V	37.8V	35.3V	38.0V	35.6V	38.2V	35.9V
Maximum Power Current (Imp)	8.56A	6.83A	8.66A	6.89A	8.74A	6.94A	8.82A	6.99A	8.91A	7.05A
Open-circuit Voltage (Voc)	46.4V	43.0V	46.7V	43.3V	46.9V	43.6V	47.2V	43.8V	47.5V	44.0V
Short-circuit Current (Isc)	9.05A	7.36A	9.10A	7.40A	9.14A	7.45A	9.18A	7.52A	9.22A	7.58A
Module Efficiency STC (%)	16.49%		16.75%		17.01%		17.26%		17.52%	
Operating Temperature(℃)	-40℃~+85℃									
Maximum system voltage	1000/1500VDC (IEC)									
Maximum series fuse rating	20A									
Power tolerance	0~+3%									
Temperature coefficients of Pmax	-0.38%/℃									
Temperature coefficients of Voc	-0.31%/℃									
Temperature coefficients of Isc	0.06%/℃									
Nominal operating cell temperature (NOCT)	45±2℃									

Figure B.1: Module specifications [100].

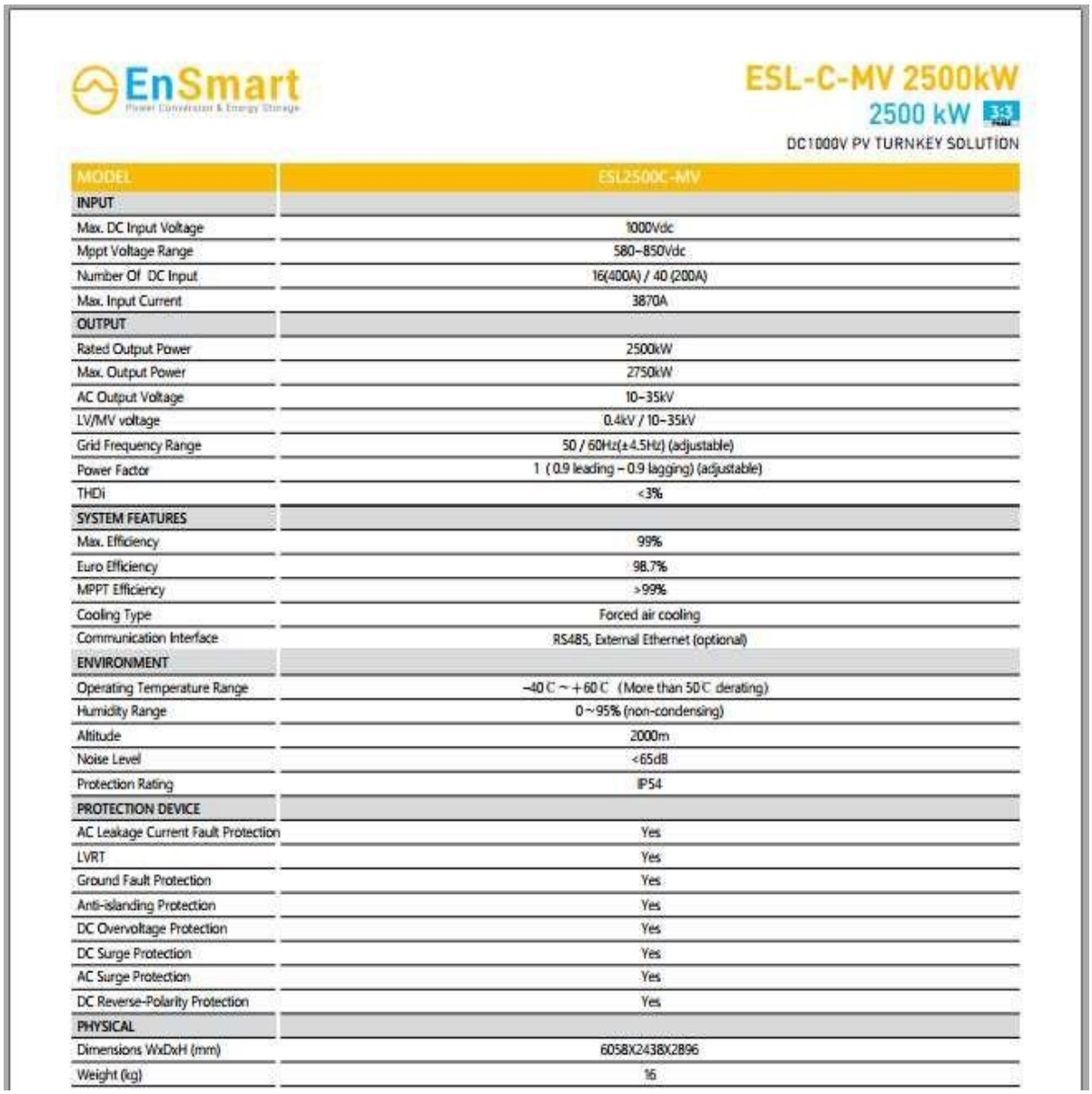

EnSmart

Power Conversion & Energy Storage

ESL-C-MV 2500kW

2500 kW

DC1000V PV TURNKEY SOLUTION

MODEL	ESL2500C-MV
INPUT	
Max. DC Input Voltage	1000Vdc
Mppt Voltage Range	580~850Vdc
Number Of DC Input	16(400A) / 40 (200A)
Max. Input Current	3870A
OUTPUT	
Rated Output Power	2500kW
Max. Output Power	2750kW
AC Output Voltage	10~35kV
LV/MV voltage	0.4kV / 10~35kV
Grid Frequency Range	50 / 60Hz(±4.5Hz) (adjustable)
Power Factor	1 (0.9 leading ~ 0.9 lagging) (adjustable)
THDi	<3%
SYSTEM FEATURES	
Max. Efficiency	99%
Euro Efficiency	98.7%
MPPT Efficiency	>99%
Cooling Type	Forced air cooling
Communication Interface	RS485, External Ethernet (optional)
ENVIRONMENT	
Operating Temperature Range	-40℃ ~ +60℃ (More than 50℃ derating)
Humidity Range	0~95% (non-condensing)
Altitude	2000m
Noise Level	<65dB
Protection Rating	IP54
PROTECTION DEVICE	
AC Leakage Current Fault Protection	Yes
LVRT	Yes
Ground Fault Protection	Yes
Anti-islanding Protection	Yes
DC Overvoltage Protection	Yes
DC Surge Protection	Yes
AC Surge Protection	Yes
DC Reverse-Polarity Protection	Yes
PHYSICAL	
Dimensions WxDxH (mm)	6058X2438X2896
Weight (kg)	16

Figure B.2: Technical Data of the inverter [101].

APPENDIX C: Determining AC Active power and nominal power ratio

The active AC power fed into the grid under optimal weather conditions is determined by the design AC output power of the inverter, the power factor (cos (φ)), the apparent power of the inverter and the AC voltage of the Network. Figure C.1 shows the dependence of the AC active power on the power factor.

The following formula determines the AC active power:

□ = □ ∗ cos (□) ', [C.1]

where □ = AC active power, □ = Apparent power of the inverter, and cos(□) = Power factor. The DC input power of the inverter and its efficiency determine the DC input power required to achieve the desired active AC power to be exported to the grid. Furthermore, it should be mentioned that the efficiency of the inverter is influenced by the voltage of the photovoltaic field which decreases at high input voltages. This input power can be found using the following equation:

□ = ___ [C.2]

where □ is the DC input power of inverter, □ is the AC active power, and □ is the efficiency of the Inverter. The maximum efficiency measured for the selected inverter is 99%. The ratio that describes the ratio between the DC power of the inverter and the DC power of the photovoltaic field (Nominal Power Ratio) is important to calculate in order to avoid oversizing

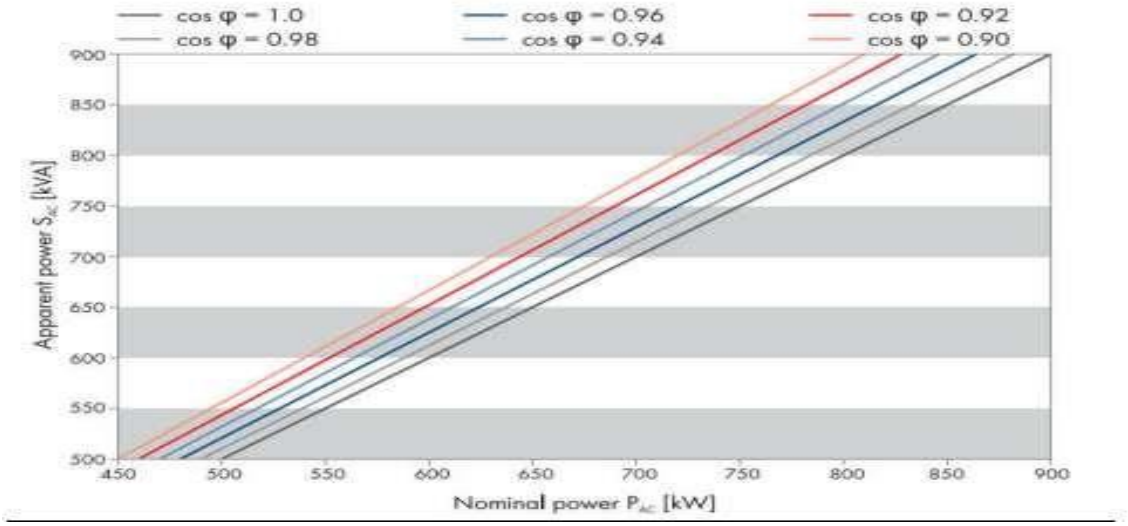

Figure C.1: AC active power depending on the power factor cos(φ) [88].

the inverter since its performance is maximum for a given absorbed power, and decreases when this power is small compared to the nominal value.

□□□ = _____ [C.3]

where NPR is the Nominal power ratio and □ is the PV array power.

APPENDIX D: Voltage dimensions

The electrical output of photovoltaic modules is negatively influenced by the temperature. This parameter affects the voltage more than the current as can be seen in Figure D.1 below. Therefore, the module voltage or string current must be calculated taking into account the

climatic data of the PV location. However, FSPV has less of an impact due to the cooling effect of the water directly below the installation.

As can be seen from the figure; the open circuit voltage decreases with the temperature. This dependence leads us to calculate the maximum open circuit voltage of the module for the lowest temperature that can be expected at the mounting location.

$$\square_{,\ ,\ } = \square * \left(1 + \frac{T_{min} * \Delta T}{100}\right)_{\%} \qquad [D.1]$$

where $\square_{,,}$ is the Maximum PV module voltage, $\square$ is the open-circuit voltage of the PV module, $\square$ is the Temperature coefficient at minimum expected temperature and $\Delta\square$ is the temperature variance between STC and minimum expected temperature. According to the Lesotho meteorological services data, the lowest temperature registered at the site in winter time is -5 ^{o}C.

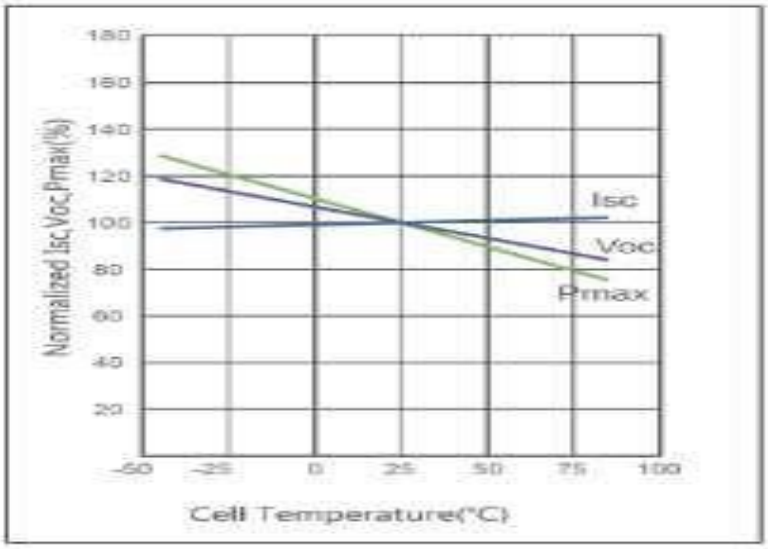

Figure D.1: Temperature dependence of Isc, Voc and Pmax [87]

.

To calculate the minimum voltage of the PV module (Equation D.2), the highest temperature to be expected at the installation site must be considered. The highest temperature in the bodies of water appears to be lower compared to terrestrial temperatures due to the cooling effect. Despite this, the operating temperature of the cells is usually between 45 °C and 70 °C. Therefore, it is assumed that the panels will operate at 50°C in summer, the temperature which is considered to be the expected maximum temperature.

$$\square_{,\ ,\ } = \square * \left(1 + \frac{T_{max} * \Delta T}{100}\right)_{\%} \qquad [D.2]$$

where $\square_{,,}$, $\square$, $\square$, and $\Delta\square$ are the minimum PV module voltage, voltage of the PV module at maximum power, temperature coefficient at maximum expected temperature and the temperature variance between STC and maximum expected temperature respectively.

As seen on Figure D.1, current is less dependent on temperature than voltage, the maximum PV module current in short-circuit conditions, calculated considering the maximum expected temperature that can be expected at the installation place using equation (D.3).

□ , , = □ * $\left(\frac{T_{max} * \Delta T}{\%}\right.$ [D.3]

where □ ,, is the maximum string current, □ is the short-circuit current of the PV module, □ is the temperature coefficient at the maximum expected temperature and Δ□ is the temperature variance between the STC and the maximum expected temperature.

APPENDIX E: String dimensions

The voltage of a PV module string must be below the maximum input voltage of the inverter. If it is exceeded, yield losses can occur. In this design, the system DC-link is rated at 1000 VDC to reduce the output current ripple and regulate the voltage at the DC side of the inverter; therefore the number of necessary PV modules per string was calculated as:

□ , , ≤ _____, , [E.1]
, ,

where □ ,,, □ ,, and □ ,, are the maximum number of PV modules per string, the maximum input voltage of the inverter and the maximum PV module voltage respectively. To avoid yield losses due to sub-optimal MPP, tracking is also necessary to maintain the string voltage above the minimum MPP voltage of the inverter. Therefore, the minimum number of PV modules per string was calculated using Equation (E.2):

□ , , ≥ _____, ,
[E.2]
, ,

where, □ ,, is the minimum number of PV modules per string, □ „, is the minimum voltage of the inverter and □ ,, is the minimum PV module voltage. The optimum number of PV modules per string must be between the minimum and maximum string voltage as is shown in the following Equation:

□ , , ≤ □ , ≤ □ , , [E.3]

Once the number of modules per string has been established, the maximum and minimum string voltage was calculated using the following equations:

□ , , = □ , * □ , , [E.4]

□ , , = □ , * □ , , [E.5]

where: □ , , is the maximum voltage per string, □ , , is the minimum voltage per string, □ , number of modules per string, □ , , is the maximum PV module Voltage and □ , , is the minimum PV module Voltage. These values must be in the MPP voltage range of the inverter, between 580 V and 850 V in this study.

The maximum number of strings depends on the maximum input current of the inverter and the minimum number of strings depends on the PV array power. They are calculated by using the following Equations:

□ , = _____, [E.6]
, ,

□ , = _____, * ’ , [E.7]

where: □ , is the maximum number of strings, □ , is the minimum number of strings, □ , is the number of modules per string, □ , is the PV array power, □ , is the maximum PV module power, □ , is the maximum input current of the inverter, and □ , , is the maximum string current. The number of strings per inverter is given by:

□ , , ≤ □ , ≤ □ , , [E.8]

Lastly, the number of modules per string, the number of strings per inverter and the number of inverters, the total number of PV modules which are needed can be calculated using Equation (D.9):

□ = □ , * □ , * □ [E.9]

APPENDIX F: Row module spacing

The minimum spacing between the neighbouring arrays of PV panels is determined according to the day with the smallest height of the Sun. This spacing enables us to ensure that there are no losses due to a mutual shadowing of PV panels in the power plant. Figure F.1, determines the module inter-row spacing. Based on the figure, the first step in calculating the module interrow spacing was to calculate the height difference from the back of the module to the surface using Equation (F.1):

□□□□*h*□ □□□□□□□□□□□ = sin(□) ∗ □□□□□□ □□□□*h* [F.1] Where □ is a

PV tilt angle (°) of the installed array.

To calculate the Module row spacing, the Sun path chart program of the Solar Radiation Monitoring Laboratory of the University of Oregon (UO Solar Radiation Monitoring Laboratory) [102] was used to determine the Sun's Elevation Angle by entering the latitude and longitude of the location. This study chose the worst-case scenario during the winter solstice (June 21st) between 9 AM and 3 PM where winter is at its peak and solar irradiance at a minimum as shown in Figure F.2. It should be noted that these calculations are done for a system with fixed axis solar panels. From the chart data, the window was highlighted and a horizontal line drawn out to the left of the chart to narrow in on the Solar elevation angle at those times. Hence, angle 22^0 will be used to determine the Module row spacing using Equation (F.2):

$$Module\ row\ spacing = \frac{Heigh\ \ Difference}{Tan(angle\ of\ elevation)} \quad [F.2]$$

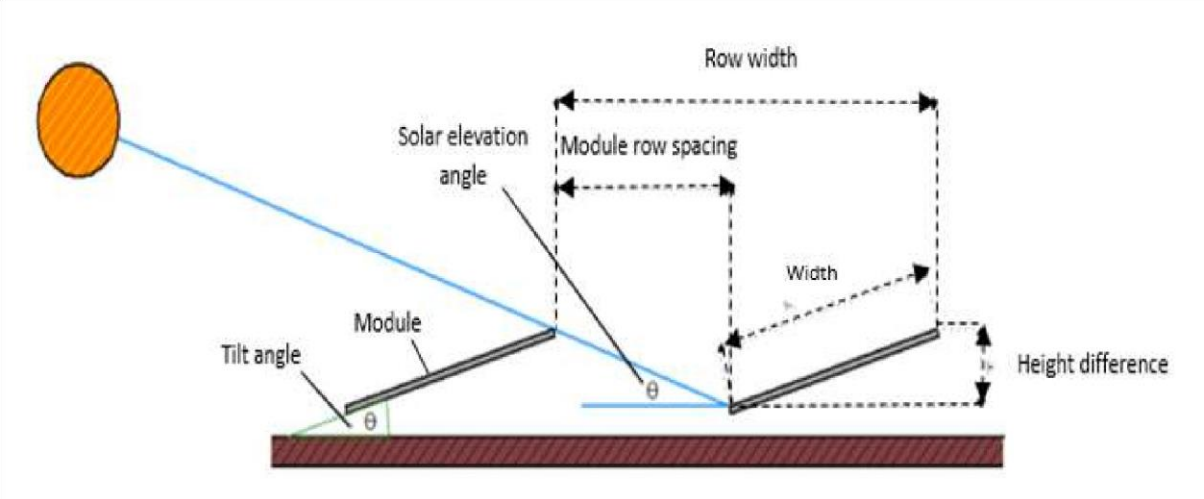

Figure F.1: The calculation of the minimum module spacing between the neighbouring arrays of PV panels [103].

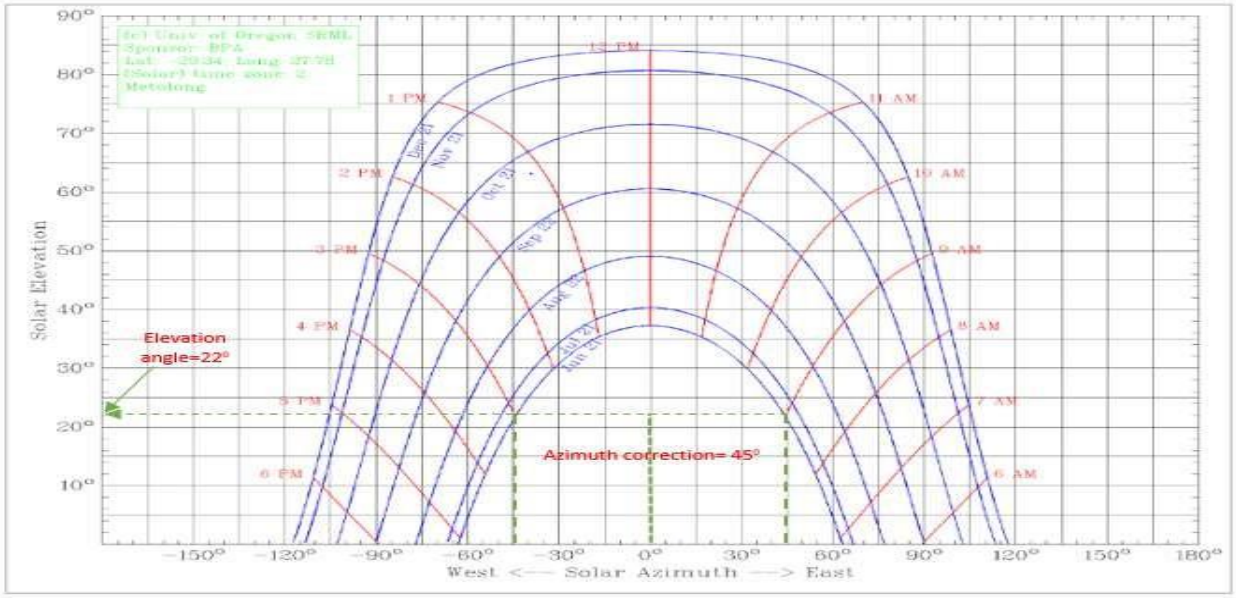

Figure F.2: Sun path chart for Metolong [102].

The next step is to account for the Azimuth angle and use the Metolong Sun path chart to apply another formula. As from the chart, two vertical reference lines are drawn down from each time reference. The difference between South going in either direction turns out to be 45^0 (Azimuth correction) and this angle was used to determine the minimum module row spacing using Equation (F.3).

□□□□□□□ □□□□□□ □□□ □□□□□□□ = □□□□□□ □□□ □□□□□□□ ∗ cos (□□□□□□*h* □□□□□□□□□□ □□□□□) [F.3]

Lastly, Equation (F.4) gives the distance from the trailing edge of one row to the trailing edge of the subsequent row or row width as:

□□□ □□□□*h* = □□□□□□□ □□□ □□□□□□□ + cos(□) ∗ □□□□□□ □□□□*h* [F.4]

Where, □ is the PV tilt angle (°) of the installed array.

Once the array spacing and tilt angle of each string is determined, the total area of the solar site required was calculated using Equation (F.5).

□ (□) = □ , , ∗ □ , ∗ (□□□ ∗ □□□) [F.5]

Where □ , , □ , , □□□ □□□ □□□ denote the number of modules per string, maximum number of strings, Module width (in meters) and Module row spacing (in meters) respectively.

APPENDIX G: Levelized Cost of Electricity

The Levelized Cost of Electricity (LCOE) is one of the most important economic indicators of a FSPV system. It is an indicator that measures the cost of the energy generated throughout the lifetime of the facility. In other words, it represents the minimum price of electricity that will generate enough revenue to pay for all the costs of the facility. Therefore, it is a really handy indicator to compare different power plants with different capacities or initial investments. It is specially adapted to a constant tariff system, where a fixed electricity price is set for every moment. The LCOE is calculated by adding all cash flows and dividing by the combined electrical production over the lifetime of the system. However, many factors influence the LCOE of an FSPV system including albedo, ambient temperature, module operating temperature, heat loss factor, soiling and mismatch losses, tilt angle, ground coverage ratio, and environmental loads. Because some models and the PVSyst model do not include an option explicitly to model FSPV systems yet, this study carried out a simplified LCOE analysis using the following formula (G.1).

$$\square\square\square\square = \frac{\sum_{t=1}^{n} \frac{I_t + OM_t + F_t}{(1+r)^t}}{\sum_{t=1}^{n} \frac{E_t}{(1+r)^t}} \qquad [G.1]$$

where I_t stands for the initial investment costs that may start before year 1, OM_t stands for Operation & Maintenance costs, F_t stands for fuel costs and E_t stands for electricity generation. All these parameters are evaluated along their lifetimes and have to be adjusted by a discount rate. Using the time value of money, this rate is used to bring a future value to the present to be able to represent a current situation. The rate is normally fixed as it is hard to predict how the market and interest rate change with time. The increase in capacity, salvage values and tax incentives may also be included in the formula and will always be evaluated within the discount rate.

APPENDIX H: Net Present Value

The NPV indicates all future cash flows, both positive and negative, that is, Revenue and maintenance costs over the lifetime of the power system discounted to the present. It represents the profitability of a project and is used to determine which alternative projects to prioritize. The NPV was calculated by the following Equation (H.1):

$$\square\square\square = -\sum \frac{\quad}{(\quad)} + \sum \frac{\quad}{(\quad)} \qquad [H.1]$$

where $\square_{\square\square}$ represents the initial investment, which may be considered to be done at year 0 of the project and in turn simplifies that equation to a -$\square_{\square\square}$ term. It also may start at N years prior to year 0 and therefore should be discounted to the future. $\square_{\square}$ Represents the discounted revenues that the project will earn during its lifetime.

APPENDIX I: Impact on the reduction of greenhouse gases emissions

GHG emission reductions refer to the amount of greenhouse gases produced when using a fossil energy system to generate the same amount of electricity produced by a renewable energy system.
Carbon dioxide (CO_2) emission: Indicates the total manufacturing emissions of the components of the photovoltaic system. The life cycle CO_2 emissions of the polycrystalline silicon modules were taken from the literature at 0.053 $kgCO_2eq./kWh$ [104], [105]. The CO_2 emissions for one year and during the service life of a PV system were evaluated using equations (I.1) and (I.2), respectively.

□□ □□□□□□□□ □□ □□ □□□□□□ = □ _ ___ ∗ □□ [I.1]

Where $E_{a,out}$ is the annual output energy, LC_{e_PV} is the life cycle CO_2 emission from the PV, and t is the life of the PV system.

□□□□□□□□ □□ □□□□□□□□□□ □□ □□ □□□□□□ = ∑ □ _ ___ ∗ (□ − □) ∗ □ ∗ 0.053 (In kg)

[I.2]

In the Equation (I.2), d is the degradation rate of the polycrystalline PV module which is taken as 0.6%/year [106].

CO_2 mitigation is shown as the amount of CO_2 emission reduction from generating the power that the coal-fired power plant releases to generate an equal amount of electricity. The annual CO_2 mitigation can be evaluated by using Equation (I.3).

□□□□□□ □□ □□□□□□□□□□ = □ _ ___ ∗ □□ [I.3]

The average CO_2 emission is 0.98 kg for the generation of electricity per unit from the coalfired power plant. In South Africa, the transmission and distribution losses increase the emissions per unit of CO_2 and can be assumed to be 1.58 kg which is the grid emission factor represented as EF_{grid} [107]. The net CO_2 reduction for a PV system is estimated using the difference between CO_2 emissions and lifetime reduction as shown in Equation (I.4).

□□□ □□ □□□□□□□□□□ = □□ − □□ _ ∗ ∑ □ _ ___ ∗ (1 − □) ∗ □ [I.4]

Earned carbon credits: The carbon credit can generally be understood as a compensation term that attaches value to the reduction of GHG emissions. A carbon credit is earned by trading $1tCO_2e$ on the international market. The price of carbon credits is $17.95/tCO2e [108]. Here, the earned carbon credits was estimated using Equation (H. 5).

□□□□□□ □□□□□□ □□□□□□□□ ($) = [1.58 − 0.053] ∗ ∑ □ _ ___ ∗ (1 − □) ∗ □ ∗ 17.95

[I.5]

APPENDIX J: Mathematical model for the estimation of reduction of water evaporation

The evapotranspiration rate (ET_0) in millimetres per day (mm/day) is calculated using the variation of the Penman formula developed by [90] that requires relative humidity, mean air temperature, wind speed, and solar radiation data:

$$\square\square = 0.051(1-\alpha)R_s\sqrt{T-9.5} - 0.188(T+13)\left(\frac{R_s}{R}-0.194\right) * 1 - 0.00014(0.7\square + 0.3\square + 46)\sqrt{\frac{RH}{100}+0.049(T_{max}+16.3)\left(1-\frac{RH}{100}\right)(a_u+0.536u)} \quad [J.1]$$ [J.1]

Where $\square$ is the water albedo or reflectivity with the value of 0.08, $\square$ is the mean air temperature (°C), T_{max} is the maximum air temperature (°C), T_{min} is the minimum air temperature (°C), $\square\square$ is the relative humidity (%), $\square\square$ is the global horizontal solar radiation (MJ/m^2/day), $\square\square$ is the extra-terrestrial radiation (MJ/m^2/day), $\square$ is the wind speed at 2 m above the water surface (m/s), and $\square\square$ is 0 if using [109] and 1 if using [110].

The mean temperature was derived from the average of the maximum and the minimum temperature instead of the average daily temperature [90]. The temperatures was acquired from the Lesotho meteorological service; a dataset consists of different climate variables.

The daily total sunshine hours (n) were estimated based on the monthly sunshine duration. Monthly R_s was calculated based on monthly Ra, daylight hours (N), and daily total sunshine hours (n) by [90]:

$$\square = \square \times 0.5 + 0.25 \times \_ \quad [J.2]$$

The extra-terrestrial radiation R_a or radiation received in the upper part of the Earth's atmosphere on a horizontal surface at various latitudes relative to reservoirs was provided by the Food and Agriculture Organization of the United Nations (FAO, 1998). N can be calculated for each month based on the following Equation by [90]:

$$\square = 4\square\square\square\square(0.53\square - 1.65) + 12 \quad [J.3]$$

Where i is the rank of the month (e.g. January has rank 1), $\emptyset$ is the latitude of the site (radians) which is positive for the Northern hemisphere. Relative humidity was calculated based on the water vapour pressure using the formula below:

$$\square\square = \frac{\_\_\_\_\_}{\_\_\_\_\_} * 100\% \quad [J.4]$$

It is important to note that Penman (1963) [110] and Linacre (1993) [109] suggested the incorporation of the wind function to estimate the potential evaporation from open water, which appears in Equation (J.5) as:

□ = □ + 0.536□ [J.5]

The wind speed at 10 m above the water surface was found based on the equation for the wind speed at different heights, provided by FAO (1998) [72]:

$$□ = □ \frac{4.87}{\ln(67.8z-5.42)} \quad [J.6]$$

Where □□ is the measured wind speed at z meter above ground surface (m/s). The average speed shown was assumed to be the wind speed at the reservoir. The total volume of water that evaporates from free surfaces can be calculated according to the following Equation:

□(□ /□□□) = □(□/□□□) × □ [J.7]

The reduction in reservoir water evaporation after the construction of the FSPV can be estimated based on the ratios of the area covered by the reservoir, that is, the total FSPV platform area (A_{FSPV}) and the total open area of the reservoir before the construction of FSPV ($A_{reservoir}$) according to the following equation:

Δ□(□ /□□□) = □ × □(□/□□□) × □ [J.8]

Where the coefficient k < 1 accounts for the fact that part of the additional irradiated energy on the FSPV is handed to water, increasing its potential for evaporation. The values of the coefficient k depend on the type and reflective characteristics of the platform, its coverage level with PV modules and the efficiency of these modules.

APPENDIX K Reservoir data J.1. Water level variations (Metolong reservoir)

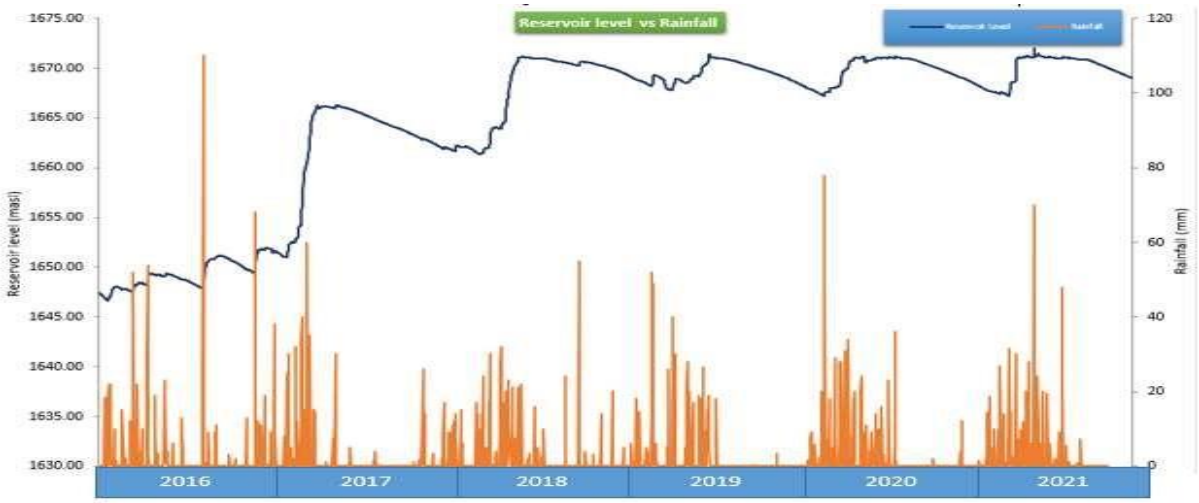

APPENDIX J.1: Reservoir level vs rainfall

J.2. Simplified bathymetry map of the Metolong Dam.

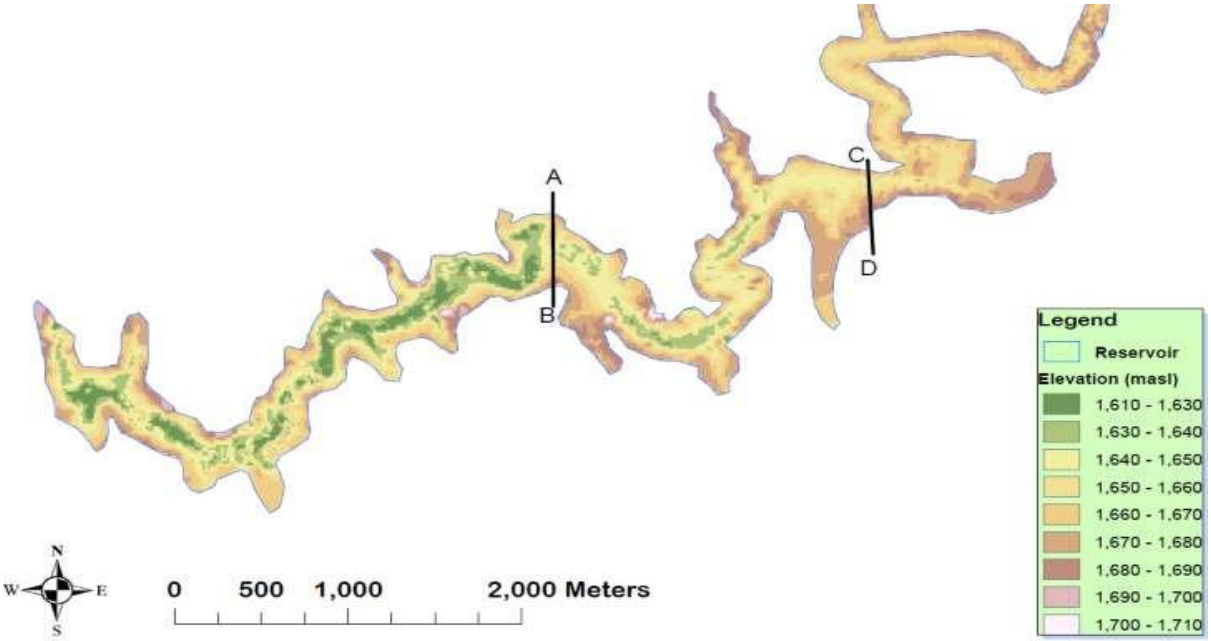

APPENDIX J.2: Showing bathymetric layout of the Metolong Dam.

J.3. The graph showing the changing of reservoir volume and surface area with elevation.

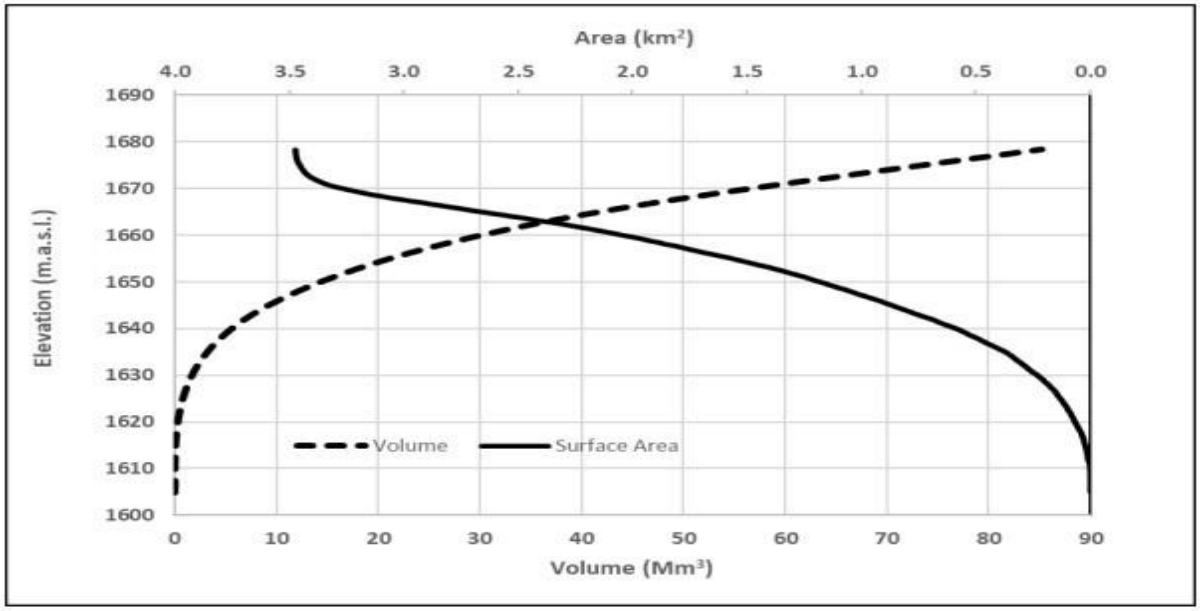

APPENDIX J.3: Storage-area-elevation curve of Metolong Dam.

J.4. Summary of Metolong reservoir data parameters.

Column1	Column2	Column3	Column32	Column4	Column5	Column6	Column7	Column8	Column10	Column11	Column12	Column13	Column14	Column15	Column14	Column15	Column16	Column17
Date	Reservoir Level	Diference in EL	Spillway Discharge Head (m)	Total diff in EL since 1 Nov 2014	Live Storage %	Live Storage m3	Precipitation in mm (dam site)	Precipitation cumulative mm	US Weir Daily Average Inflow Depth (m)	Daily avarage inflow (m^3/sec)	IFR flo- Outlet house meter l/sec	IFR recomended l/sec	V-notch 1 right gauge depth m	V-notch 2 left gauge depth m	V-notch 1 (gauge level (m) Right	V-notch 2 (gauge level (m) Left	Daily outflow from V-Notch (l/s)	D/S crump weir plate depth m
21 June 2021	1670.08	(0.02)	0.00	7.99	95.30	53573258	0	4975.20	0.104	0.406	274	270	0.28	0.29	0.2713	0.258541667	307	0.07
22 June 2021	1670.05	(0.03)	0.00	7.96	95.15	53488624	0	4975.20	0.081	0.271	274	270	0.28	0.29	0.2713	0.258541667	307	0.07
23 June 2021	1670.03	(0.02)	0.00	7.94	95.05	53432258	0	4975.20	0.042	0.088	274	270	0.28	0.29	0.2713	0.258541667	307	0.07
24 June 2021	1670.00	(0.03)	0.00	7.91	94.90	53347793	0	4975.20	0.009	0.004	274	270	0.28	0.29	0.2713	0.258541667	307	0.07
25 June 2021	1669.98	(0.02)	0.00	7.89	94.80	53291540	0	4975.20	0	-0.001	274	270	0.28	0.29	0.2713	0.258541667	307	0.07
26 June 2021	1669.96	(0.02)	0.00	7.87	94.70	53235333	0	4975.20	0.016	0.014	274	270	0.28	0.29	0.2713	0.258541667	307	0.07
27 June 2021	1669.94	(0.02)	0.00	7.85	94.60	53179170	0	4975.20	0.09	0.322	274	270	0.28	0.29	0.2713	0.258541667	307	0.07
28 June 2021	1669.92	(0.02)	0.00	7.83	94.50	53123052	0	4975.20	0.044	0.096	274	270	0.28	0.29	0.2713	0.258541667	307	0.07
29 June 2021	1669.89	(0.03)	0.00	7.80	94.35	53038960	0	4975.20	0.033	0.057	274	270	0.28	0.29	0.2713	0.258541667	307	0.07
30 June 2021	1669.86	(0.03)	0.00	7.77	94.20	52954970	0	4975.20	0.033	0.057		270	0.28	0.29	0.2713	0.258541667	307	0.07
01 July 2021	1669.84	(0.02)	0.00	7.75	94.10	52899032	0	4975.20	0.033	0.057		130	0.09	0.10	0.0813	0.068541667	20	0.005
02 July 2021	1669.83	(0.01)	0.00	7.74	94.05	52871081	0	4975.20	0.032	0.054	132	130	0.09	0.10	0.0813	0.068541667	20	0.005
03 July 2021	1669.81	(0.02)	0.00	7.72	93.95	52815211	0	4975.20	0.032	0.054	132	130	0.18	0.19	0.1713	0.158541667	104	0.04
04 July 2021	1669.79	(0.02)	0.00	7.70	93.85	52759385	0	4975.20	0.032	0.054	132	130	0.18	0.19	0.1713	0.158541667	104	0.04
05 July 2021	1669.77	(0.02)	0.00	7.68	93.75	52703605	0	4975.20	0.031	0.051	132	130	0.18	0.19	0.1713	0.158541667	104	0.04
06 July 2021	1669.75	(0.02)	0.00	7.66	93.65	52647870	0	4975.20	0.031	0.051	132	130	0.18	0.19	0.1713	0.158541667	104	0.04
07 July 2021	1669.73	(0.02)	0.00	7.64	93.55	52592179	0	4975.20	0.031	0.051	132	130	0.18	0.19	0.1713	0.158541667	104	0.04
08 July 2021	1669.71	(0.02)	0.00	7.62	93.46	52536633	0	4975.20	0.030	0.048	132	130	0.18	0.19	0.1713	0.158541667	104	0.04
09 July 2021	1669.69	(0.02)	0.00	7.60	93.36	52480932	0	4975.20	0.030	0.048	132	130	0.18	0.19	0.1713	0.158541667	104	0.04
10 July 2021	1669.67	(0.02)	0.00	7.58	93.26	52425375	0	4975.20	0.030	0.048	132	130	0.18	0.19	0.1713	0.158541667	104	0.04
11 July 2021	1669.65	(0.02)	0.00	7.56	93.16	52369863	0	4975.20	0.030	0.048	132	130	0.18	0.19	0.1713	0.158541667	104	0.04
12 July 2021	1669.63	(0.02)	0.00	7.54	93.06	52314396	0	4975.20	0.030	0.048	132	130	0.18	0.19	0.1713	0.158541667	104	0.04
13 July 2021	1669.61	(0.02)	0.00	7.52	92.96	52258873	0	4975.20	0.030	0.048	132	130	0.18	0.19	0.1713	0.158541667	104	0.04
14 July 2021	1669.59	(0.02)	0.00	7.50	92.86	52203595	0	4975.20	0.030	0.048	132	130	0.18	0.19	0.1713	0.158541667	104	0.04
15 July 2021	1669.57	(0.02)	0.00	7.48	92.76	52148262	0	4975.20	0.030	0.048	132	130	0.18	0.19	0.1713	0.158541667	104	0.04
16 July 2021	1669.54	(0.03)	0.00	7.45	92.62	52065344	0	4975.20	0.030	0.048	132	130	0.18	0.19	0.1713	0.158541667	104	0.04